SNS 000000000000000

Preliminary Design Report

Superconducting Radio Frequency Linac for the Spallation Neutron Source

November 1999

SNS XXXXXXXXXXXX

PRELIMINARY DESIGN REPORT

SUPERCONDUCTING RADIO FREQUENCY LINAC FOR THE SPALLATION NEUTRON SOURCE

November 1999

DRAFT

Prepared for the
U.S. Department of Energy
Office of Science

LOCKHEED MARTIN ENERGY RESEARCH CORPORATION
managing the
Spallation Neutron Source Activities at the
Argonne National Laboratory
Brookhaven National Laboratory Lawrence Berkeley National Laboratory
Los Alamos National Laboratory Oak Ridge National Laboratory
under contract DE-AC05-96OR22464
for the
U.S. DEPARTMENT OF ENERGY

Table of Contents

List Of Figures

List of Tables

ACRONYMS

ANL	Argonne National Laboratory
APT	accelerator production of tritium
ATLAS	Argonne Tandem-Linear Accelerator System
BCP	buffered chemical polishing
BPM	beam position monitor
CCDTL	coupled cavity drift tube linac
CCL	coupled cavity linac
CEA	Centre d'Energie Atomique
CEBAF	Continuous Electron Beam Accelerator Facility
CERN	European Laboratory for Particle Physics
CERN SPS	CERN Super Proton Synchrotron
CESR	Cornell Electron Storage Ring
CHL	central helium liquifier
CM	cryomodule
CW	continuous wave
DESY	Deutsches Elektronen-Synchrotron
DTL	drift tube linac
DOE	U.S. Department of Energy
ESS	European Spallation Neutron Source
FEL	free electron laser
FWHM	full width half maximum
HEBT	high energy beam transport
HEPL	High Energy Physics Laboratory
HERA	electron-proton accelerator at DESY
HOM	higher-order mode
IGBT	insulated gate bipolar transistor
INFN	Instituto Nazionale di Fisica Nucleare
IPS	iron pipe size (manufactured in U.S.)
JAERI	Japan Atomic Energy Research Institute
JLab (or TJNAF)	Thomas Jefferson National Accelerator Facility
KEK	High-Energy Accelerator Research Organization
KEK-B	KEK B factory
KFA	Kern Forschung Anlage
LANL	Los Alamos National Laboratory
LANSCE	Los Alamos Neutron Science Center
LEBT	low energy beam transport
LEP-200	Large Electron Positron Collider at CERN
LHC	large hadron collider
LLrf	low-level radio frequency
MEBT	medium energy beam transport
NC	normal conducting
OFHC	oxygen-free high-conductivity
rf	radio frequency
RFQ	radio frequency quadrupole
RGA	residual gas analyzer
rms	root mean square
RRR	residual resistivity ratio
SC	superconducting

SRF	superconducting radio frequency
TESLA	TeV Energy Superconducting Linear Accelerator
TJNAF	Thomas Jefferson National Accelerator Facility
TL	transfer line
TTF	TELSA Test Facility
TVA	Tennessee Valley Authority
WBS	work breakdown structure

DEFINITIONS

a/b	aspect ratio
B'	gradient
B_p	peak magnetic field
E_a	$E_a = E_oT$ accelerating gradient
E_o	average gradient
E_p	peak surface electric field
q	charge
Q_o	quality factor
Qext	external quality factor
T	transit time factor
β	particle velocity divided by the speed of light
β_g	cavity geometric β
ΔE	energy gain

Executive summary

A preliminary design of a superconducting linac (SC) option for the Spallation Neutron Source (SNS) was undertaken by an ad hoc working group established by SNS management to assess the technology choice of the SNS linac. Based on the analysis performed and recorded in this report, the group recommends that the SNS management incorporate the SC linac option into the SNS baseline. Technologies required for the SC SNS linac have already been demonstrated in other existing SC accelerator facilities, and the demonstrated performance exceeds the SNS requirements. There is a strong industrial base for SC linac construction to expedite this schedule.

Construction of the superconducting linac is feasible within the baseline schedule, provided that prototyping efforts are organized expeditiously. Parallel efforts using existing infrastructure and expertise from partner laboratories can facilitate this fast-track startup.

The general advantages of a superconducting linac for the SNS are:

1) Construction and operating costs are considerably less compared to the warm linac. Expected power consumption is about 12 MW less than in the normal-conducting case.
2) Availability of the SC linac can be designed to be higher than that of the warm linac with a similar construction cost. This is due to fact that each SC cavity has substantial reserve capability.
3) The reserve capability can be used later to upgrade the linac energy by increasing the klystron power.
4) Energy stability is better than for the warm linac.
5) Ultra-high vacuum from the cryogenic system creates less beam-gas scattering.
6) The much larger bore of the SC cavity reduces linac component activation due to beam loss.

Specifically, the impacts to the SNS of changing to superconducting technology are:

1) Construction Cost Advantage - The total project cost of the SC linac option presented in this report is about $29.3M less than the warm baseline linac total project cost, including prototyping, technical equipment, and conventional facility scope reduction.

2) Operating Cost Advantage - Due to the reduction of electric power and cooling required to operate the facility, the operating cost savings for the facility with SC linac are estimated to be at least $3.5M per year.

3) Schedule Advantage - Due to the fact that less hardware is required, the construction duration is much shorter. Although actual construction of the SC linac starts later than the warm linac schedule, the SC linac is completed four months earlier. This four months can be used to obtain additional float for the Project.

4) Availability Advantage – The SC linac is designed to operate with one or two klystrons or cavities deactivated. Therefore the linac availability is higher than that of the warm linac. This is due to fact that each SC cavity has substantial reserve capability.

5) Environmental Advantage – The environmental impact of about 12-MW lower power consumption is significant and translates into less heat rejection into the Walker Branch Watershed.

There are significant cost, schedule, and availability advantages to the SC option. Superconducting accelerator technology is expected to be the technology of choice in the 21st Century and may attract world-class scientists and engineers to this Facility.

1. INTRODUCTION

This report presents a preliminary design of the superconducting (SC) linac for the Spallation Neutron Source (SNS). The work was performed by an ad hoc working group established by the SNS management to assess the technology choice of the SNS linac. Based on the analysis performed and recorded in this report, the group recommends that the SNS management incorporate the SC linac option into the SNS baseline. Technologies required for the SC SNS linac have already been demonstrated in other existing SC accelerator facilities, and the demonstrated performance exceeds the SNS requirements.

Construction of the superconducting linac is feasible within the baseline schedule, provided that prototyping efforts are organized expeditiously. Parallel efforts using existing infrastructure and expertise from partner laboratories can facilitate this fast-track startup.

The advantages of a superconducting linac for the SNS are:

1) Construction and operating costs are less compared to the warm linac. Expected power consumption is 10 to 12 MW less than in the normal-conducting case.
2) Availability of the SC linac can be designed to be higher than that of the warm linac with a similar construction cost. This is due to fact that each SC cavity has substantial reserve capability.
3) The reserve capability can be used later to upgrade the linac energy by increasing the klystron power.
4) Energy stability is better than for the warm linac.
5) Ultra-high vacuum from the cryogenic system creates less beam-gas scattering.
6) The much larger bore of the SC cavity reduces linac component activation due to beam loss.

The impacts of changing to superconducting technology at this point in time are:

1) Schedule impact – Prototyping of cavities and cryomodule requires about 24 months, and the fabrication and installation also take about 24 months. In addition, an allotment for the procurement period must be added. Participation by several laboratories may shorten the prototyping period. The 24-month-long fabrication and installation period is substantially shorter than that of the warm linac.

2) A superconducting radiofrequency cavity processing facility at Oak Ridge – Industry-built niobium cavities must be cleaned, processed and tested before installing in the linac enclosure. Construction of such infrastructure at the Oak Ridge site may take 18 months. In the meantime existing facilities at other laboratories could be utilized for the prototyping. Early construction of SRF test and processing facilities at Oak Ridge enables the SNS to assemble a world-class accelerator technology staff sooner.

3) Construction Cost Advantage - The total project cost of the SC linac option presented in this report is about $29.3M less than the warm baseline linac total project cost, including prototyping, technical equipment, and conventional facility scope reduction.

4) Operating Cost Advantage - Due to the reduction of electric power and cooling required to operate the facility, the operating cost savings for the facility with SC linac are estimated to be at least $3.5M per year.

5) Schedule Advantage - Due to the fact that less hardware is required, the construction duration is much shorter. Although actual construction of the SC linac starts later than the warm linac schedule, the SC linac is completed four months earlier. This four months can be used to obtain additional float for the Project.

1.1 BACKGROUND

The SNS linac is required to deliver a 1-GeV H^- beam with an average power of 2 MW. This 60-Hz linac operates at a 6 % beam duty cycle with a 1-ms pulse duration. At these power levels and pulse structures, both normal conducting and SC linacs can be designed to meet the requirements. As the duty cycle moves towards CW and the average power rises, SC linacs have the clear advantage in terms of saving significant capital and operating costs. At the time of the formulation of the SNS baseline design, an all-normal conducting linac appeared to be a reasonable choice based on LANL's long experience with warm copper linacs and the potential concern for the stability of high-power pulsed operation of SC linacs.

During the past two years three significant developments have occurred. DESY has demonstrated more than adequate control of pulsed operation of the TESLA Test Facility (TTF) linac. TTF has also reliably achieved high gradients in nine-cell cavities delivered by four industrial vendors. Additionally, a high-power (380-kW) CW coaxial coupler that meets SNS requirements has been demonstrated at KEK-B.

The experience base with SC linacs has broadened immensely in recent years. Pioneering work at Cornell and HEPL (Stanford) led to technology that enabled construction of the 4-GeV recirculating SC linac for the Continuous Electron Beam Accelerator (CEBAF) at Jefferson Laboratory in 1987. Since then, CERN has built 288 SC cavities with a resulting 3 GV accelerating voltage, and DESY has built the TESLA Test Facility to achieve higher gradients than any other facility. As of 1999, about a kilometer of SC cavities are operating worldwide with a total installed accelerating voltage exceeding 5 GV. LEP-200 (288 cavities) and CEBAF (338 cavities) are the largest installations.

The SC linac offers a number of advantages. The large bore of SC cavities (2.5 times larger than the warm linac) alleviates the beam loss situation. The thermal stability afforded by the helium cryogenic cooling, and the lower radio frequency (rf) power input contribute to lower operational costs (10-12 MW less). Cryogenic cooling intrinsically provides better vacuum and thermal stability. Finally, the SC linac rf has an inherently large operational parameter range, which enables design of a flexible and fault-tolerant machine.

Technical and programmatic risk is minimized due to ongoing development efforts in high gradient SC cavities in Europe, Japan and the US. ACCEL, with ESS has built a five cell β_g=0.75 cavity which is being tested at CERN. In the United States, LANL, with the assistance of TJNAF (Thomas Jefferson National Accelerator Facility), is completing the design and prototyping of SC cavity and cryostat hardware for the APT.

Additional SC design efforts that are underway further strengthen the experience base for SC linacs. These efforts include the 12-GeV upgrade of CEBAF in 2004, the 10-kW upgrade to the FEL at Jefferson Lab in 2002, the joint KEK/JAERI project for neutron and nuclear physics, and

Franco-Italian efforts toward 15-20-MW SC proton linac designs by CEA-France and INFN-Italy.

Another advantage, which has evolved during the last 15 years, is the maturing of an industrial base, mainly in Europe, that can support SC linac hardware construction. Three vendors routinely produce high-quality nine-cell cavities for TTF. DESY is projecting industrial production of 20000 cavities over three years for the 34-km-long TESLA linear collider and FEL.

Surface treatment and processing for the SC cavities is similar to that used in the semiconductor industry. TJNAF recently upgraded its surface treatment and cavity processing facility with state-of-the-art equipment. The new TJNAF facilities have the capabilities required for processing, assembling, and testing both prototype and production hardware for the SNS SC linac. Similar processing and testing facilities are available at LANL, DESY, Cornell University, CEA-Saclay, and JAERI-Japan.

We propose to do initial prototyping at the above facilities. Meanwhile, SNS will develop SRF processing capability on-site, and when it is available the SNS SC activities should be centered at SNS.

Accelerator physics studies were carried out at SNS. Cryogenic, cryostat and rf studies were carried out at TJNAF. Conventional facility and SC rf facility studies were conducted by TJNAF and SNS. These topics are discussed in the remainder of this document.

Contributors to this preliminary design and participants in the working groups are:

J. Alessi	BNL	C. Leemann	TJNAF
D. Chan	LANL	D. Mangra	SNS
A. Chargin	SNS	T. Mann	SNS
Y. Cho	SNS	S. Martin	ESS-Juelich
J. Delayen	TJNAF	B. Miller	LANL
F. Dylla	TJNAF	D. Olsen	SNS
D. Edwards	FNAL	H. Padamsee	Cornell-LNS
R. Fuja	ANL	C. Pagani	INFN-Milan
J. Galambos	SNS	J. Preble	TJNAF
M. Ganapati	TJNAF	C. Rode	TJNAF
M. Gregg	SNS	W. Schneider	TJNAF
K. Hasegawa	JAREI	D. Schrage	LANL
J. Holmes	SNS	S. Simrock	DESY
L. Jacobs	SNS	R. Sundelin	TJNAF
D. Jeon	SNS	E. Temple	SNS
Y. Kang	ANL	T. Wangler	LANL
K. Kim	ANL	J. Wei	BNL
S. Kim	SNS	M. White	SNS
P. Kneisel	TJNAF	R. Wood	SNS
R. Kustom	SNS		

There were two working group meetings. The first meeting was held August 9-12, 1999, at Argonne National Laboratory. This meeting included a review of the existing state-of-the-art of

superconducting radiofrequency technology, presentations of similar superconducting linacs, both existing and proposed, and an agreement on the basic architecture of the linac system. Work assignments were divided among the group members. The working group also discussed prototyping plans and procurement strategy. The group consensus was that it is unnecessary to perform beam tests on the prototype cryomodule in light of recent favorable experience at other machines. There were presentations on the European Spallation Source and TESLA SC programs in Germany, the JAERI/KEK program in Japan, the INFN-Milan work in Italy, CEBAF at TJNAF, and the APT and an SNS study at Los Alamos. The second meeting was held September 17-18, 1999, at Jefferson Laboratory for a mid-course review.

2. INTEGRATED PHYSICS DESIGN

2.1 INTRODUCTION

The SC linac accepts a 194.3-MeV H^- beam from the warm linac and accelerates it to 1 GeV, meeting all specifications listed in Table 2.1. Most of these requirements are taken directly from the SNS parameter list dated July 8, 1999. The 194.3-MeV input H^- energy is conservatively chosen to be at the end of an rf module of the CCL and at a high enough energy so that only two beta sections suffice for the SC linac. Choice of this transition energy is driven by cavity stiffness and microphonic issues, which are more problematic at low energy.

Given an additional six months, prototyping a third velocity group cavity could be carried out, which would replace the CCL completely. Japanese and European studies indicate that this is possible [1, 2].

Table 2.1 Overall SC linac parameters

Input H^- energy	194.3 MeV
Output H^- energy	1001.5 MeV
Output average beam power	2. MW
Output average beam current	2. mA
Macropulse repetition rate	60 Hz
Macropulse beam period	0.974 ms
Beam duty factor	5.84%
Chopper transmission	65%
Chopper period	841 ns
Peak macropulse current	56 mA
Average macropulse current	36 mA
Vacuum pressure	<5E-8 torr
Uncontrolled beam loss	<1 nA/m at 1 GeV
Normalized rms emittance at 1 GeV	0.5 π-mm-mrad

2.2 LINAC PHYSICS DESIGN AND ARCHITECTURE

2.2.1 Design Choices

Several design choices are available for consideration, including: 1) choice of cavity velocity, 2) number of cells per cavity, 3) constant gradient versus constant energy gain per cavity, 4) number of cavities per cryomodule and type of focusing lattice.

During the acceleration process the particle beta varies from 0.56 to 0.88. Ideally, the cavity design varies continuously with the particle beta, but this is unnecessary in the SC linac case. This study shows that two cavity groups (β_g=0.61 and β_g=0.76) are sufficient to produce beam meeting the specifications. The cavity geometrical beta, β_g is defined by the cell length of $\beta_g\lambda/2$, where λ is the rf free space wavelength. Wangler and Martin independently obtained a similar choice of beta groupings for the same energy range at the first working group meeting.

Since the particle beta is not the same as the cavity geometric beta (β_g) throughout acceleration, there is a phase slippage as the particle traverses the cavity. This slippage reduces the ideal possible energy gain, and the transit time factor accounts for this effect. The voltage gain of a particle traversing a cavity of voltage V with phase angle ϕ is $\Delta V = VT\cos(\phi)$, where T is the transit time factor. For a particle with velocity $\beta=\beta_g$, $T=\pi/4$. The transit time factor influences the design choices including: (1) the number of cells per cavity and (2) the use of constant energy gain per cavity or constant gradient per cavity. Use of eight cells per cavity instead of six cells per cavity results in smaller transit time factors, and less efficient use of the cavity accelerating field. Use of fewer cells per cavity results in less efficient use of real estate. Additionally the six cell cavities are approximately one meter long, easy to manipulate, and able to be processed in existing facilities.

The linac can either be designed to operate with constant gradient or with constant energy gain per cavity. The limit in SC cavity accelerating gradient is generally determined by the achievable E_p. Thus conservative values of E_p are preferable. A constant-gradient design is chosen because, for a fixed accelerating length and final energy, it results in a more efficient use of the accelerating gradient, and hence a lower E_p. The constant energy gain design gives E_p modulation throughout the linac, resulting in higher values of E_p wherever the transit time factor is small, namely at the ends of the beta sections. As an illustration, the comparison of E_p for constant energy gain and constant gradient are shown in Figure 2.1. The higher peak gradient requirement for a constant energy-gain scheme is clearly seen in Fig. 2.1. For the constant energy gain case, E_p reaches 37 MV/m.

As a practical matter, with the same peak gradient limit, the difference between a six-cell, constant-energy-gain linac and a constant-gradient linac is 37 m of length or about six cryostats. To facilitate constant-gradient acceleration, the input rf power to each cavity has to be programmed.

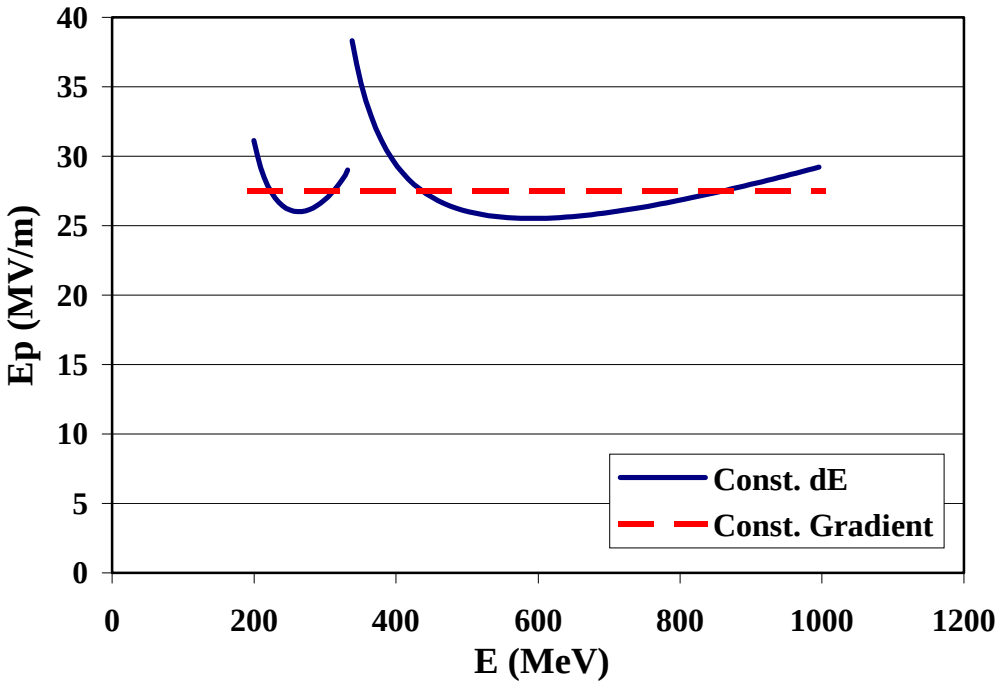

Figure 2.1 E_p versus energy for constant gradient and constant energy gain acceleration schemes for the same total linac length.

FODO, doublet, or triplet magnetic focusing lattices are all possible design choices for transverse focusing. This design choice influences the number of cavities per cryomodule. A doublet structure was chosen because its focusing period offers the maximum uninterrupted distance for accelerating cavities, resulting in higher packing factors. The quadrupole doublets and diagnostics are located in the warm sections between cryomodules. Doublet focusing allows three cavities per medium-beta cryomodule and four cavities per high-beta cryomodule, while maintaining good beam quality. These issues are discussed in more detail in Section 2.3 and in Chapter 8.

2.2.2 Cell Physics Design

This section discusses the design choices that determine the linac architecture and beam dynamics. Figure 2.2 shows the geometrical view of the half-cell along with definitions of the cell parameters. The cell parameters listed in Table 2.2 were obtained as a result of design calculations with Superfish with the assumption that B_p is less than 70mT. The 70-mT value is conservative since it is less than half of the typical value for TESLA cavities. A detailed discussion of the design, fabrication, processing, and voltage capabilities of the cavities is given in Chapter 3.

As noted earlier, cavity performance is limited by peak surface electric field and peak surface magnetic field. Currently, the TESLA Test Facility achieves about 55 MV/m and 150 mT for E_p and B_p, respectively. The ratios of the peak surface electric field, E_p, to the average gradient of an interior cell, E_o, and the peak surface magnetic field, B_p, to E_o depend on cavity geometry.

A 5-cm iris radius is used for the 805-MHz cells. This aperture is considered large enough to satisfy the beam dynamics requirements and produce negligible activation. This iris radius gives a coupling constant of about 2%. The cavities will be stiffened to reduce the effects of microphonics. Table 2.2 also lists the cavity fields when operated at a peak surface field of 27.5 MV/m. To compare these fields directly with those for β=1 accelerators, the average accelerating fields, E_a, are also listed, where $E_a = E_o \ \pi/4$.

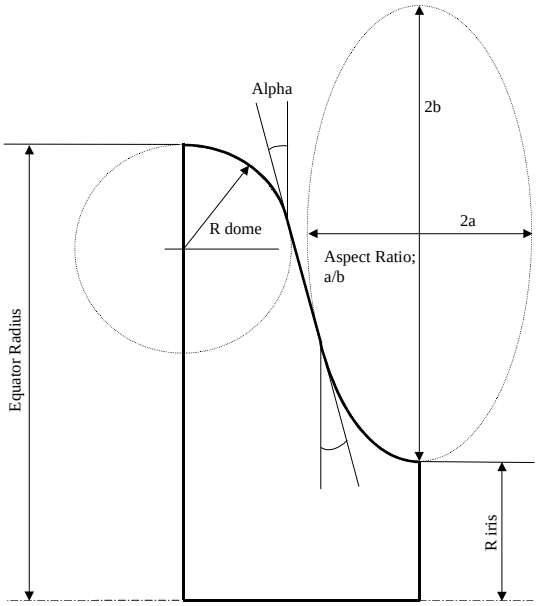

Figure 2.2: Reference geometry for the half-cells.

Table 2.2: Cell parameters and fields.

Section	Medium beta	High beta
Geometric beta	0.61	0.76
Alpha (deg)	5.0	7.0
R iris (cm)	5.0	5.0
R dome (cm)	3.7	4.6
a/b	0.7	0.7
E_p/E_o	2.33	1.82
E_p/E_a	3.0	2.35
B_p/E_p (mT/MV/m)	1.99	2.12
Coupling (%)	2.5	1.6
Parameters at E_p=27.5 MV/m:		
E_o (MV/m)	11.8	15.1
E_a (MV/m)	9.3	11.9
B_p (mT)	54.7	58.3

2.2.3 Linac Architecture

Having decided on the six-cell cavity design, the next task is to decide the cryomodule structure for each beta section. The optimum number of cavities per cryomodule is three for the β_g = 0.61 section and four for the β_g = 0.76 section. This choice also satisfies transverse focusing requirements. In addition to the active lengths of the acceleration cavities, the following length allowances were made for equipment along the linac beam line:

- 22.0-cm cavity-end lengths for couplers on both sides of the active length,
- 7.0-cm lengths on both ends of each cavity for bellows,
- 17.2-cm lengths for warm to cold transitions at both ends of each cryomodule,
- 5.0-cm for a relief valve and vacuum pumpout port for each cryomodule, and
- 10.0-cm lengths for gate valves at both ends of each cryomodule.

Warm lengths of 160 cm are allotted between cryomodule gate valves to allow for quadrupoles, diagnostics, vacuum, and alignment equipment. The layout of these warm sections is discussed in Chapter 8 and the length allowances are summarized in Table 2.3. With these length allowances and six-cell active-cavity lengths of 0.6815 m and 0.8491 m, the cryomodule lengths with gate valves are 4.239 m and 6.100 m, respectively, for the medium-beta and high-beta sections, with corresponding focusing periods of 5.839 m and 7.700 m.

Table 2.3: SC linac space allowances (cm)

Cavity ends	22.0
Bellows	7.0
Cold to warm transitions	17.2
External valve and beam pipe	10.0
Relief valve and vacuum pumpout	5.0
Warm space between valves	160.0

The remaining parameters to be determined are the number of medium-beta and high-beta cryomodules needed to accelerate the beam from 194.3 to 1001.5 MeV. With an assumed peak surface electric field of 27.5 MV/m, tradeoff studies between number of cryomodules in the medium- and high-beta sections determined the transition energy. The result is this acceleration requires 9 medium-beta cryomodules and 20 high-beta cryomodules and the transition energy between sections is 331.1 MeV. The optimum energy for this transition is weakly determined. In general, it is more efficient to have more high-beta cryomodules and less medium-beta cryomodules because the packing factors and the acceleration fields are higher for the high-beta cryomodules. The total length of the resulting SC linac is 206.6 m with an energy gain per real estate length of 3.9 MV/m. Table 2.4 lists the parameters that describe this constant-gradient linac architecture.

Figures 2.3 to 2.5 show cavity parameters as a function of energy. Figure 2.3 shows the phase of the beam bunches with respect to the rf for each cell in each cavity and shows that the end cavities have beam phase changes of more than 100 degrees. These phase changes are minimized when the beam velocity matches the cavity geometric velocity but is not reduced to zero because the end-cell effective lengths are not identical to the interior-cell lengths. The phase matching used in these calculations is discussed in section 2.3.2.

Table 2.4 Parameters that describe the architecture of the SNS SC linac

Total real estate length (m)	206.6	
Total cavity length (m)	86.3	
Energy gain per real estate meter (MeV/m)	3.90	
HOM couplers	yes	
Power couplers per cavity	one	
Klystrons per cavity	one	
Transverse magnetic focusing lattice	warm doublets	
Frequency (MHz)	805	
Starting energy (MeV)	194.3	
Family transition energy (MeV)	331.1	
Ending energy (MeV)	1001	
Sections	**Medium-beta**	**High-beta**
Beta	0.61	0.76
Cell length (m)	0.1136	0.1415
Number of cells per cavity	6	6
Active cavity length (m)	0.6815	0.8491
Cavities per cryomodule	3	4
Number of cryomodules	9	20
Number of cavities	27	80
Number of cells	162	480
Cryomodule length (m)	4.239	6.100
Warm space between valves (m)	1.60	1.60
Transverse focusing period (m)	5.839	7.700
Filling factor	0.350	0.441
Total section length (m)	52.5	154.0
E_p (MV/m)	27.5	27.5
B_p (mT)	54.7	58.3
E_o for interior cells (MV/m)	11.8	15.1
E_a for interior cells (MV/m)	9.3	11.9
Average cavity transit time factor	0.689	0.690
Average E_0 per cavity (MV/m)	13.1	16.1
Max energy gain per cavity (MeV)	5.33	9.06
Min energy gain per cavity (MeV)	4.45	6.04
Max power per cavity (kW)	192	326
Min power per cavity (kW)	160	217

Figure 2.4 shows the average cavity transit time factors for each cavity as a function of beam energy. The transit time factors vary between 0.58 and 0.78. Also shown in the figure is the cosine of the cell phase angles averaged over each cavity.

Figure 2.5 shows the average beam power requirement for each cavity for the design 2 MW beam. No other power losses are accounted for except beam power. The linac will have one input power coupler per cavity; consequently, Fig. 2.5 also shows the input coupler power per cavity. The coupler power in the high-beta section is 326 kW, well below the 380 kW achieved in CW operation with the KEK-B couplers.

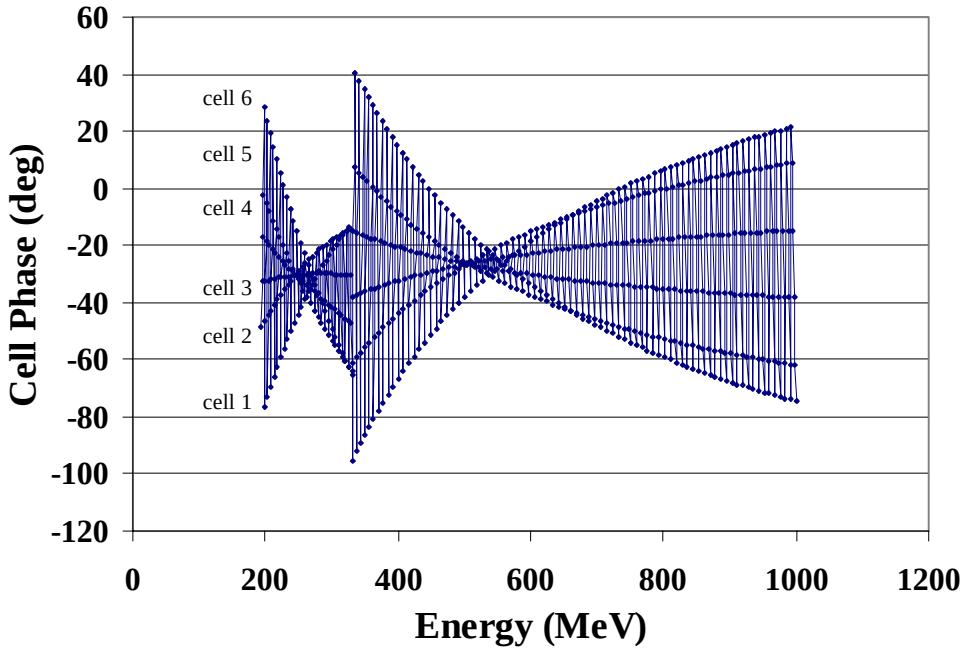

Figure 2.3: Beam phases for each cell of each cavity as a function of beam energy. Cell numbers are indicated in the figure.

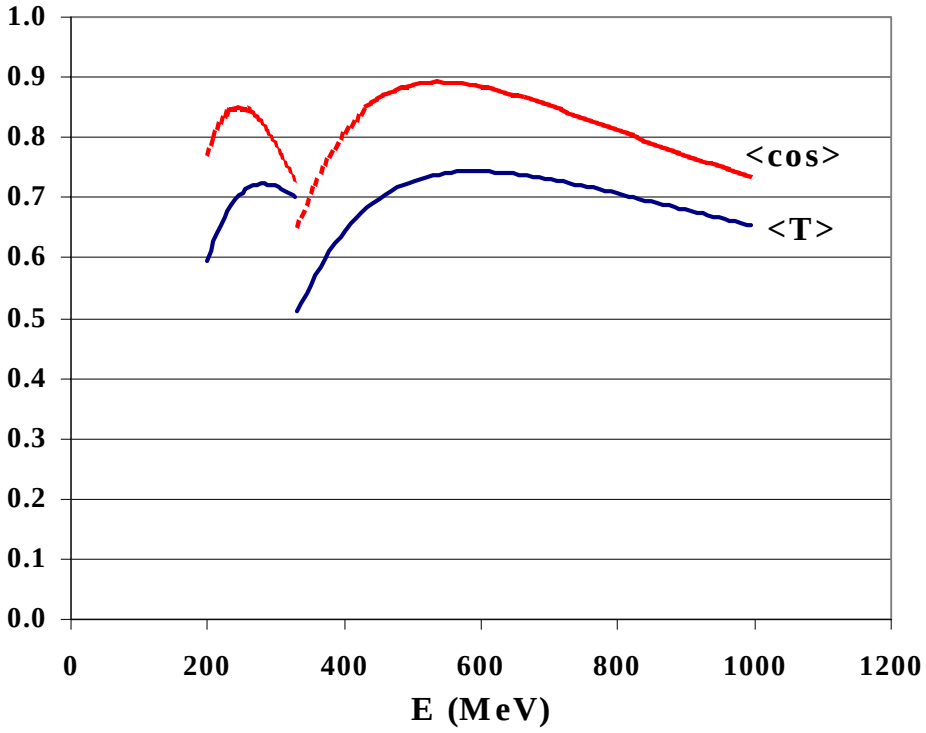

Figure 2.4: Transit time factor (bottom) and cosine of the cell phase angle (top), averaged over each cavity.

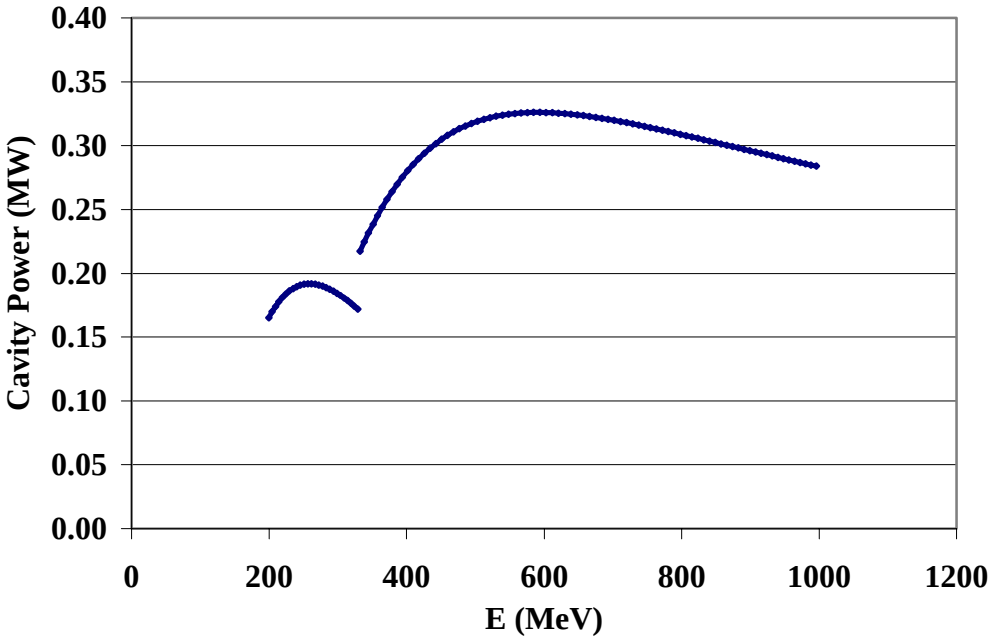

Figure 2.5: Cavity or coupler beam power as a function of energy.

2.3 BEAM DYNAMICS

2.3.1 Interfaces and Configuration

Beam matching and particle tracking studies for the SC SNS linac were carried out using the configuration described in Table 2.5. The normal conducting section is taken from the present SNS design up to 194.3 MeV, and the parameters shown in the table pertain to the CCL at that energy. The quadrupole lengths are 8 cm in the CCL and 40 cm in the SC sections. The spaces between the doublet pairs in the SC linac are taken to be 30 cm. The doublet lattice periodicity is 5.839 m in the $\beta_g = 0.61$ SC section and 7.700 m in the $\beta_g = 0.76$ SC section.

Table 2.5: Linac configuration used in matching and tracking calculations

Linac type	CCL	SC $\beta_g = 0.61$	SC $\beta_g = 0.76$
Energy range (MeV)	79.2 to 194.3	194.3 to 331.1	331.1 to 1001.5
Lattice type	FODO	Doublet	Doublet
Lattice period (m)	2.451 at 194.3 MeV	5.839	7.700
Quadrupole gradient B′ (T/m)	17.40	5.15	5.15
Energy gain / cavity (MeV)	2.4	4.71 to 5.55	6.45 to 8.93
Rf phase	–30.0°	–21.0° to –33.0°	–26.5°

2.3.2 Matching

Beam matching is carried out using the TRACE3D code [3] assuming a full beam current of 56 mA, a cavity frequency of 805 MHz, and 4.4×10^8 H^- ions per micro-pulse. The TRACE3D

code transports a beam ellipse in six-dimensional (6-D) phase space linearly through a user-defined lattice. Space charge forces are treated with a linear approximation.

The first matching step is the calculation of periodic solutions, within the FODO or doublet lattice periods, for a number of periods on either side of the CCL to cold linac β_g = 0.61 transition. CCL parameters are deduced from the baseline warm linac, and the doublet quadrupole field gradient B' and the rf phase are adjusted in the β_g =0.61 section to give continuous phase advances per unit length for both transverse and longitudinal motion across the transition. The results for current-independent matching, listed in Table 2.5, are B' = 5.51 T/m and $\phi = -21.0°$.

A similar procedure is carried out for the transition from the β_g = 0.61 section to the β_g = 0.76 section. In this case, the doublet quadrupole field gradient of B' = 5.15 T/m in the β_g = 0.61 section and the rf phase of $\phi = -26.5°$ in the β_g = 0.76 section are taken from the results above, and the quadrupole field gradient in the β_g =0.76 section and the rf phase in the β_g = 0.61 section are varied. The results in this case are B' = 5.15 T/m in the β_g =0.76 section and $\phi = -33.0°$ in the β_g = 0.61 section. To accommodate the different phases required at the low- and high-energy ends of the β_g =0.61 section, the rf phase is ramped linearly from $\phi = -21.0°$ to $\phi = -33.0°$ in 1.5° steps through each of the nine cryostats in the β_g = 0.61 section.

Next, the Courant-Snyder parameters of the 6-D phase space beam envelope for these solutions are matched across each transition. Six lattice parameters are varied in each transition region to facilitate the matching. In the 6-D phase space, it is natural to select four quadrupole field gradients and two rf cavity phases to vary. Matching from the CCL into the β_g = 0.61 section of the SC linac is performed using the final two CCL quadrupoles and the first doublet pair for transverse matching. The first and the fourth cavities in the SC linac are used for longitudinal matching. The resulting parameters, listed in Table 2.6 provide a matching of the periodic solution in the CCL to that in the β_g = 0.61 section.

Both TRACE3D and multi-particle simulations showed that matching between the β_g = 0.61 and β_g =0.76 sections is already good enough so that further matching is unnecessary, even with a slight change in the beta functions.

Table 2.6: Parameters for matching between the CCL and the β_g =0.61 section.

Parameter varied	Value
CCL quadrupole	-14.85 T/m
CCL quadrupole	11.59 T/m
1st Quad of SC doublet	-5.008 T/m
2nd Quad of SC doublet	4.804 T/m
1st SC cavity rf phase	-30.36°
4th SC cavity rf phase	-21.4°

Figure 2.6 is a TRACE3D plot summarizing the beam transport for a matched solution from 79.2-MeV through the third cryostat of the high beta section (416 MeV), traversing both matching transitions. The upper figures show the initial (left) and final (right) beam ellipses in transverse (upper) and longitudinal (lower) phase space. The plot at the bottom shows the horizontal (top), vertical (bottom), and longitudinal (heavy curve at top) amplitudes along the

linac. The transition from FODO structure to doublet structure is clearly seen. The transition between the two beta sections is less drastic. In the SC linac, the TRACE3D envelope size never exceeds 1 cm in the transverse direction or 5 degrees in the longitudinal direction, indicating that the matched beam is well behaved.

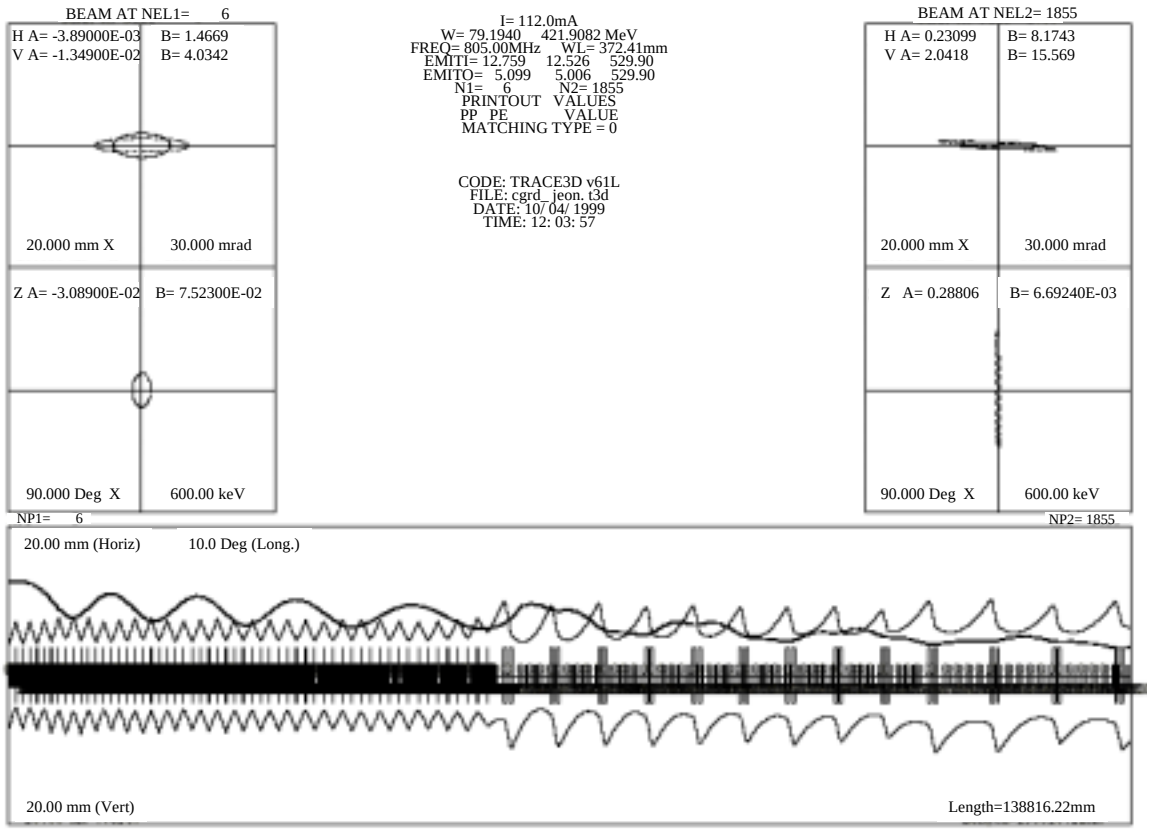

Figure 2.6: TRACE3D calculation of beam transport from 79.2-MeV through the third cryostat of the high beta section (416 MeV), through the matching transitions.

2.3.3 Multiparticle Simulations Without Construction Tolerances

To verify the overall architecture and beam matching, a more detailed beam dynamics calculation is carried out using multiparticle simulations. First, simulations of the ideal machine are conducted without consideration of construction imperfections and tolerances. This is done using the LINAC code, a version of the PARMILA code, [4] and the lattice obtained from the previous TRACE3D matching as input. The PARMILA code is used for the simulations of the front end and DTL, while the LINAC code is used for the CCDTL, CCL, and the SC linac. Both codes carry out particle tracking, treating the space charge interaction nonlinearly via a two-dimensional (2-D) PIC model in cylindrical geometry, with rotational symmetry about the beam axis. In the calculations, a beam of 10,000 macroparticles is tracked from an initial distribution at the beginning of the RFQ to the end of the SC linac at 1.0 GeV. The initial distribution is taken from the tracking calculations, including construction imperfections and tolerances [5] starting with an initial four-dimensional (4-D) waterbag distribution at the entrance to the RFQ. Figure 2.7 shows that, without construction imperfections and tolerances, the rms emittances in the horizontal, vertical, and longitudinal directions remain below 0.4π mm mrad throughout the linac. Figure 2.8 shows, for the same calculation, the values of the maximum and rms particle

transverse displacements and indicates that the maximum transverse displacements are less than 1.5 cm throughout the linac. Both figures show that the beam matching between the linac interfaces is satisfactory.

The results indicate that the behavior of the beam is quite acceptable, clearing the 5.0-cm radius in the SC section with a 3.5-cm margin. Figures 2.9 and 2.10 show the beam phase space and transverse distributions at the beginning and end of the SC linac, respectively.

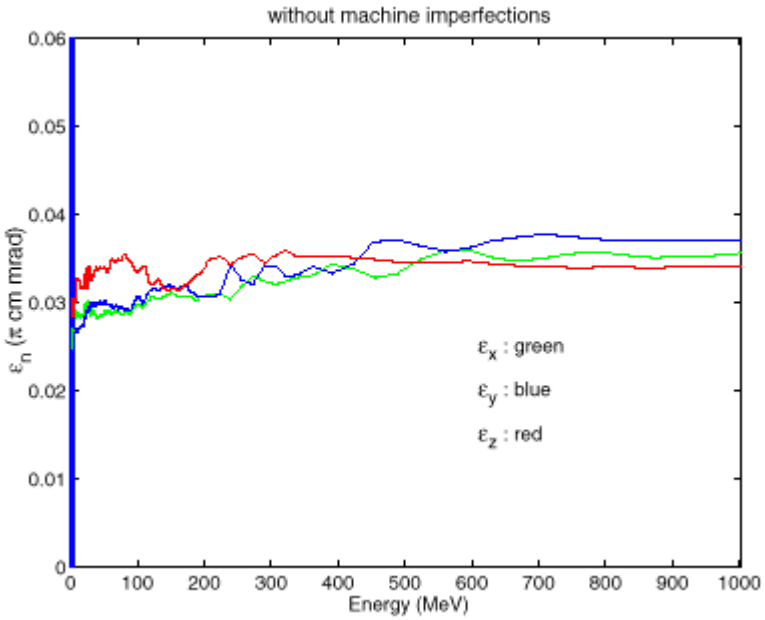

Figure 2.7: LINAC calculation of the rms beam emittances through the matched SC linac versus energy. The longitudinal emittance in the plot is expressed in units of π-MeV-degrees for 805 MHz and must be multiplied by 10.

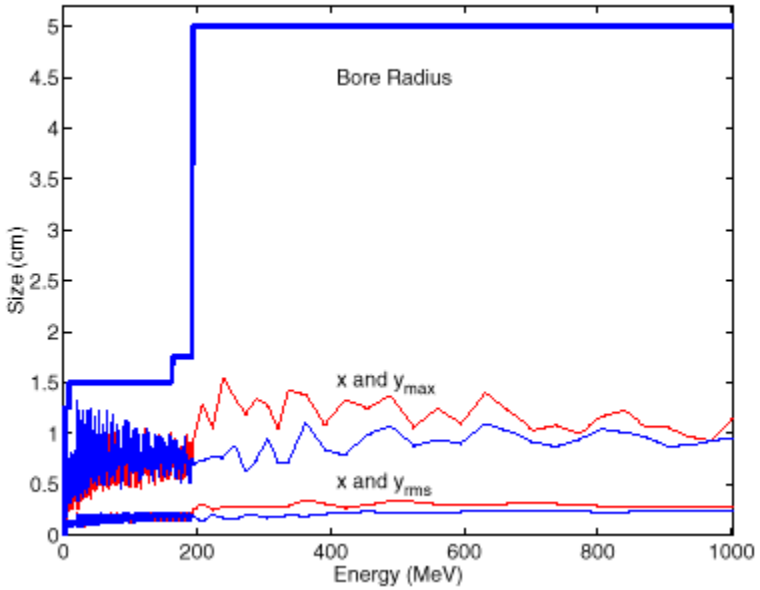

Figure 2.8: LINAC calculation of both the maximum and rms transverse particle displacements through the matched SC linac. Machine imperfections and tolerances are not included.

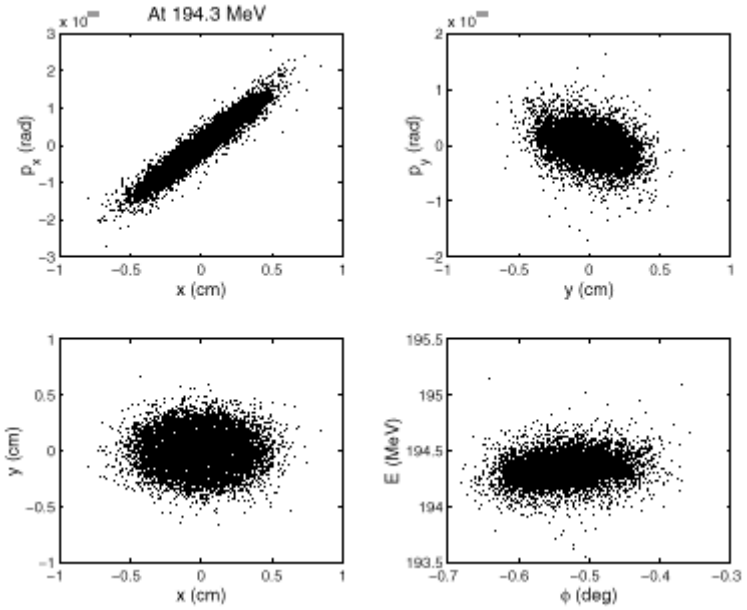

Figure 2.9: Beam distributions at the beginning of the SC linac at the design energy of 194.3 MeV.

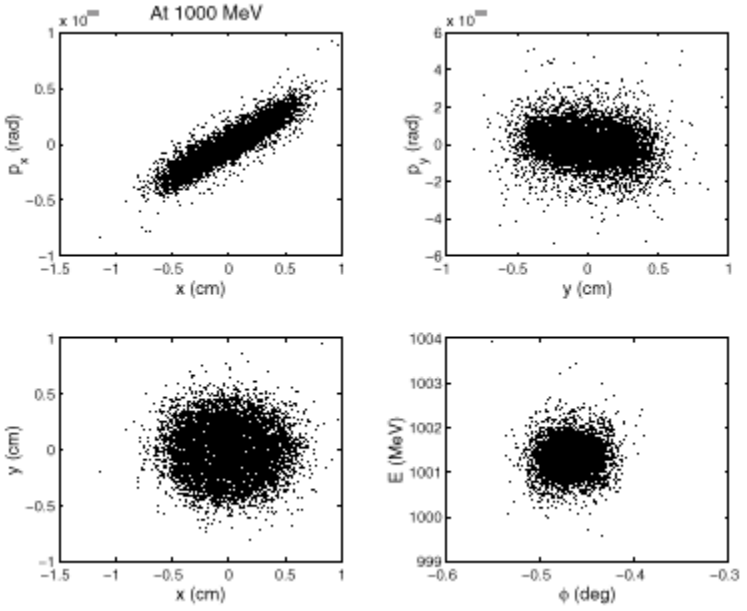

Figure 2.10: Beam distributions at the end of the SC linac at 1.0 GeV.

2.3.4 Multiparticle Simulations With Construction Imperfections andTolerances

A preliminary study is carried out on the impact of construction imperfections and tolerances in the warm and SC linacs. Table 2.7 lists the assumed extremes of uniformly distributed errors for the baseline warm linac system, based on work by the LANL team. Table 2.8 lists the values of error limits on the two sections of the SC linac used in this study. These values are comparable to those assumed for the warm linac. Microphonics effects are not included in the SC linac errors because it has been demonstrated that they can be compensated. Figure 2.11 shows the plots of the energy centroid jitter and the phase centroid jitter due to inclusion of the aforementioned imperfections. These results are obtained from the 10,000 imperfection runs from 20 MeV to 1.0 GeV. These histograms show that the energy spread from the SC linac is less than $\pm$ 1.5 MeV, which is below the design criteria of $\pm$ 2.2 MeV. This energy jitter level is easily correctable with the existing HEBT rf cavities and is acceptable for ring injection.

Table 2.7: Values of error limits used in tracking studies.

DTL, MEBT:	
Quadrupole transverse displacement	0.0508 mm
Quadrupole roll	4.36 mrad
Quadrupole tilt	9.95 mrad
Quadrupole gradient error	0.5% (DTL), 1.732% (MEBT)
Rf field phase error in tank	8.73 mrad
Rf field amplitude error in tank	0.5%
Rf field tilt error in tank	0.1%
CCDTL, CCL:	
Quadrupole transverse displacement	0.127 mm
Quadrupole roll	5.0 mrad
Quadrupole tilt	5.0 mrad
Quadrupole gradient error	0.25 %
Error in distance between end gaps of adjacent segments	0.254 mm
Error in distance between adjacent gaps of a segment	0.0508 mm
Segment transverse displacement	0.25 mm at ends[a]
Module field amplitude error (dynamic)	0.5 %
Module phase error (dynamic)	0.5°
Module field amplitude error (static)	1.0 %
Module phase error (static)	17.45 mrad
Segment field amplitude error (static)	1.0 %
Segment phase error (static)	0.0
Field amplitude tilt in module	1.0 % at ends[b]

[a] Independent misalignments of the two ends, resulting in displacements and tilts.
[b] Low at one and high at the other, or vice versa.

Table 2.8: Values of error limits used in tracking studies in the SC linac.

Doublet transverse displacement	0.1 mm
Doublet rotation	2.5 mrad
Doublet tilt	2.5 mrad
Doublet gradient error	0.25%
Cavity displacement within cryostat	1.0 mm
Klystron amplitude error	0.5%
Klystron phase error	0.5°

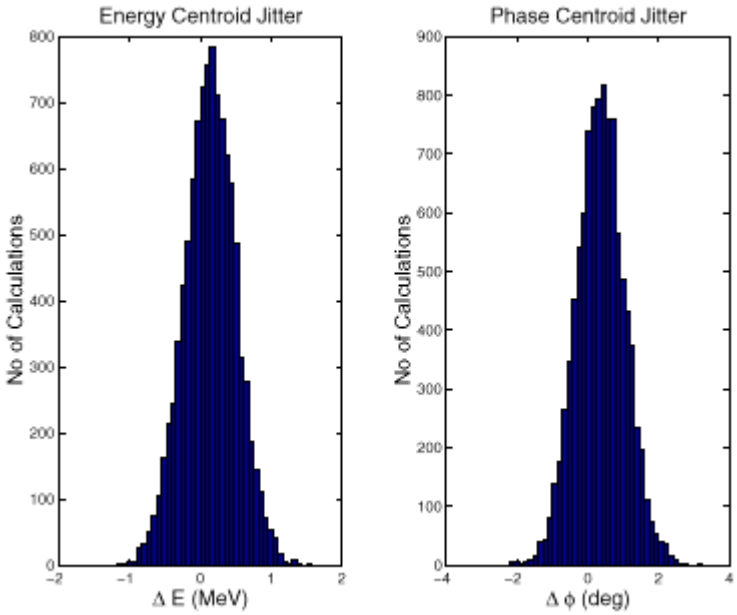

Figure 2.11: Histogram of the beam energy centroid jitter and the phase centroid jitter at 1.0 GeV, caused by klystron amplitude and phase jitter.

Figure 2.12 shows the normalized rms emittances for ten Monte-Carlo calculations. Each calculation uses different random number seeds, thus simulating ten independent linacs with machine construction imperfections. The number of macroparticles used in the simulations is 10,000. The blue curves are the vertical emittance, the green curves are the horizontal emittance, and the red curves are the longitudinal emittance. The maximum transverse extent of the 10,000 macroparticles in the beam and the rms beam sizes are shown in Figure 2.13. The blue curves in Figure 2.13 are for the horizontal beam size and the red curves are for the vertical beam sizes. The horizontal beam size is consistently larger than the vertical beam size because the plotted points are always taken at focusing quadrupole locations. The maximum transverse extent of the beam radius is well below 2 cm.

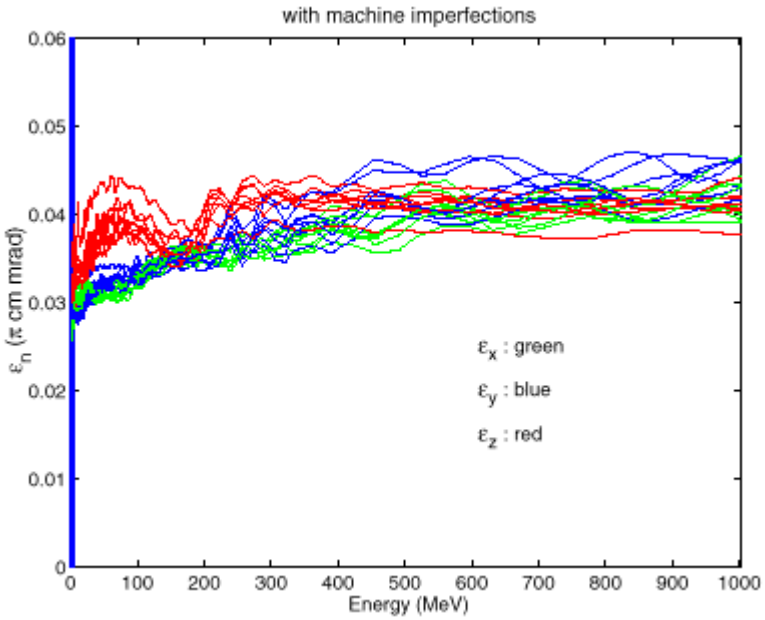

Figure 2.12: Normalized rms emittances versus energy for ten independent linac calculations with about 10,000 macroparticles. Each calculation was made with different random number seeds for simulating errors.

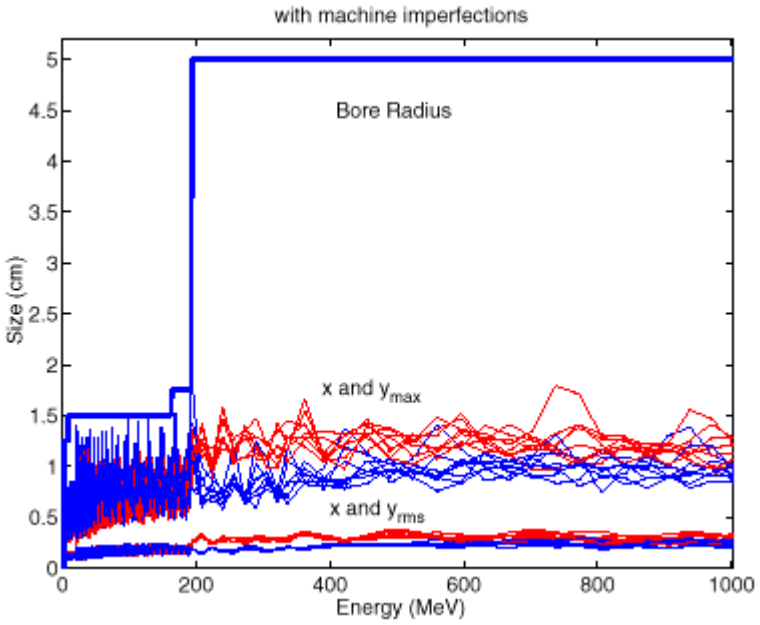

Figure 2.13: The maximum transverse extent of the macroparticles in the beam and the rms beam sizes versus energy for ten independent calculations with about 10,000 macroparticles. Each calculation was made with different random number seeds.

2.4 CAVITY FAILURE FAULT TOLERANCE

The SC linac has an inherent reserve capability. This reserve can be used to maintain operation with one or more non-functioning cavities. Fault tolerance is investigated by performing multi-particle simulations with non-functional cavities.

Initial beam dynamics calculations do not include linac machine imperfections and tolerances. Initially, a failure of two cavities in the same cryomodule of the high-beta section is considered. In this case, the linac can still operate. This conclusion is based on results shown in Figure 2.14, where the resultant transverse and longitudinal normalized rms emittances through the acceleration cycle are still acceptable even without rematching. Figure 2.15 shows the transverse and longitudinal emittances, also without rematching, when two cavities in the same cryomodule of the medium-beta section fail. In this case, the emittance growth is more pronounced because of the stronger space charge effects. However, we can reduce either the transverse rms emittances or the longitudinal emittance depending on which is more critical. This reduction can be achieved by choosing an appropriate set of cavities and quadrupole doublet pairs for rematching. Figure 2.16 shows two different rematching schemes for the medium-beta case. Transverse emittance can be improved at the expense of longitudinal emittance if needed, or vice-versa. However, the linear sum of emittances cannot be reduced simultaneously.

Figure 2.17 shows the beam phase space distributions immediately after passing through the two failed cavities of the medium-beta section. Because of the cavity failure, a significant deformation in the longitudinal phase space takes place, which then induces strong envelope oscillations and halo formation. Through the coupling, a significant enhancement of halo formation in the transverse phase spaces is also induced. The resultant halo at 1 GeV is shown in Fig. 2.18. The total energy spread is ±1.2 MeV, whereas the total energy spread of the core is only ±0.5 MeV. Without cavity failure the energy spread is ±1 MeV. In addition to this energy spread in the bunch, the total centroid energy jitter of ±1.5 MeV remains essentially unchanged. These conditions may be acceptable considering the energy acceptance of the ring, and momentum collimators in the HEBT line intercept halo particles beyond ±3 MeV. Figure 2.19 shows the normalized emittances with machine imperfections and tolerances and with rematching when two medium-beta cavities in the same cryomodule are nonfunctional. The transverse emittances and the energy spread are acceptable for normal operation. Since two cavity failures in a medium-beta section would have a more severe effect than a two-cavity failure in a high-beta section, the linac is operable with any two cavities off.

This simulation study also indicates that failure of a complete cryomodule is not tolerable in either the medium-beta or high-beta sections. In this case the total energy spread in the beam is ±2.5 MeV, and the longitudinal phase space is severely distorted, as shown in Fig. 2.20. Considering the energy centroid total jitter of ±1.5 MeV in addition to this energy spread in the beam, the total energy spread is not tolerable for the ring energy acceptance. Figure 2.21 shows the normalized rms emittance growth caused by failure of one cryomodule in the high-beta section. The growth of the transverse and the longitudinal emittances is appreciable.

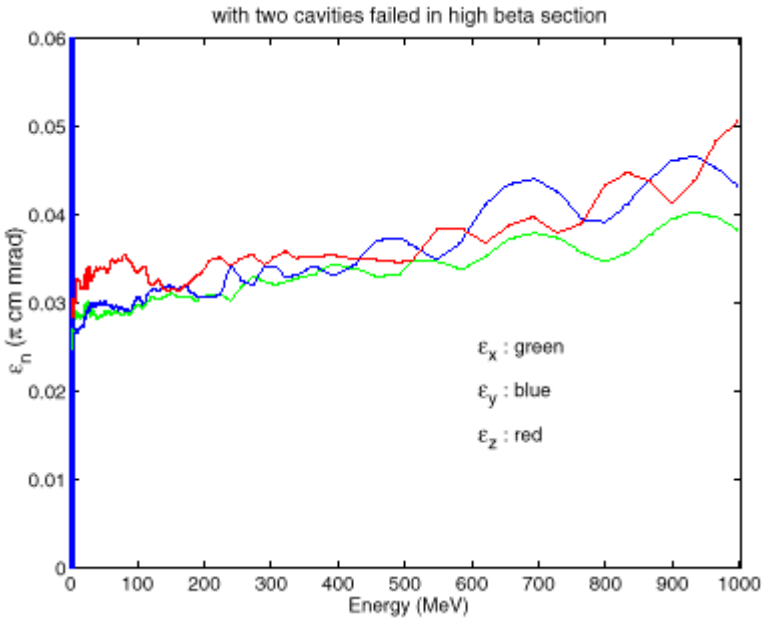

Figure 2.14: Plots of the normalized transverse and longitudinal emittances versus energy when two cavities in the high-beta section fail at about 550 MeV, without rematching.

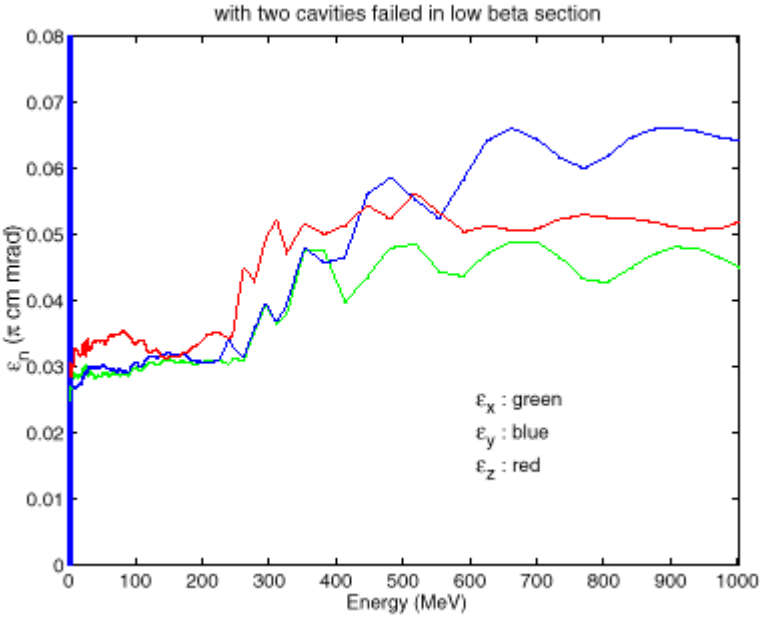

Figure 2.15: Plots of the normalized transverse and longitudinal emittances versus energy when two cavities in the medium-beta section fail at about 262 MeV, without rematching.

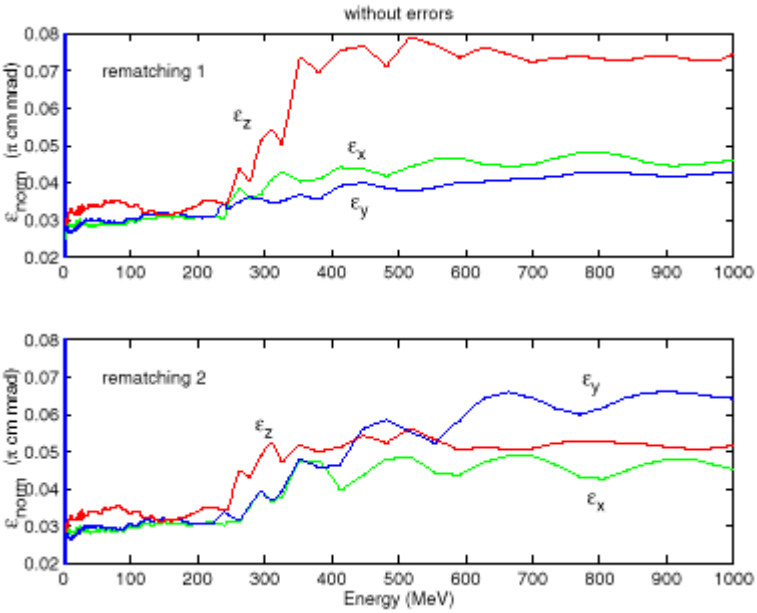

Figure 2.16: Plots of the normalized rms emittances for two different rematching schemes by adjusting two cavities and four quadrupoles around the two failed cavities of the medium-beta section.

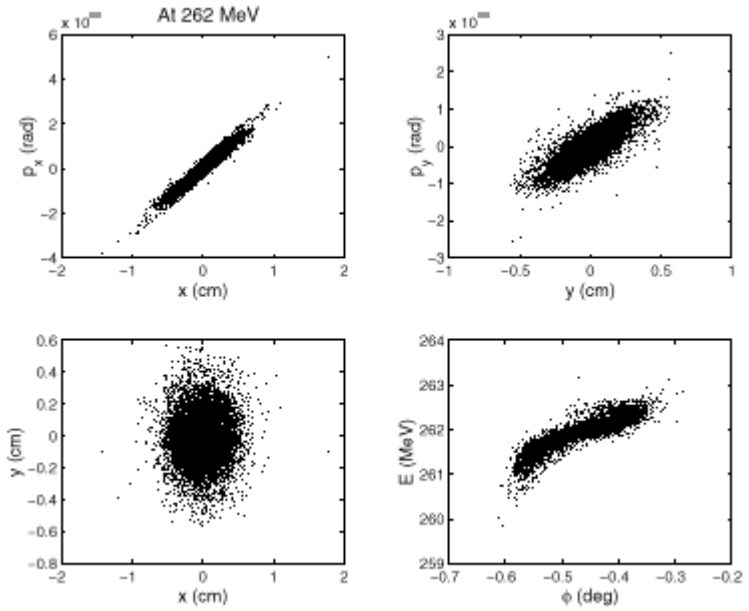

Figure 2.17: Plots of the beam distribution immediately after passing through the two failed cavities of the medium-beta section. A pronounced deformation in the longitudinal phase space is visible.

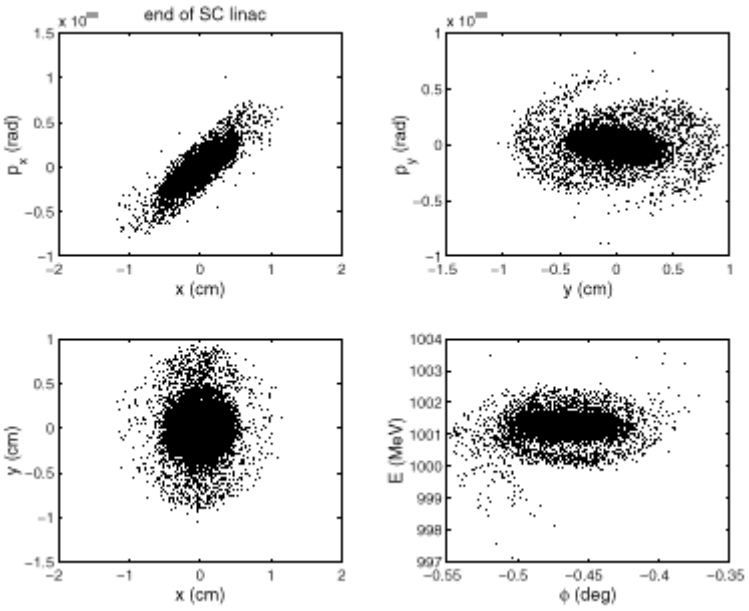

Figure 2.18: Plots of the distribution of the same beam as in Figure 2.17 at the end of the linac. Because of the coupling, halo formation takes place in the transverse phase space as well as in the longitudinal phase space, leading to rms emittance growth.

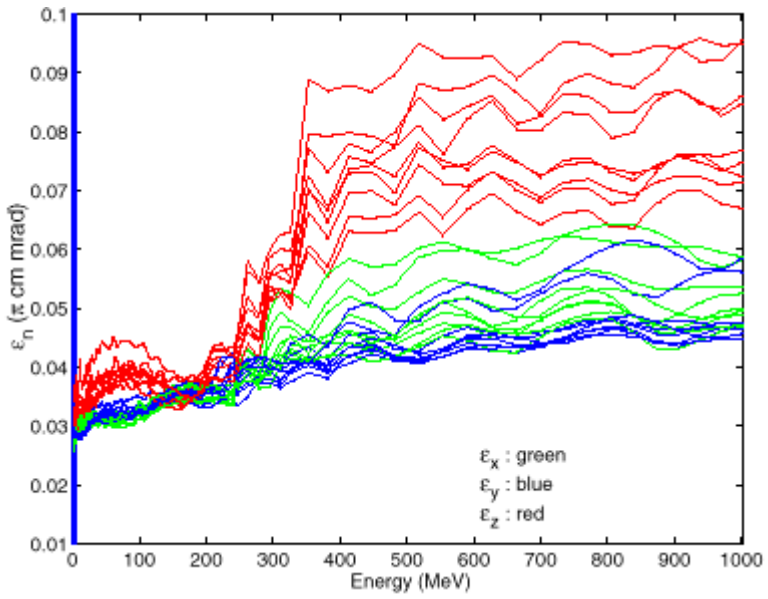

Figure 2.19: Emittance plots including machine tolerances and imperfections with rematching for the case that two cavities in the same medium-beta cryomodule are nonfunctional. The transverse emittances and the energy spread are acceptable.

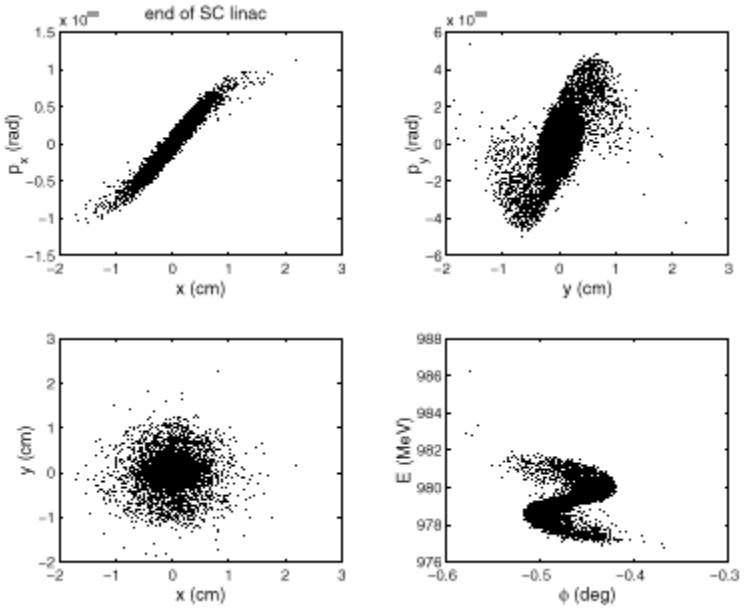

Figure 2.20: Plots of the beam phase space distributions before compensating the final beam energy after one cryomodule fails in the high-beta section. The energy spread of the beam is ±2.5 MeV, and a significant halo formation is observed.

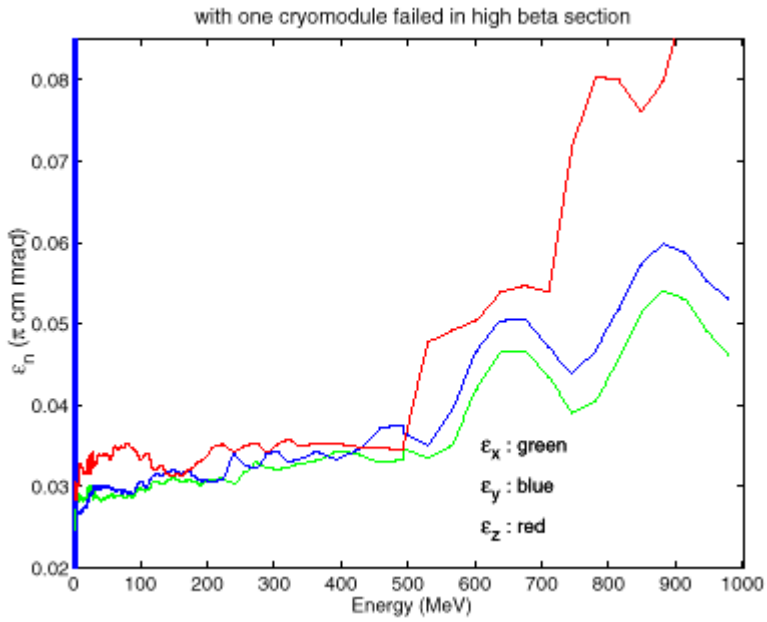

Figure 2.21: Plots of the normalized rms emittances after one cryomodule fails in the high-beta section.

The fault tolerance study shown here is preliminary in nature. As the SC linac design matures, detailed fault tolerance analysis will be carried out and remedial procedures in conjunction with appropriate application software will be developed. Nevertheless, this initial study is extremely encouraging.

2.5 SUMMARY OF INTEGRATED PHYSICS DESIGN

A satisfactory SC linac architecture has been developed to accelerate the H^- beam from 194.3 to 1001.5 MeV. This linac is 207 m long with 27 $\beta_g = 0.61$ cavities in 9 cryomodules and 80 $\beta_g = 0.76$ cavities in 20 cryomodules. The linac design is based on a constant gradient per cavity with an average gradient of 9.3 MV/m for the medium beta section and 11.9 MV/m for the high beta section. The parameters of this linac are listed in Table 2.4.

A satisfactory 6-D matching was obtained between the normal conducting linac and the $\beta_g = 0.61$ section of the SC linac and between the $\beta_g = 0.61$ and the $\beta_g = 0.76$ sections of the SC linac. Multiparticle simulations show that emittance growth is minimal across the interfaces. Without consideration of construction imperfections and tolerances, the normalized rms emittances grow from 0.32 π mm-mrad at 194 MeV to 0.35 π mm-mrad at 1.0 GeV. The maximum extent of the beam profile stays below 1.5 cm. When construction tolerances are included in the simulations, 10 out of 10 Monte Carlo machines show rms transverse emittance less than 0.46 π mm-mrad. This magnitude is similar to the rms emittance of the baseline warm linac in the presence of construction tolerances and imperfections. Although the 0.5 π mm-mrad is a soft requirement, this area needs further investigation to assure the output emittance is acceptable.

The energy centroid jitter and the phase centroid jitter are both acceptable assuming 0.5% klystron amplitude errors and 0.5° phase errors in the SC linac with one rf system per cavity. More detailed systematic studies will be carried out, including the effects of cavity microphonics. Preliminary fault tolerance calculations indicate that the linac may be operable with two non-functional cavities in a single beta section.

3. ACCELERATION CAVITIES

3.1 ACCELERATION CAVITIES

3.1.1 Introduction and Specifications

The principal feature of SC cavities is that they operate at high accelerating gradients with low wall losses, a factor of 10^5 less than copper. Essentially all available RF power can therefore be used to accelerate the beam. As a result, more than half the RF power required for the warm copper baseline design can be eliminated, along with the associated equipment, such as high-voltage power supplies, high-power klystrons, and controls. There are corresponding reductions in cooling water needs. The total power reduction is about 12 MW. The higher operating gradient permits a significant reduction in the overall length of the linac, about a 137-m reduction from the baseline. With the large Q accompanying the higher gradient, beam chopping will cause reduced cavity field perturbations and improve the beam dynamics.

The potential for higher gradients available with SC cavities allows flexibility to increase the bucket size. The large bucket size can help prevent longitudinal beam loss and thereby improve availability. The larger aperture permitted by SC cavity designs reduces alignment, steering, and matching tolerances, as well as the risk of radioactivation from proton beam loss, which is an important consideration. The short 1-m cavities have a large velocity acceptance to provide additional advantages in flexible operation and increased availability. Finally, the excellent vacuum at the 2 K operating temperature reduces beam loss from H^- stripping to a negligible level, and this excellent vacuum will exist from the first cool down.

The SC linac design adopted for the SNS makes maximum use of developments in SC accelerator technology, as described in Section 3.2. Nevertheless the design choices leave ample safety margin when compared with recent demonstrated performance. The strong capabilities of several industries to fabricate SC cavities and cryomodules allow the SNS to meet an aggressive production schedule. The extensive testing capabilities of several laboratories worldwide will properly complement the industrial fabrication capabilities.

The linac design uses two beta sections, the medium-beta section with geometrical $\beta_g = 0.61$ from 194 to 331 MeV, and the high-beta section with $\beta_g = 0.76$ from 331 to 1001 MeV. The choice of just two beta sections has the additional advantage that it limits the number of cavity types, minimizes the prototyping and production effort, and allows for spare cavities.

Extensive beam dynamics simulations on these and similar designs show that the selection of two beta sections provides adequate beam dynamics properties. Experience with low-beta cavities in heavy-ion accelerators, such as ATLAS, confirms the appropriateness of using a single beta section for a large range of velocities. There is the possibility of constructing a third low-β_g section of cavities at $\beta_g = 0.5$ to cover the energy range from 87 MeV to 194 MeV and thus totally eliminate the CCL. Prototyping of these cavities would be necessary.

With the constant beta of each section, the transit time factor varies with the beam velocity. The cavity phase is adjusted to provide longitudinal beam match. As a result, the energy gain is adjusted, as required, to provide a constant peak surface field of 27.5 MV/m for both medium- and high-beta sections. For the medium-beta section, the corresponding energy gain ranges from 4.45 to 5.33 MeV. For the high-beta section, the energy gain per cavity ranges from 6.04 to 9.06 MeV.

Figure 3.1 shows the rf profile designs for the six-cell medium-beta and high-beta cavities. One port is available for the input coupler and one port at each end of the cavity for two HOM couplers. An additional port will be available for the field monitor probe. The cavity is stiffened to reduce the Lorentz-force-detuning coefficient. Based on mechanical modeling of similar low-beta cavities, we expect a Lorentz force detuning coefficient of about 2 Hz per $(MV/m)^2$ for the medium-beta and less than 2 Hz per $(MV/m)^2$ for the high-beta cavity. A titanium helium vessel will be welded to the cavity. Conflat flanges can be brazed using techniques developed at LANL for APT. Alternatively we can use the niobium-titanium flanges developed by DESY for TTF.

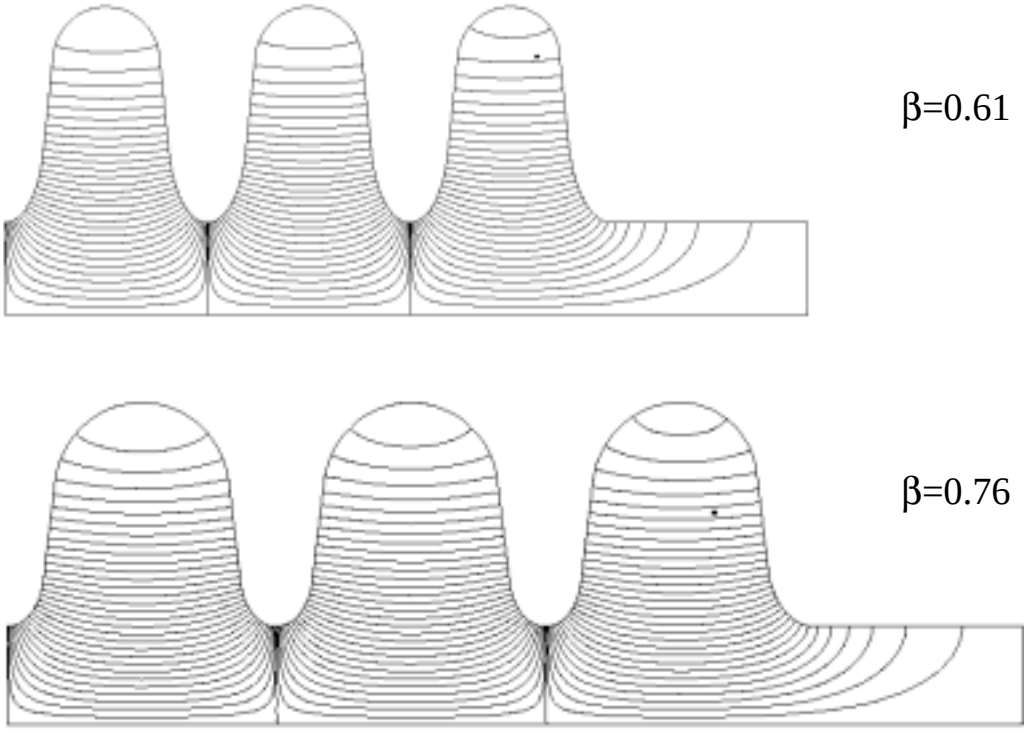

Figure 3.1: RF profile designs for the six-cell medium-beta and high-beta cavities.

Figure 3.2 shows a 3-D cut view of a five-cell niobium $\beta_g = 0.64$ cavity fabricated by industry for the APT linac. The cavity has ports for input, HOM, and field monitor couplers. The figure also shows the helium vessel end plates integrated with the cavity ends.

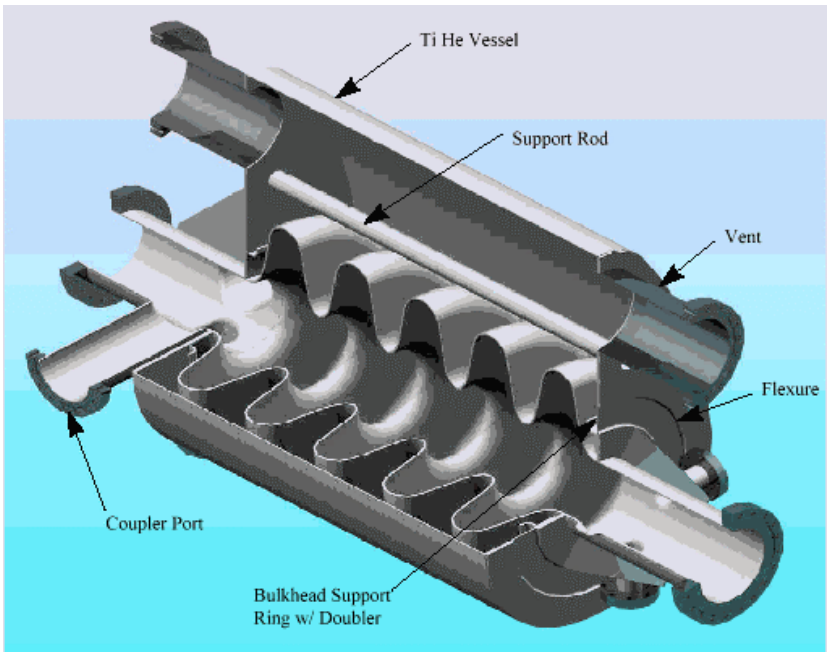

Figure 3.2: 3-D cut view of a 700-MHz, five-cell niobium beta = 0.64 cavity fabricated by industry for the APT linac.

Table 3.1 lists the cavity parameters for the two beta sections. The peak surface field is maintained constant throughout a beta section by adjusting the energy gain per cavity or adjusting the input power to compensate for variations in transit time factor and cavity phase. The Q_{ext} is chosen so that the cavity is matched to the beam. The typical value for Q_{ext} for this high-power linac (5×10^5) is much lower than for existing applications such as at CEBAF (6×10^6) or TTF (3×10^6). As a result, the effects of Lorentz force and microphonic detunings are expected to be much less for the SNS than TTF. Details of these effects on SNS are discussed in Section 3.2.

Table 3.1 Cavity parameters.

Section	Medium beta	High beta
Geometrical beta	0.61	0.76
Rf frequency (MHz)	805	805
Number of cells per cavity	6	6
Active cavity length (m)	0.682	0.849
Number of cavities	27	80
Aperture radius (cm)	5.0	5.0
Cell-to-cell coupling factor (%)	~ 2	~ 2
Lorentz force detuning coef. $Hz/(MV/m)^2$	~ 2	< 2
Ep (MV/m)	27.5	27.5
Hp (mT/MV/m)	54.8	58.4
Ep/Ea	3.00	2.35
Hp/Ea (mT/MV/m)	5.96	4.98
Gradient Ea (MV/m)	9.17	11.7
Beam power per cavity (kW)	160–192	217–326
Energy gain per cavity (MeV)	4.45–5.33	6.04–9.06
Qo	5×10^9	5×10^9
R/Qo (Ohm/m)	~ 350	~ 500
Typical Q_{ext}	$\sim 5 \times 10^5$	$\sim 5 \times 10^5$
Typical bandwidth (Hz)	~ 1400	~ 1400
Rf duty factor (%)	8	8
Average wall loss per cavity (W)	3.7	5.1
Total dynamic heat load for section (W)	100	370
Operating temperature (K)	2.1	2.1

The cavities are made from 3.5-to-4-mm-thick niobium sheets, nominal RRR = 300, by the standard procedures of deep drawing and electron beam welding. Each sheet is scanned for quench-causing inclusions using the eddy-current method developed at DESY. After fabrication, the cavities are cleaned in the standard manner by buffered chemical polishing (BCP) of about 100 μm and high-pressure water rinsing, followed by a two-hour bake at 800°C. If recent good results on single cell cavities with electropolishing [KEK] or sulfuric acid buffering [CEA-Saclay] prove to be beneficial with multicell cavities, we plan to adopt the improved chemical processing procedures.

Based on TTF experience, we expect to reach the desired field without 1400°C heat treatment. Each cavity is tested in a vertical cryostat. If the prototyping stage shows that 800°C heat treatment is not sufficient to reach the required gradients, the cavities will be postpurified with titanium at 1400°C to reach the desired field levels. BCP is carried out after postpurification, as determined by TTF experience. The possibility of a 1400°C heat treatment provides for a substantial safety margin and performance contingency.

After qualifying the performance of the cavity, the rest of the helium vessel is welded to prepare the cavity for insertion into the cryomodule. Techniques for integrating the helium vessel have been developed at DESY for the TTF and at LANL for the APT.

3.2 DESIGN BASIS

As a result of experience at LEP, CEBAF, HERA, TTF, Cornell, CEA-Saclay, and KEK, the science and technology of SC cavities and couplers are highly developed. Structures can be designed to be free of multipacting. Material selection, surface treatment, and preparation techniques can be performed to ensure that the required goals of the SNS cavities are achieved. High-power couplers can be designed, incorporating recent developments at KEK, CEA-Saclay, and LANL, so that multipacting is not a limiting factor. Cavities and couplers built according to modern state-of-the-art technology meet our requirements. Several mature cryomodule designs are available, such as those of CEBAF and TTF, and are easily adapted to the SNS.

A broad experience base exists for beta = 1 cavities, as discussed in Section 3.3. Briefly, experience from TTF shows that SC cavities provide accelerating gradients of 25 MV/m and Q values above 5×10^9, as measured during tests with beam on eight cavities in a single cryomodule. The corresponding surface fields are $E_p = 50$ MV/m and $B_p = 107$ mT, substantially above the SNS requirements. The design chosen for the SNS SC linac is therefore based on parameter choices that have been demonstrated and surpassed in operating accelerators with beam.

LANL, CEA-Saclay, and JAERI have developed cavity designs for beta = 0.50, 0.64, and 0.82. Single-cell cavities have been built and tested to be free of multipacting and to reach surface electric fields of E_p = 40 to 45 MV/m. Several multicell cavities have been designed and built. Laboratories at TJNAF, CERN, INFN-Genova, JAERI, CEA-Saclay, and the industrial company ACCEL, GmbH have already started testing multicell units with beta between 0.5 and 0.75. An ESS beta = 0.5 five-cell cavity is undergoing tests at CERN. All of these cavities have reached respectable fields and have been shown to be free of multipacting. At LANL, tests of multicell cavities for APT are nearing their final stage. Cryomodules developed recently for several of these accelerating structures incorporate the many valuable lessons from LEP and TTF experience.

In connection with the APT project, proton irradiation studies conducted on both warm and cold cavities show that there is no danger of performance degradation from the long-term radiation dose expected from nominal proton beam loss.

Cavities can be detuned either by mechanically-induced vibration (microphonics) or by electromagnetically induced Lorentz force. Special attention must be given to the tuner, the mechanical rigidity of the cavity, its helium vessel, and the actual tuning mechanism. The Lorentz force of the pulsed electromagnetic field in the cavity causes time-dependent mechanical deformations to the cavity and results in changes in resonant frequency. For the beta = 1, TTF structures at 1.3 GHz, the average Lorentz force detuning coefficient is 1 Hz/(MV/m)^2. Because of the lower SNS frequency (805 MHz) and lower-beta geometry, the average coefficient for the stiffened SNS structure is expected to be 2 Hz/(MV/m)^2. Since the SNS design gradient is more than a factor of two lower than for TTF, the detuning is expected to be reduced by a factor of four. Also, because the SNS operating bandwidth is a factor of four wider than for TTF, the impact of Lorentz force detuning and microphonics is expected to be reduced by a factor of 16. The addendum to this Chapter discusses these scaling laws.

SC cavity applications over the last decade have generated a strong industrial base of cavity and cryomodule suppliers, as well as suppliers of high-purity niobium. The most experienced company has delivered more than 300 m of cavities. Comprehensive preparation, assembly, and test facilities exist at these companies as well as at various laboratories. The existence of industrial capabilities and national laboratory facilities benefits the SNS schedule.

Worldwide development activities are in progress for SC low-beta cavities for high-intensity proton linacs. These laboratories include TJNAF, LANL, CEA-Saclay, JAERI, INFN-Genova, INFN-Milan, and CERN.

3.3 COMPARISON TO ESTABLISHED PERFORMANCE

During the last decade there have been remarkable strides in the application of SC cavities around the world. In all, cavities totaling nearly 1 km in length have been installed and routinely provide about 5 GV of acceleration. The largest installation is for LEP-200 at CERN, where nearly 500 m of cavities provide more than 3 GV of acceleration. CEBAF, at Jefferson Lab, is the next largest application with 165 m of cavities. For comparison, the SNS will require about 100 m of SC cavities.

Although the original CEBAF design energy was 4.0 GeV, CEBAF now operates at 5.5 GeV because of on-line gradient improvements made possible by the intrinsic gradient potential of SC cavities. Compared with originally-planned gradients of 5 to 6 MV/m, the average operating gradient at LEP and at CEBAF is now 7 MV/m. Therefore, these laboratories have benefited significantly by progressing toward the intrinsic potential of SC cavities. More recently, the CEBAF-FEL operates with 10 cavities at gradients between 9.0 and 12.5 MV/m.

For proton applications, it is important to appreciate that two four-cell cavities have been operating routinely at the CERN SPS for many years, where the intensity is 3.5×10^{13} protons/pulse and the average circulating beam current is 300 mA. Three single-cell 500-MHz SC cavities have been operating in the high-current storage ring CESR at Cornell University, and four one-cell cavities are operating in the KEK-B factory. These cavities routinely run with CW beam currents of more than 500 mA.

Since the construction of the large installations at CERN and JLAB, several advances in cavity design and performance have been made in connection with the TESLA project and the associated TTF, now under construction at DESY. The number of cells per cavity has increased from the typical four to five cells to the present nine-cell design. Cavities have been stiffened to reduce Lorentz-force detuning and have been operated in pulsed mode with beam. TTF routinely operates with a 2-ms rf pulse length, a 10-Hz repetition rate, and with average field regulation of better than 0.1% and phase regulation of 0.1 degrees.

Cavity performance has improved by more than a factor of three since CEBAF and LEP were constructed. In acceptance tests of 73 TTF cavities, each of which has nine cells and a 1-m active length, the accelerating gradients reached 20 to 29 MV/m. These gradients correspond to peak surface electric fields of 40 to 58 MV/m and peak surface magnetic fields of 86 to 125 mT.

Because cavity performance is governed by peak fields, it is convenient to compare the SNS desired performance with the TTF established performance in terms of peak fields rather than accelerating fields. The peak field comparison is also more convenient because the ratios of peak to accelerating fields change with beta values of the structures. Figure 3.3 shows E_p achieved by

TESLA 9-cell cavities as a function of construction year, as supplied by the four separate vendors. The cavities constructed in 1998 and 1999 have E_p greater than 38 MV/m, except one cavity that had a construction defect. This should be compared with 27.5 MV/m used for the SNS design. The figure clearly shows an improvement in the achievable E_p since 1995, as well as a reduction in the number of construction defects.

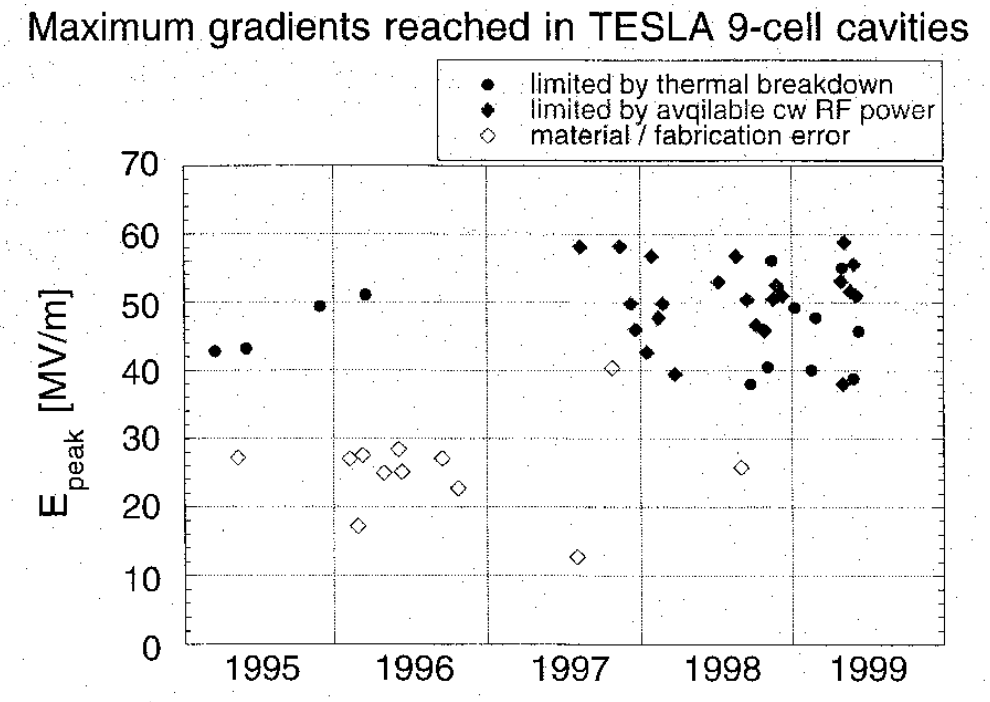

Figure 3.3 Values of E_p achieved in TESLA 9-cell cavities versus construction year.

Figure 3.4 shows a Q_0 versus E_a curve for a nine-cell TESLA cavity. Note that the Q_0 value was always above 10^{10} for $E_a < 15$ MV/m. The figure shows Q_0 versus E_a curve for three cases: no heat treatment, 800 °C heat treatment, and 1400 °C heat treatment. Without heat treatment, the RRR was 400 and a quench occurred at 17 MV/m. With 800 °C heat treatment, the RRR was unchanged and a quench occurred at 21 MV/m. The 1400 °C heat treatment increased the RRR to 770 and the E_a was limited only by the available amplifier power.

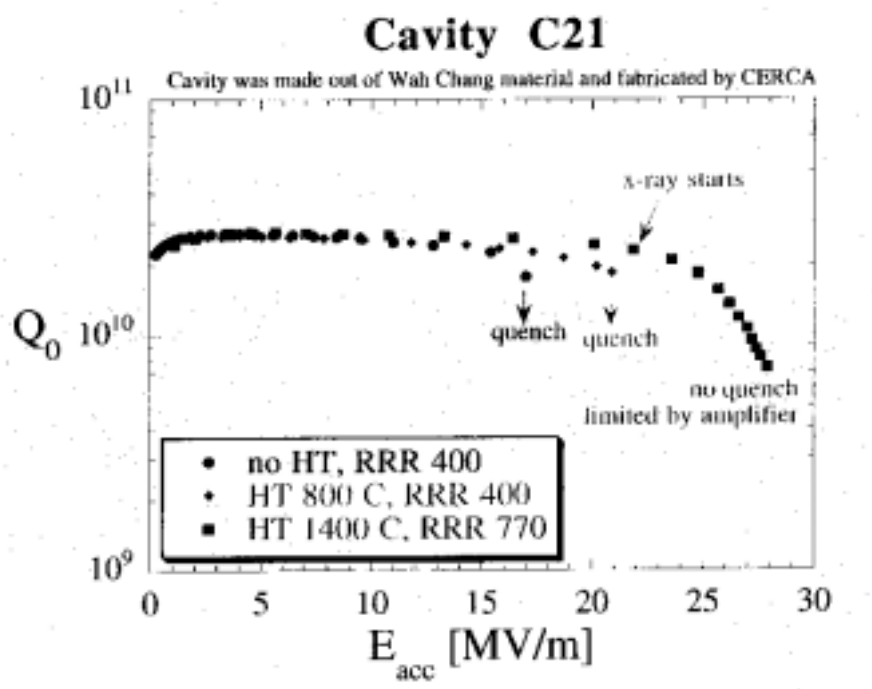

Figure 3.4 Q_0 versus E_a for a nine-cell TESLA cavity. Q_0 is above 10^{10} for $E_a < 15$ MV/m. CERCA (France) is one of four manufacturers of the TESLA nine-cell cavities, and Wah Chang (USA) is one of at least three suppliers of high-quality niobium.

Several reasons exist for the sharp advances in the performance of TTF cavities. The purity of niobium has improved, which increases the field at which quenches will occur from heating at inclusions and other imperfections. Two main avenues exist to achieve high-purity niobium, as characterized by the residual resistivity ratio (RRR), a convenient determination of niobium purity:

1. The niobium industry is delivering material with a higher RRR.
2. A postpurification process doubles the as-received RRR.

Additionally, by prescreening the material with an eddy-current scanning device, it is possible to eliminate the occasional bad sheet that may have tantalum or iron inclusions. The typical rejection ratio at TTF is less than 5%. Field emission is avoided by better surface preparation, in particular, high-pressure water rinsing. Any remaining field emission can be reduced by processing with pulsed high-peak-power rf. Mainly employed in the horizontal cryostat, when the high-power coupler is attached to the cavity, the high-power processing technique allows cavities to reach nearly the same gradient as in the vertical cryostat acceptance tests. At Cornell, this technique has been shown to recover the gradient of cavities contaminated by deliberate vacuum accidents. Processing with the available peak power is routinely used on-line at CERN and TTF. For the SNS, peak powers of 230 to 340 kW per cavity will be available for field emission processing.

Heat treatments have also increased cavity performance. Eight TTF cavities were tested with only 800° C heat treatment but without the 1400° C titanium postpurification technique. Of these, four had a measured RRR of 180 to 280 and reached E_a = 14 to 24 MV/m. The other four had a measured RRR between 350 and 440 and reached E_a = 21 to 25 MV/m. Based on these results,

we anticipate that the less expensive 800° C annealing may be sufficient for the SNS. We intend to verify this strategy during the prototyping stage. If necessary, and as a backup, the cavities can be prepared using the postpurification technique.

At TTF, two eight-cavity cryomodules were assembled and tested with beam with a peak electron beam current of 8 mA. The on-line accelerating gradient was 16 MV/m for the first cryomodule and 20 MV/m for the second. The first cryomodule was limited to 16 MV/m because it contained cavities with weld defects as mentioned earlier. Figure 3.5 shows the CW, 1-Hz, and 10-Hz performance of one of the best cavities as measured in the horizontal cryostat. The conservative SNS operating range is also depicted in the figure for comparison.

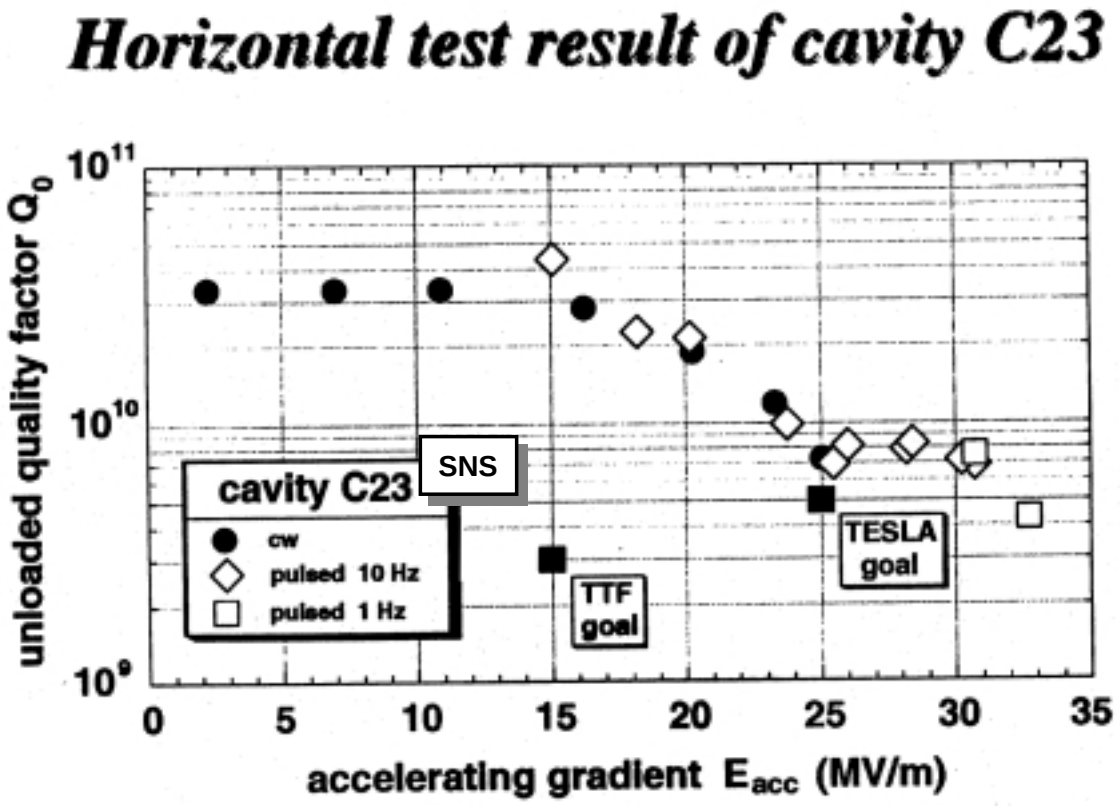

Figure 3.5 CW and pulsed performance of one of the best cavities as measured in the horizontal cryostat. The conservative SNS operating range is also shown for comparison.

In conclusion, the peak fields of 27.5 MV/m and acceleration gradients of less than 12 MV/m for the SNS cavities are relatively modest and have been exceeded with existing technology.

ADDENDUM FOR LORENTZ FORCE DETUNING

The rf field produces a Lorentz force on the cavity walls that detunes the cavity by a static frequency shift Δf given by

$$\Delta f = K \cdot E_a^2$$

where *K* is the static Lorentz force detuning sensitivity factor, which depends on the cavity shape and construction, and E_a is the cavity field measured in terms of the accelerating gradient. If the rf generator frequency is fixed during detuning, then more power is needed to maintain the cavity voltage constant to maintain constant acceleration. The required increase in generator rf power $P_{\Delta f}$ to maintain a constant voltage for a detuned cavity is given by

$$P_{\Delta f} = P_{\Delta f = 0}(1 + (\frac{\Delta f}{f_{1/2}})^2) \ ,$$

where $P_{\Delta f = 0}$ is the required generator power for a tuned cavity, Δf is the Lorentz force frequency shift, and $f_{1/2}$ is the full-width half maximum bandwidth of the cavity, loaded by the input coupler.

With the SNS cavity parameters of K ~ 2 Hz /$(MV/m)^2$ and E_a ~ 12 MV/m, the frequency tune shift Δf is 290 Hz. With a bandwidth of $f_{1/2}$ ~ 1400 Hz, the required increase in drive power $P_{\Delta f}$ is about 4%, compared with the undistorted case with Δf = 0. This 4% increase in rf power compares with about a 20% increase in required rf power for the TESLA case because of TESLA's higher gradient, higher frequency, and smaller bandwidth. This increase in rf power should be easily compensated with the operating TTF-type digital adaptive feedback rf control system.

4. COUPLERS

4.1 INPUT COUPLER

4.1.1 Introduction and Specifications

The function of the input coupler is to transfer rf power from the klystron to the beam, to maintain accelerating field in the cavity in the absence of beam, to provide peak rf power for processing cavity field emission, and to damp the nonaccelerating modes of the fundamental passband.

Table 4.1 shows the number of couplers, available forward power per coupler, beam power to be delivered by each coupler, and the accelerating mode Q_{ext} for the low- and high-beta cavity types. In order to process field emission with available power, it should be possible to reach accelerating fields of about twice the operating field if desired.

Table 4.1: Coupler parameters for SNS medium- and high-beta sections.

	Medium beta (0.61)	High beta (0.76)
No. of couplers	27	80
Max beam power (kW)	192	326
R/Q (Ω per m)	350	500
ΔV per cavity (MeV)	4.45–5.33	6.04–9.06
E_p (MV/m)	27.5	27.5
Q_{ext}	5×10^5	5×10^5

4.1.2 Input Coupler Design and Basis

The antenna-type coaxial design is chosen based on the successful experiences of CERN (LEP), DESY (HERA and TTF), and especially the success of the KEK input coupler for KEK-B.

Since the KEK-B coupler provides the highest power transmission of any presently operating coupler (at least 380kW CW), the current plan is to copy and scale it for the SNS.

Figure 4.1 shows the KEK-B cryostat, rf cavity, and associated tuner, damper, and coupler. Figure 4.2 shows the KEK-B 508-MHz coupler, which will be scaled proportionately to 805 MHz. The lengths of the various sections will be adjusted to fit the SNS cavity and cryostat. The waveguide-to-coaxial transition is of the doorknob variety. As in all high-power applications, the main window is at room temperature and is remote from the cavity. The window is a disk-shaped, water-cooled, 95% pure alumina ceramic with a central hole for the inner conductor. Figure 4.3 shows the window in more detail. A Teflon™ coaxial centering disk between the window and doorknob serves to limit the flow of air to the cavity in the unlikely event of a ceramic window break. The inner conductor is made of oxygen-free high-conductivity (OFHC) copper pipe and is water cooled. The outer conductor is made of copper-plated (30 μm) stainless steel and has fins (shown in Figure 4.2) cooled by a 4.5 K stream from the refrigerator. It is planned to attach the input coupler to the cavity under a dust-free clean jacket after the sealed cavity is assembled into the cryostat.

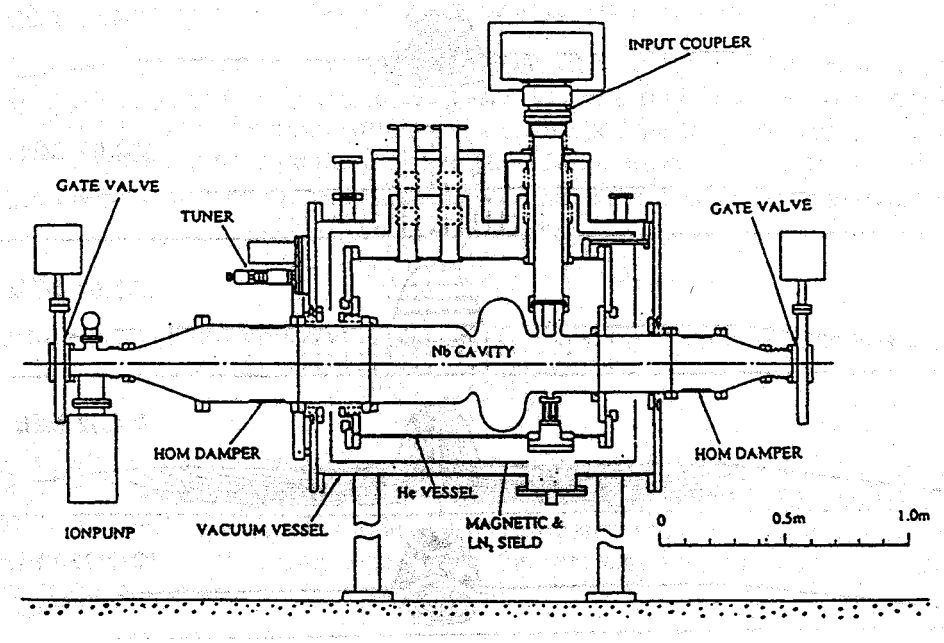

Figure 4.1: The KEK-B rf module, including cryostat, rf cavity, and associated tuner, damper, and coupler.

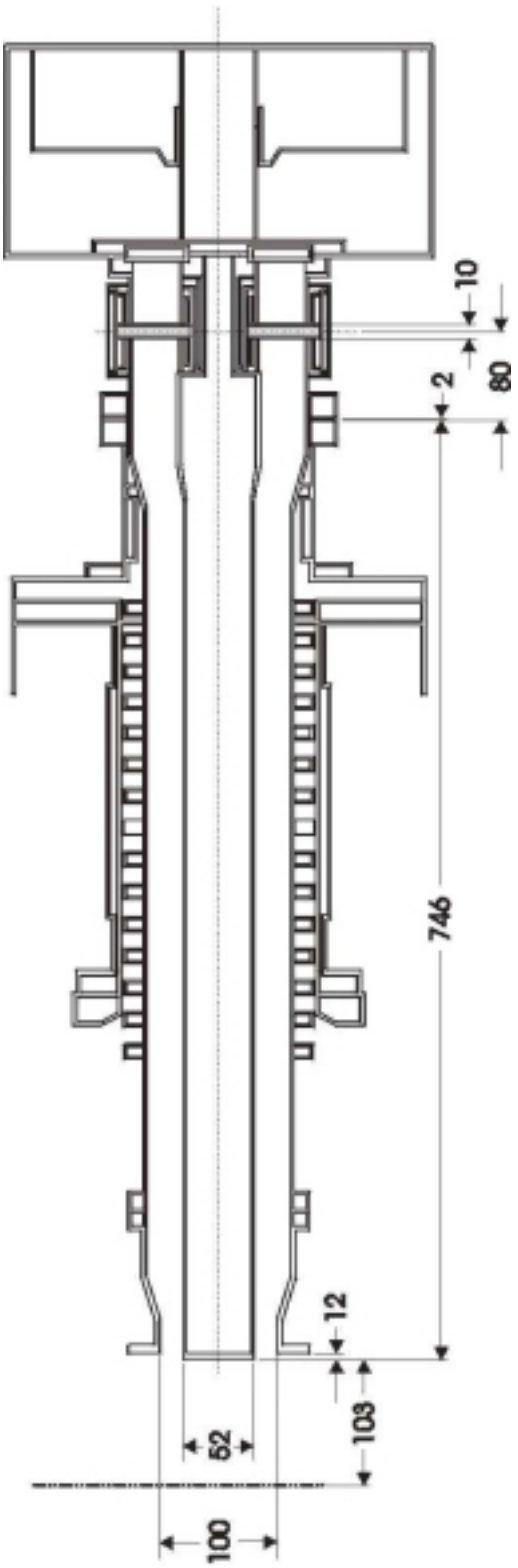

Figure 4.2: The KEK-B 508-MHz coupler.

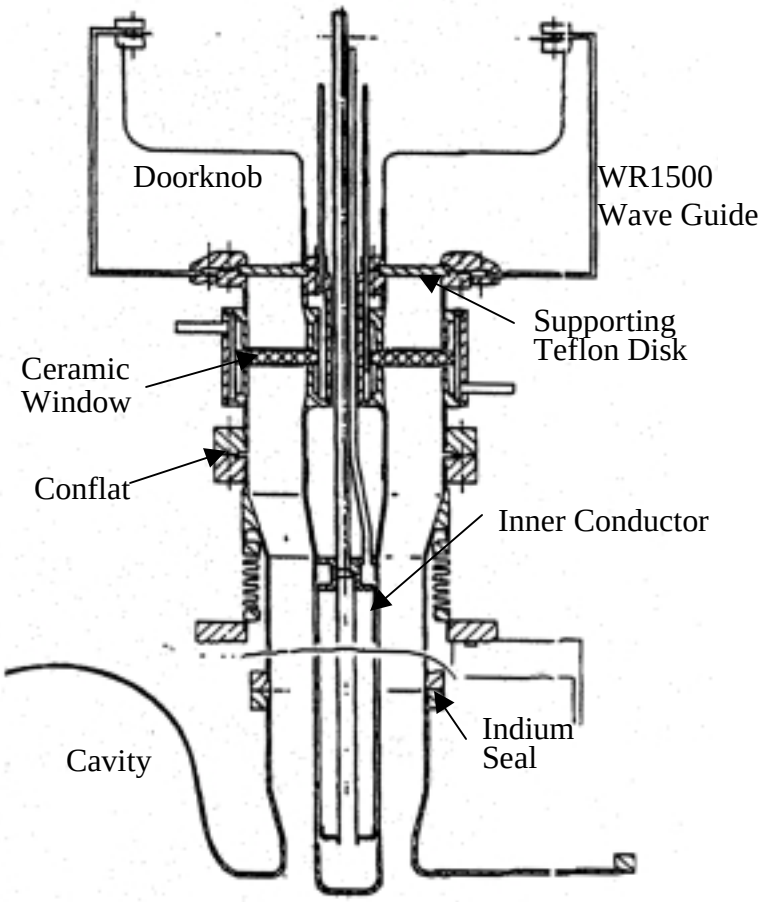

Figure 4.3: Detail of the KEK-B main coupler window.

The dimensions of the inner and outer conductor are such that multipacting will not be a serious problem as estimated by the simulation codes. The vacuum side of the window has a 100-Å-thick anti-multipactor coating. In addition, the design permits the application of a dc bias voltage between the two conductors to curb any possible multipacting.

The Q_{ext} value will be fixed after initial adjustment of the position of the inner conductor by the use of appropriate spacing washers during final assembly. From past experience we expect that the Q_{ext} for the nonaccelerating modes of the fundamental passband will be of the same order as the Q_{ext} for the accelerating mode (i.e., a few $\times 10^5$).

The coupler will be equipped with standard diagnostics for vacuum, gas species (RGA), temperature, and light monitoring. Vacuum and light levels will be used to trip the rf in case of an arc.

Before attachment to the cavity, each coupler will be high-power tested and conditioned to 500 kW in travelling wave and to 125 kW in standing wave operation.

4.1.3 Comparision With Existing Technology

With the four SC cavities (508 MHz) now in routine operation at KEK-B, the four input power couplers have each delivered beam power of 370 to 380 kW CW to a 500-mA-stored beam. This performance is in excess of the SNS maximum requirement of 345 kW. Moreover, the SNS will operate in the pulsed mode with < 10% duty factor, which is generally less demanding on coupler performance than the CW operation carried out at KEK-B. Before installation into the cavities, the KEK couplers were successfully conditioned to a travelling wave power level of 800 kW as well as a full-reflected power level of 300 kW. Cooling provisions for the outer conductor and the window can be simplified because of the low duty cycle for SNS. These minor design improvements will be carried out during the prototyping stage. The high-power coaxial coupler for APT (LANL) has now been tested to reach in excess of 1 MW CW in a room-temperature test. Additional high-power coupler efforts are underway at DESY and CEA-Saclay.

4.2 HIGHER-ORDER MODE COUPLERS

4.2.1 Introduction and Specifications

The function of the HOM couplers is to damp the higher-order modes to Q_{ext} values of 10^4 to 10^5 to prevent resonant buildup of beam-induced fields that may make the beam unstable or increase the HOM power. The HOM couplers extract beam-induced HOM power from the cavity and deposit it into room-temperature loads rather than into the cryogenic system. Two couplers are needed with a relative azimuthal angle of about 90 degrees to ensure damping of both polarizations of dipole modes. One coupler is attached to each end of the cavity. The HOM couplers must reject the accelerating mode by means of a filter.

Detailed calculations will be carried out during the prototyping stage for the HOM spectra, trapped modes, and expected HOM power. Codes exist, and procedures have been well established for electron applications. As for proton machines, the expected HOM power for the 700-MHz APT CW five-cell cavities is 7 W for the medium-beta and 17 W for the high-beta cavities. Expected SNS HOM power loads are much less than those for APT.

4.2.2 Higher-Order Mode Coupler Design and Basis

The coaxial, demountable, loop-type coupler shown in Figure 4.4 is chosen because of its demonstrated performance, compactness, relaxed mechanical tolerances, and demountability. The plane of the loop is orthogonal to the beam axis. The loop couples mainly to the magnetic field of dipole modes and mainly to the electric field of longitudinal modes. The rejection filter is formed by the inductance of the loop and the capacity between the loop end and the outer conductor. A capacitive coupling links the loop to the external load via a type-N connector. The loop is cooled by conduction through an upper stub, which is connected to the 2 K bath through a thermal shunt. The final tuning of the filter can be carried out outside the clean room once the coupler is attached and the cavity is sealed.

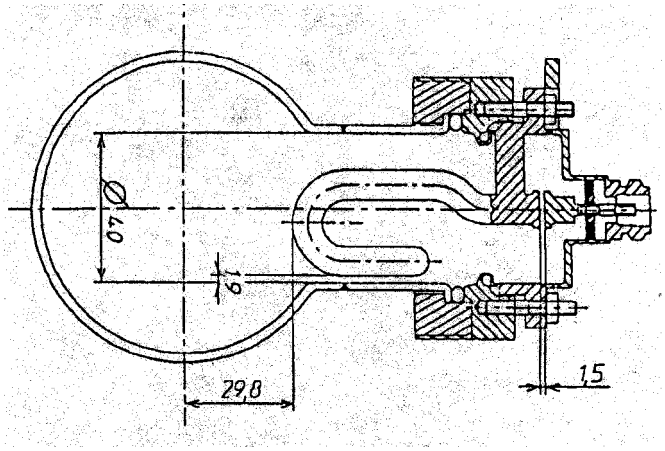

Figure 4.4: Coaxial, demountable, loop-type coupler from TTF.

4.2.3 Comparision With Existing Technology

Table 4.2 is representative of the typical Q_{ext} values achieved with this coupler on a nine-cell, 1.3-GHz TTF cavity for the highest impedance monopole and dipole modes. Power tests carried out in the CW modes with this coupler showed good thermal behavior up to an accelerating field of 21 MV/m. Coupler performance exceeds the SNS requirements.

Table 4.2: Damping measurements with the demountable TTF coupler.

Mode	Frequency (MHz)	R/Q	Q_{ext} ($\times 10^4$)
TE111	1706.43	10.0 Ω/cm^2	0.22
	1707.57		0.45
TE111	1734.11	15.4 Ω/cm^2	0.36
	1734.50		0.16
TM110	1874.41	8.7 Ω/cm^2	7.3
	1874.92		5.4
TM011	2448.29	67.0 Ω	5.8
TM011	2454.03	79.5 Ω	11.0

4.3 TUNER

4.3.1 Introduction and Specifications

The function of the tuner is to match the cavity resonance frequency with the desired accelerator operating frequency. If the cavity is not being used for acceleration, the tuner must detune the cavity frequency a few bandwidths away from resonance, so that the beam will not excite the fundamental mode. During accelerator operation, the tuner must correct for slow changes in the cavity frequency caused by

changes in the liquid helium bath pressure or in the lengths of the cavity and helium vessel support system.

The role of the tuner is to adjust the cavity frequency to an accuracy of $1/20^{th}$ of the cavity bandwidth. From the Q_{ext} of the input coupler, the expected bandwidth is 1600 Hz, giving a required resolution of 80 Hz. The tuning coefficient of the cavity is 200 kHz/mm, and the desired tuning range is 500 kHz or 2.5 mm.

4.3.2 Tuner Design and Basis

The cavities must be tuned while preserving field flatness. Tuning is achieved by varying the total length of the cavity. The length of the cavity is controlled by an electromechanical system acting differentially with respect to the cavity body. As each cavity is enclosed in its helium vessel, the latter must show some flexibility.

The tuning system is generally composed of a stepping motor, gearbox, screw-and-nut assembly, and a lever arm with a flex mechanism attached. The rf control system stabilizes frequency, amplitude, and phase variations induced by sources such as the rf drive, beam current variations, Lorentz force detuning, and microphonics. Tuners are an active part of the complete rf control system.

4.3.3 Comparision With Existing Technology

The tuner design will be finalized during the prototyping stage and will be based on several successful tuner designs presently in operation at CEBAF and TTF.

5. CRYOSTATS

5.1 INTRODUCTION AND SPECIFICATION

SNS requires nine 4.239-m-long cryomodules and twenty 6.1-m-long cryomodules. The total length of the SC linac is 206.6 m, including warm sections. For comparison, CEBAF uses 43 9.6-m-long cryomodules, which is about twice the scope of the SNS SC linac. Table 5.1 lists the SNS cryomodule parameters.

Table 5.1: Cryomodule Parameters

	Medium beta	High beta
Number of cryomodules	9	20
Cavities per cryomodule	3	4
Slot length	5.839 m	7.700 m
Cryomodule length (bore tube)	4.239 m	6.100 m
Cryomodule diameter	0.914 m (36 IPS)	0.914 m (36 IPS)
2 K static heat load per cryomodule*	25 W	28 W
2 K dynamic heat load per cryomodule	16 W	18 W
Shield heat load*	170 W	200 W
Control valves per cryomodule	5	5
Bayonets per cryomodule	4	4
Tunnel (height × width)	10 × 12 ft	10 × 12 ft
Radiation hardness	10^8 rads	10^8 rads
Pressure rating - 2 K system:		
warm	3 bar	3 bar
cold	5 bar	5 bar
Pressure rating - shield and 4.5 K systems	20 bar	20 bar

* includes transfer line

5.2 CRYOMODULE DESIGN

The cryomodule design is based on the CEBAF cryomodule with improvements borrowed from LHC, TESLA, and the JLab 12-GeV Upgrade, and uses the frequency-scaled KEK fundamental power coupler.

Figure 5.1 shows the tunnel cross section including the cryomodules and related piping, and Figure 5.2 shows the plan and elevation views of the high-beta cryomodule. Figure 5.3 shows the schematic flow-diagram of the cryogenic transfer system and Figure 5.4 shows the medium-beta cryomodule. Figure 5.5 is a 3D rendering of half of the space-frame fixture for the high-beta cryomodule. Two cavities in helium jackets are shown.

The KEK-B coupler, described in Section 4.1, requires a 4.5-K lead flow to cool its outer conductor; therefore, the LHC concept of producing the 2 K in the cryomodule rather than in the refrigerator is used. The refrigerator produces a 3-bar, 4.5-K stream, which feeds two cryomodule cooling loops in parallel: (1) The first loop exchanges heat with the return stream through a small subcooler in the cryomodule and then Joule-Thomson valves are utilized to cool the cavity. (2) The second loop feeds the outer conductor of the power coupler.

The 50-K cryomodule shield is cooled by a 4-bar, 35-K stream, which first cools the supply transfer line shield, then the cryomodule shield, and finally the return transfer line shield before returning to the refrigerator at 55 K.

The bayonet design permits replacement of a cryomodule in less than a day, if needed, without warming up. In the eight years since the initial CEBAF cool down, the linacs have never been warmed up.

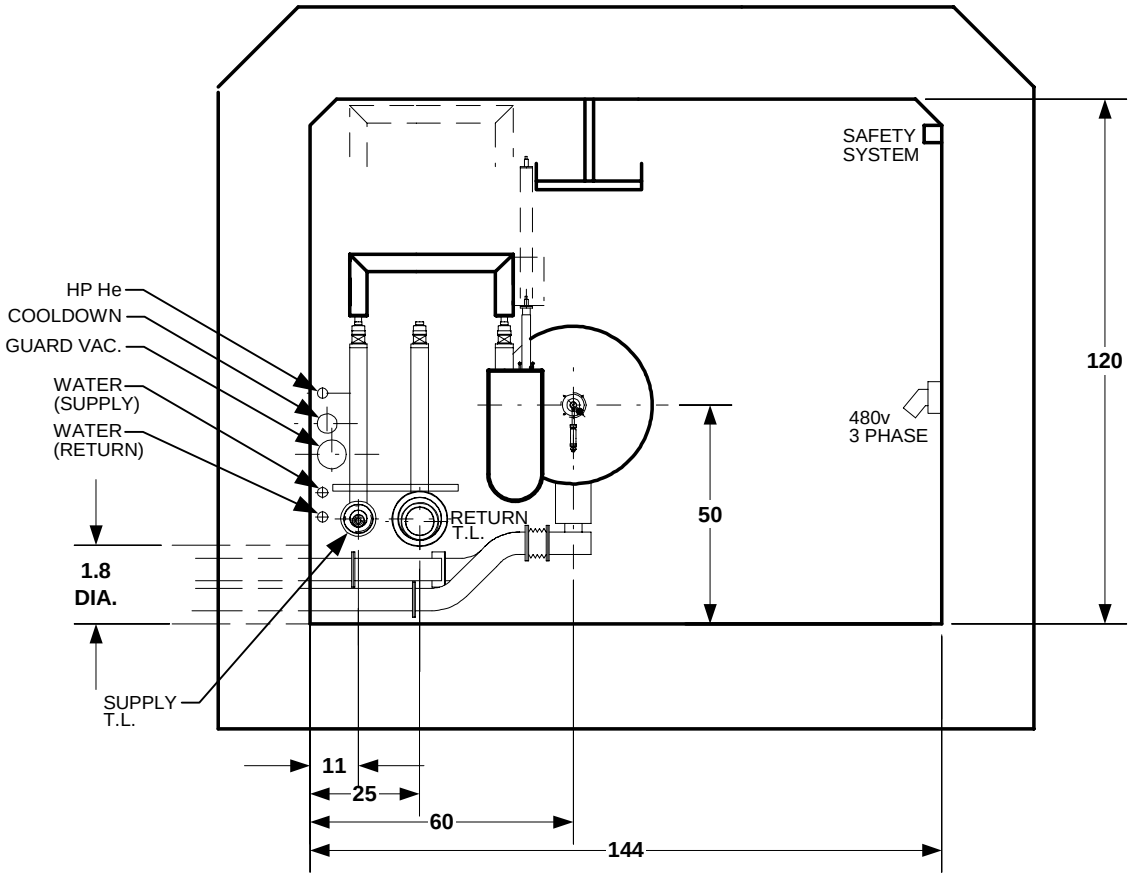

Figure 5.1: SC linac tunnel cross section

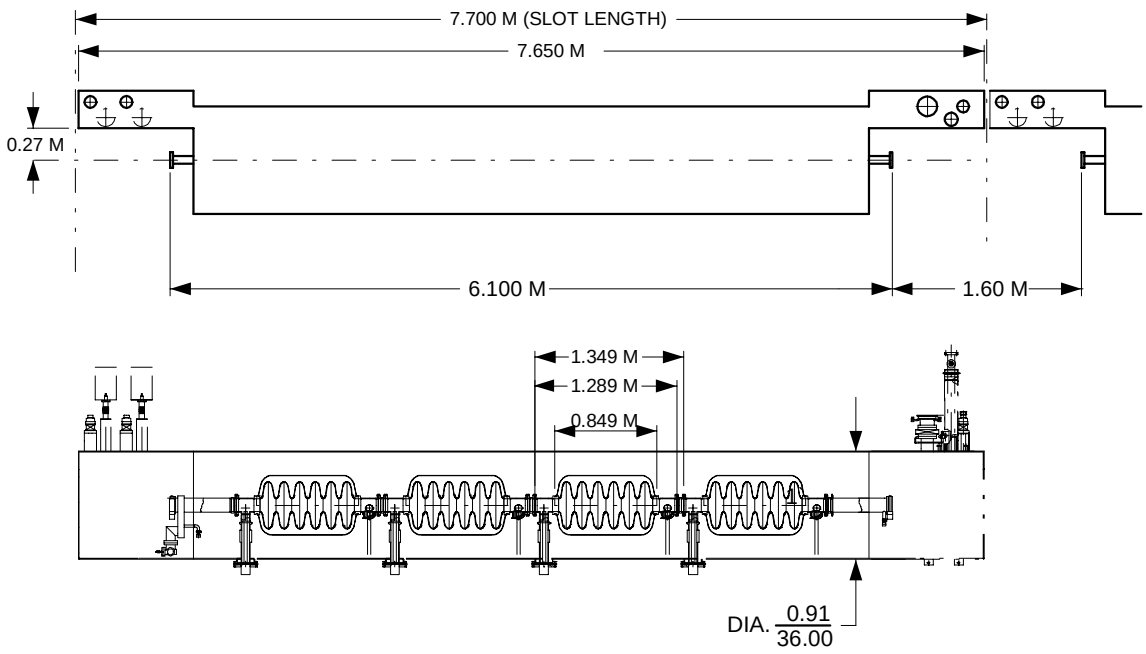

Figure 5.2: High-beta cryomodule ($\beta_g = 0.76$).

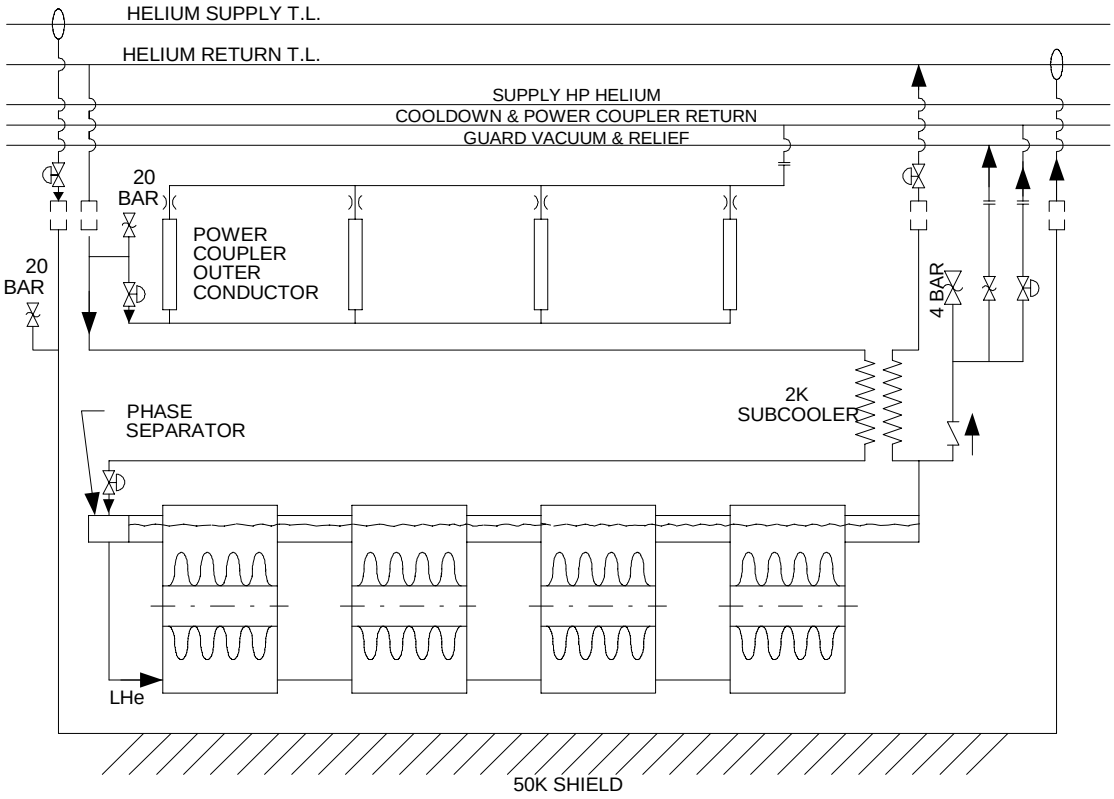

Figure 5.3: Schematic flow diagram of the cryogenic transfer system.

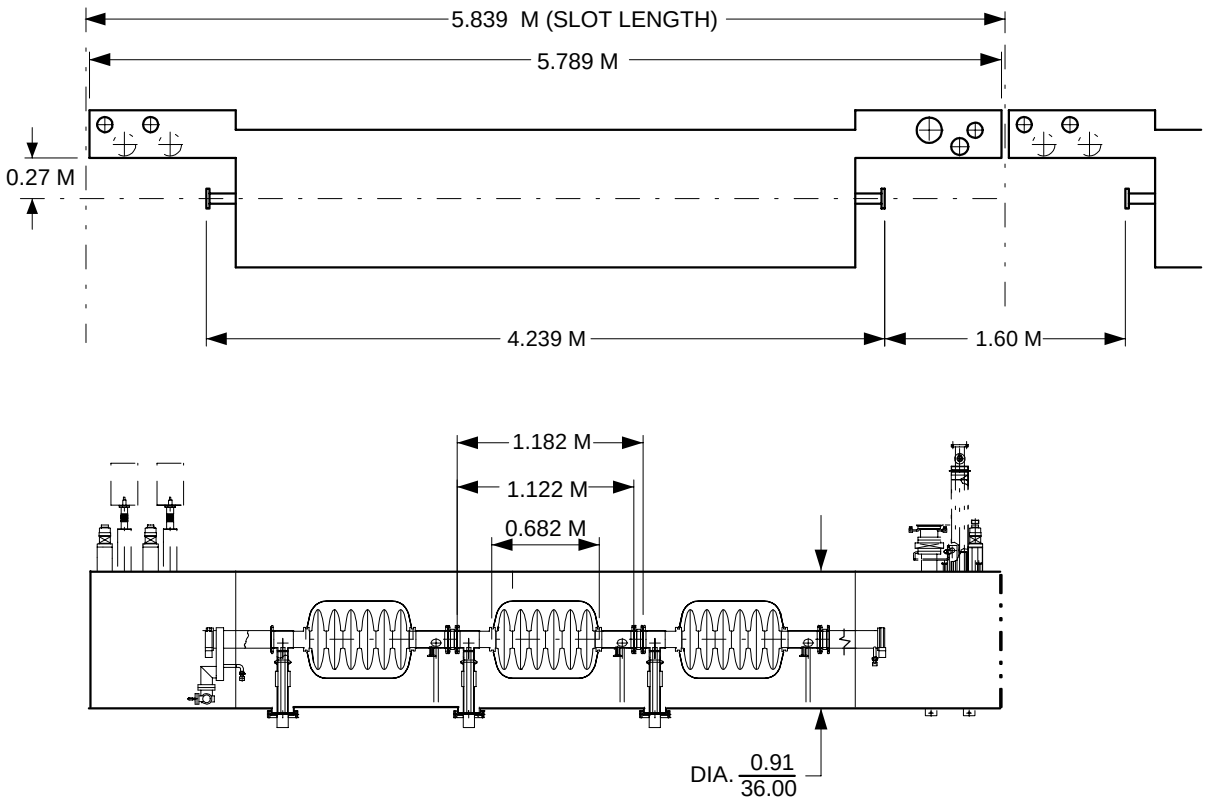

Figure 5.4: Medium-beta cryomodule ($\beta_g = 0.61$).

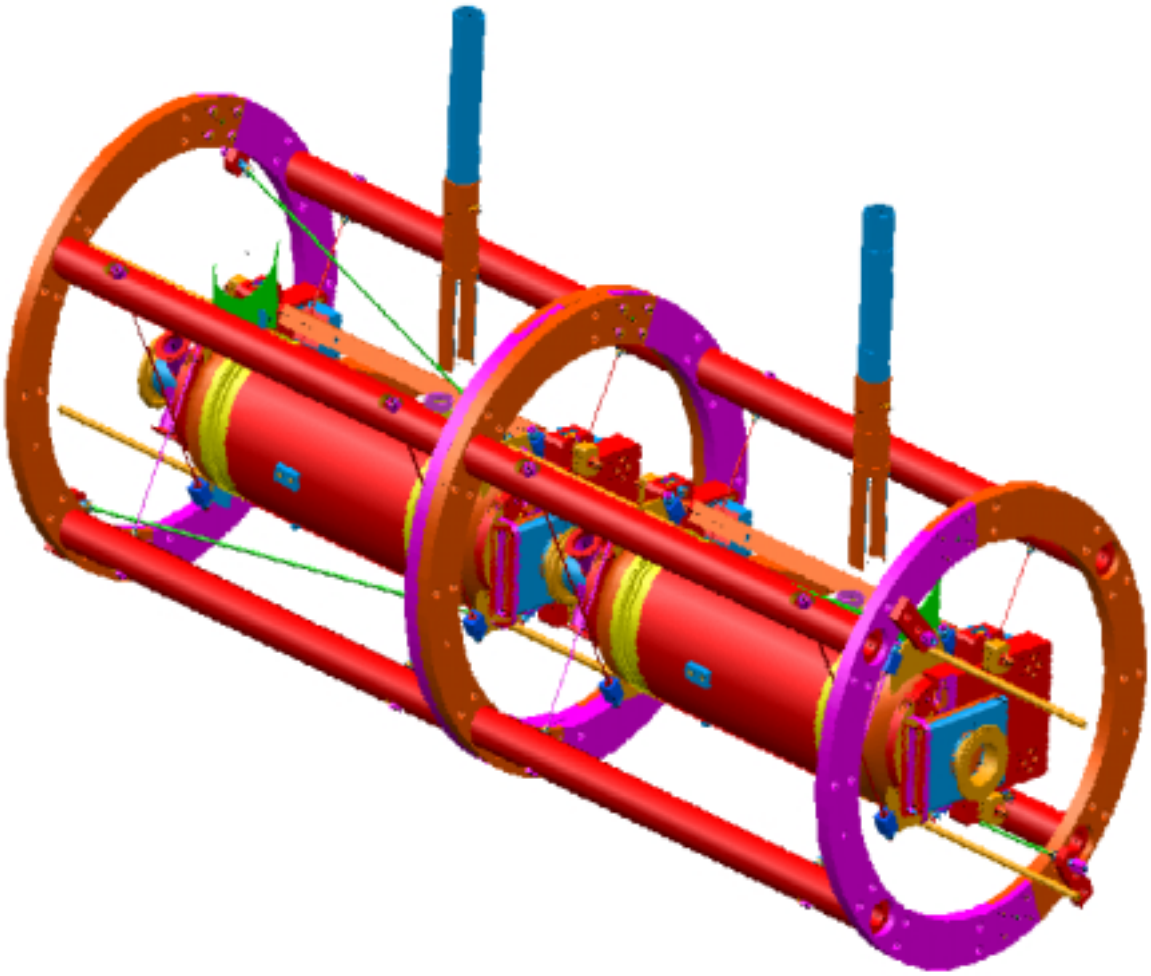

Figure 5.5 Detail showing half of the space-frame fixture for a high-beta cryomodule.

6. CRYOGENICS

6.1 INTRODUCTION AND SPECIFICATION

The required SNS cryogenic system is about half the size of the JLab cryogenic system. The JLab system can be adapted for SNS use with only minor modifications. Requirements of the SNS cryogenic system are listed in Table 6.1. Because SNS uses a lower frequency, 805 MHz versus 1500 MHz, its optimum temperature is just below the lambda point. A temperature of 2.10 K is specified for the refrigerator, which provides a large margin of 0.07 K for pressure drops in the return of the transfer line and cryomodule (0.005,7 bar).

Table 6.1 Cryogenic circuit loads.

	Primary	Secondary	Shield
Temperature (K)	2.10	5.0	35–55
Pressure (bar)	0.041,3	3.0	4.0–3.0
Static load	785 W	5.0 g/s	5530 W
Dynamic load	~500 W	2.5 g/s	0 W
Capacity	2,250 W	15 g/s	8300 W
Margin (%)	~50	100	50

To meet the SNS schedule of a 1-GeV beam in July 5, 2004, the cryomodule installation schedule requires linac cooldown on October 1, 2003. Contracts for the refrigerator and transfer lines should be placed in FY 2000 since the refrigeration system is on the critical path.

6.2 TRANSFER LINE

The CEBAF transfer line system consists of two tee-shaped 240-m-long linac feeds, each capable of supplying a maximum capacity of 5 kW at 2.0 K. SNS can use the existing CEBAF design for one linac (206.6 m) with only the cryomodule spacing changed.

The SNS cryogenic supply transfer line is 6-IPS (168 mm OD) with a 1-IPS (30 mm ID) primary supply and eccentric 35 K shield. The return transfer line is a 12-IPS (324 mm OD) with a 6-IPS (163 mm ID) primary subatmospheric return and eccentric 55 K shield. Figure 6.1 shows the transfer line cross sections for the SNS linac as well as the central helium liquifier (CHL). The transfer lines are made in modules that are 15 m long, as shown in Figure 6.2.

There is a 40-m-long branch supply to the center of the SC linac that is identical to the piping cross section in the tunnel with only the 1-IPS replaced with a 1.25-IPS (39 mm ID). The branch return can either be a single 16-IPS (406 mm OD) with an 8 IPS (214 mm ID) primary subatmospheric return or two 12 IPSs with the return piping cross section in the tunnel. In addition, there are three helium gas headers as listed in Table 6.2.

Table 6.2: Helium gas header parameters

Helium Gas Header	Header Size	Pressure
Warm gas supply for bayonets and coupler	2 IPS	3 bar
Cooldown and coupler relief	4 IPS	1.05 bar
Guard vacuum and relief	6 IPS	0.01 bar

In case the fundamental coupler design is changed to something besides the KEK coupler, and does not use 4.5 K helium cooling, the sizes of the first two headers in Table 6.2 decrease to ¾ and 2 IPS, respectively.

6.3 REFRIGERATION

The SNS SC linac requires about half the CEBAF refrigeration capacity. A simple scaling of the CEBAF system leads to the refrigeration system described in Table 6.3 below.

Table 6.3: Refrigeration system description

Warm compressor system:	two stages of two 321-mm screw compressors 10 ppm oil removal on each compressor 0.01 ppm final oil removal
4.5 K cold box:	Liquid nitrogen (LN2) precooling four turbines dual 80 K absorbers single 20 K absorber 4.5 K subcooler
2.1 K cold box:	four stages of cold compressors compression ratio of 25 for 2.10 K Note: 2 K subcooler is removed to the cryomodules
Auxiliary equipment:	10,000-gal liquid helium (LHe) Dewar 20,000-gal LN2 Dewar four 30,000-gal gaseous helium (GHe) storage tanks dual external 50 grams per second purifier absorber regeneration skid local control room

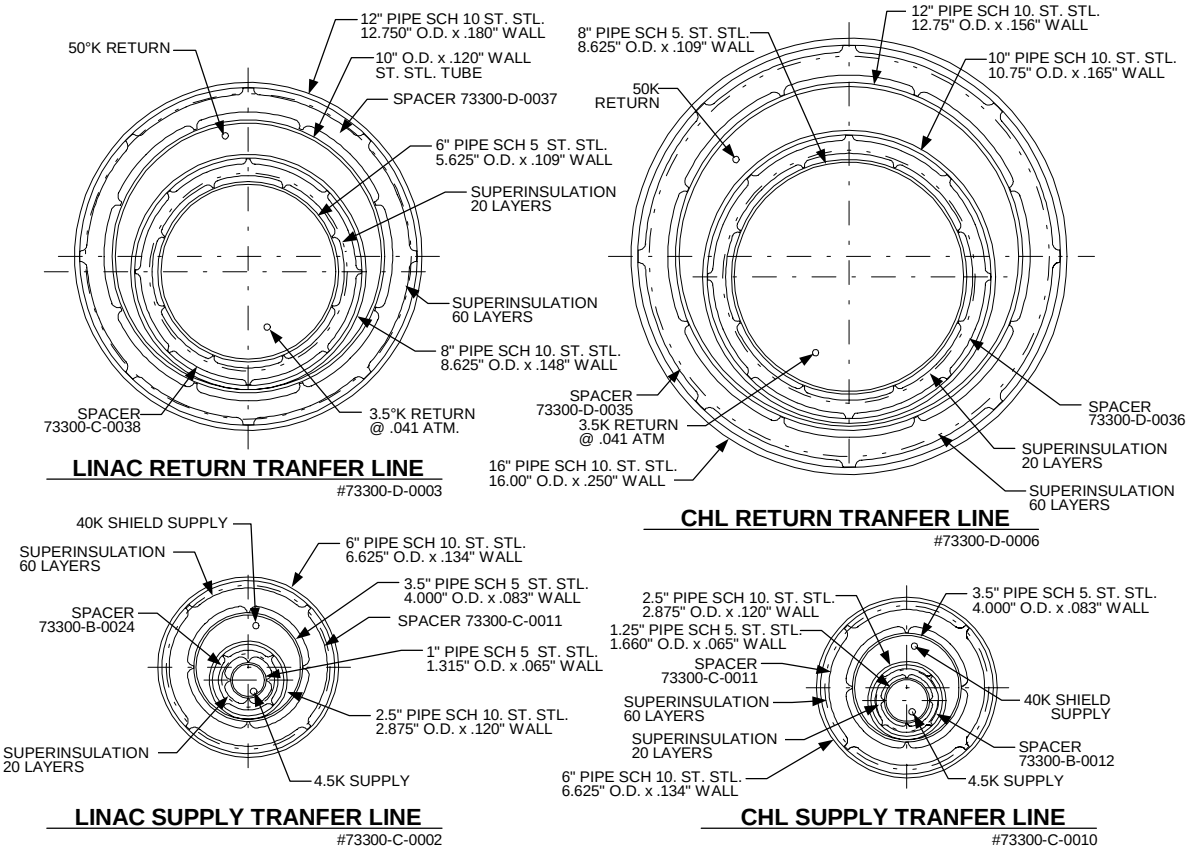

Figure 6.1: Cross sections of the linac and central helium liquifier (CHL) cryogenic transfer lines.

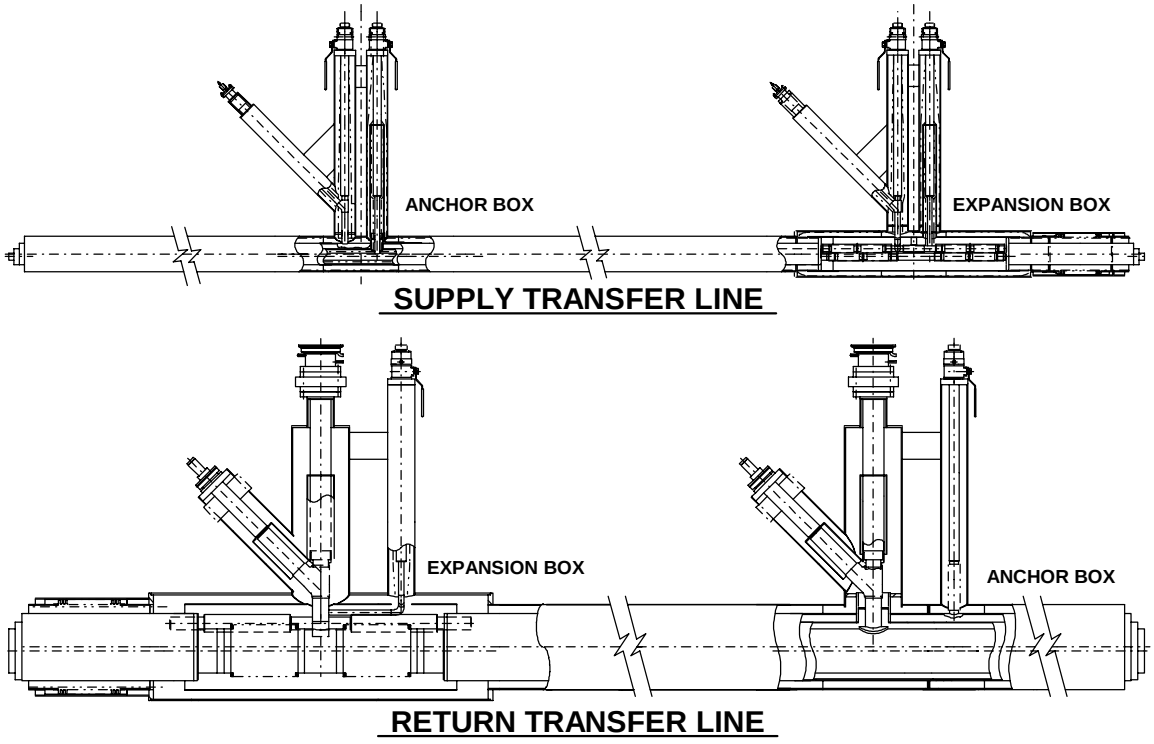

Figure 6.2: Supply and return transfer line modules in the linac tunnel.

7. RF SYSTEM

7.1 HIGH-LEVEL SYSTEM

7.1.1 Requirements

The high-level rf system includes the klystrons, modulators, circulators, and high-power distribution waveguide and directional couplers. The system provides the rf power required to accelerate the beam from 194.3 to 1001.5 MeV, with a change from $\beta_g = 0.61$ cavities to $\beta_g = 0.76$ cavities at 331.1 MeV.

7.1.2 Design Basis

In order to provide the best rf stability (through quadrature addition of uncorrelated errors), the greatest simplicity of operation, and the greatest flexibility for continued operation in the event of a single rf failure, one klystron per cavity is used.

Each klystron delivers 400 kW of pulsed power at 805 MHz. This power level includes a > 20% margin to make up for waveguide losses and to allow for phase and amplitude control. The repetition rate is 60 Hz, and the rf duty cycle is 7.02%. The klystron efficiency is 65%. There are 107 klystrons, each of which powers a single cavity.

There are several ways to supply power to the klystrons; one power supply per klystron or one power supply per several klystrons. In the case of one power supply per klystron, the power supply system reliability is less than that of a system with fewer power supplies. As discussed in Chapter 2, the SNS SC linac can still operate with one or two nonfunctional cavities. The availability of the linac in that case can be made high since the mean time for reconfiguration is expected to be a minute or two. When one supply powers several klystrons, the mean time between failures of a single large supply is longer than multiple small supplies, however failure of the supply can result in significant downtime for the entire linac system resulting in lower overall availability.

Because the SNS linac can operate with two cavities off in either section, the plan is to power two klystrons with one modulator supply. Figure 7.1 shows a schematic of the plan to power the klystrons.

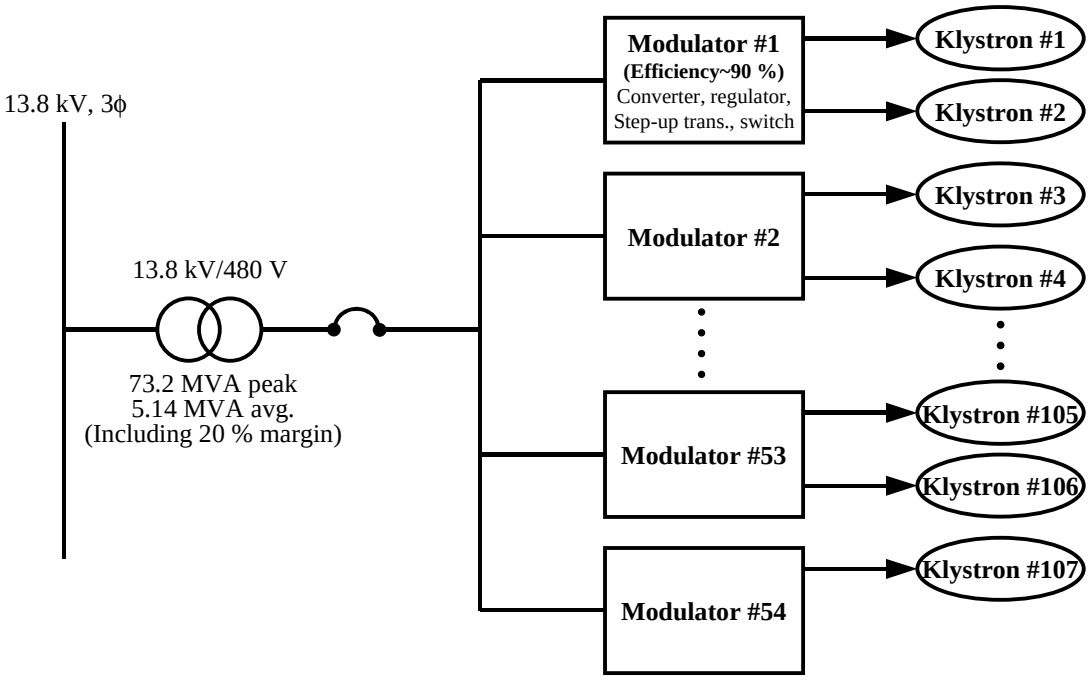

Fig. 7.1: The klystron modulator power supply scheme.

A circulator with a full-power load is installed on the output of each klystron to protect the klystron from reflections. The klystrons and circulators can either be mounted directly on the cryomodule or installed in the klystron building. Installation of the klystrons in the tunnel has the advantage that no waveguide penetrations are required between the linac tunnel and the klystron building, resulting in less neutron dose in the klystron building. The disadvantage is that tunnel access is required to replace klystrons, possibly resulting in machine downtime. A detailed feasibility study is planned. A dual-directional coupler is used to provide reference information on the phase and amplitude of the forward and reflected power. High-power phase shifters are not required.

7.1.3 Comparison with existing technology

The klystrons, while not a stock item, are well within the range of peak power, average power, and frequency that are commonly used. A reputable and reliable vendor states that delivering 120 klystrons over a two-year period is attainable.

In the case a single power supply per klystron is used, the average power of 40 kW and peak power of 400 kW do not require new technology. In case a single, large supply is used to power several klystrons, the power supply design could be similar to the IGBT-based modulator design used in the warm linac.

7.2 LOW LEVEL SYSTEM

7.2.1 Requirements

The low-level rf (LLRF) system includes the low rf power control circuitry, the tuner control, and the rf interlocks. The system controls the amplitude and phase of the fields in the cavities, controls the

resonant frequency of the cavity, and protects the cavity and klystron from fault conditions. The baseline pulse-to-pulse tolerance on the rf amplitude in the cavity is ± 0.5%, and on the rf cavity phase is ± 0.5°. The tuner must adjust the resonant frequency of the cavity so that the incident rf power is used efficiently; this frequency is a function of the beam current, since the bunches are off-crest. The interlocks must protect the system from any credible condition that can cause permanent damage or, where this is not possible, must limit the extent of the damage.

Since a constant-gradient design was chosen for the SNS SC linac, the LLRF system must be able to power each cavity separately.

7.2.2 Design Basis and Commissioning

The rf power control circuitry determines the amplitude and phase of the rf voltage in the cavity based on the signal extracted from the cavity by a reference probe. The phase is measured relative to the phase of a reference rf signal from the master oscillator. The circuitry compares the measured amplitude and phase in the cavity to the desired amplitude and phase and, based on the beam current and other operating conditions, makes corrections to the phase and amplitude of the rf drive signal that is sent to the klystron. Feed-forward based on anticipated beam current is also used to achieve the required regulation tolerances during transients.

The low-level rf system is critical during the commissioning stage. At the start of commissioning, the initial amplitude and phase calibration is performed. Klystrons are turned on sequentially, proceeding from the low-energy end of the linac to the high-energy end at low time-averaged beam current with short pulses. As each cavity is added to the cavities already powered, the phase of the added cavity is square-wave modulated and the central phase is adjusted so that the beam energy does not show the modulation frequency. Initially, downstream cavities are unpowered and off resonance, and the quadrupoles are adjusted to transport the beam to a spectrometer at the end of the linac. The modulation is then removed, and the phase is offset by the appropriate angle to provide phase focussing. The amplitude is calibrated without beam by measuring the cavity bandwidth, the incident power, and the reference probe output power; this determines the reference probe calibration of output power vs. accelerating gradient.

The vector voltage in the cavity is compared to the vector voltage incident on the cavity, with knowledge of the beam current, to determine appropriate adjustments to the tuner. The intrinsic resonant frequency of the cavity is determined by measuring the frequency during ring-down at the end of the rf pulse.

Rf system interlocks protect against consequences of rf window arcs, rf window overheating, rf coupler multipacting, rf breakdown, low cryogen level, tuner position error, bad cavity vacuum, cryogen pressure error, and similar phenomena.

7.2.3 Comparison with existing technology

A pulsed superconducting proton accelerator does not exist. TTF is a pulsed SC electron accelerator, and CEBAF is a CW SC electron machine. The major difference between the SNS and electron machines is that proton beam bunches do not pass through the cavity at the peak of the rf wave and are traveling at less than the speed of light. CEBAF has a state-of-the-art LLRF control system for a CW machine, and TTF has a state-of-the-art LLRF control system for a pulsed machine. The SNS LLRF system is adapted from the CEBAF and TTF LLRF systems, while taking into account the difference between proton and electron acceleration.

The required rf control circuit can be very similar to those used in TTF and CEBAF. The principal sources of phase and amplitude variations requiring correction are cavity microphonics, cavity Lorentz forces, cryogen pressure changes, and variations in klystron high voltage. In CEBAF, the rms errors between 0 and 100 kHz are 7.0×10^{-5} in amplitude, and 1.6×10^{-2} degrees in phase [6] for CW operation.

In TTF, using feedback and feed-forward and measuring the vector sum, the rms errors are less than 1.0×10^{-3} in amplitude, and 5×10^{-2} degrees in phase for pulsed operation, both of which are well within the SNS requirements of 0.5 % in amplitude and 0.5° in phase. Feed-forward, based on anticipated beam current, is added to improve regulation during transients. No difficulty in achieving the specified amplitude and phase regulation is anticipated, as demonstrated at TTF. The fact that the cavities are powered and controlled separately minimizes the effect of the uncorrelated amplitude and phase fluctuations on the output beam energy and simplifies calibration and operation.

The tuner control is also similar to that used in TTF. The principal difference is that the optimum cavity resonant frequency is a function of beam current in the SNS, since the bunches are off-crest, and this is not a substantial complication. The SNS cavity Q_{ext} is a factor of 12 below that in CEBAF and a factor of six less than TTF. The stability against microphonics and Lorentz forces is improved accordingly.

The required interlocks are essentially equivalent to those in use at other SC rf accelerators and are not an issue.

8. WARM SECTIONS IN THE SUPERCONDUCTING LINAC

As discussed previously, most of the SNS SC linac beam line consists of cryomodules and warm sections. The cryomodules are based on the CEBAF cryomodule with improvements borrowed from LHC, TESLA, and the CEBAF 12-GeV upgrade. The warm sections consist of 1.60-m-long spaces between the cryomodules that contain the following elements:

- Quadrupole doublets for transverse focusing and both horizontal and vertical steering dipoles for equilibrium orbit correction.
- Beam diagnostics, including special diagnostic devices.
- Two bellows in the vacuum beam line and a tee for a flange to accommodate a pumping port and valve for warm-section pump out.
- A precise alignment system and supporter for quadrupole alignment.

Gate valves and hardware to pump out the cryomodules are already included in the medium- and high-beta cryomodule lengths of 4.24 m and 6.10 m, respectively.

The magnetic quadrupoles provide transverse focusing and matching for the H^- beam. Dipole correction is accomplished by dipole windings on the quadrupole magnet poles. The end caps located at the ends of the cryomodules (Figs. 5.2 and 5.4) must accommodate quadrupoles that are located in the warm sections. Although a detailed design of these rather standard quadrupoles has not been made, the radial dimensions of the quadrupoles do not exceed 27.5 cm from the beam line axis. This allows the outside diameter of the quadrupoles to be five times the bore diameter, which is sufficient radial space. The magnetic fields from the gradients for expected beam radii are below the level at which magnetic stripping is a concern. Some preliminary parameters of these quadrupoles are summarized in Table 8.1.

Table 8.1: Parameters of the quadrupole magnets

Number of quadrupole singlets	58
Aperture diameter (m)	0.11
Maximum outer diameter (m)	0.55
Iron core length (m)	0.35
Effective length (m)	0.41
Max pole tip field (T)	0.4
Max gradient (T/m)	7.2
Max integrated gradient (T)	2.98

Table 8.2 summarizes the beam instrumentation required to commission and operate the linac. Beam diagnostics include systems to measure beam current, beam position, beam profile, beam loss, beam energy, beam phase, bunch length, and energy spread. Most of the instruments are installed in the warm sections. Both horizontal and vertical transverse micro-strip-line pickups are located in each warm section to measure the beam centroid position and angle. These beam position monitors (BPMs) are located in the quadrupole apertures. Each warm section also contains a pair of pickups for measurements of the beam energy and phase centroids. Other diagnostic elements are located above the pumping ports at the center of the warm sections. These diagnostics include six 2-plane beam profile monitors that are used for transverse matching, two dc current toroids, and nine pulsed-beam current monitors. The fast and slow

beam loss monitors are located outside the vacuum chamber. Additionally, halo scrapers can be used along the linac.

Table 8.2: Beam instrumentation and required quantities

Beam position monitor, 2 planes	29
Beam profile monitor, 2 planes	6
Beam loss monitor	58
Fast beam loss monitor	3
Dc beam current monitor	2
Pulsed beam current monitor	9
Halo scraper	0 or 1
Beam phase and energy probe, pairs	29

Figure 8.1 shows a conceptual layout of the warm section. To minimize activation from beam loss, the beam pipe 10-cm inner diameter in the warm sections is the same as the aperture of the acceleration cavities. The length of warm sections is 160 cm, and the preliminary core length of the quadrupole is 35 cm. The 160-cm length is adequate and provides a 5-cm margin. Transverse and longitudinal beam centroid monitoring systems are required at every cryomodule for transverse matching and to measure the longitudinal phase and the energy, respectively. The ionization chamber for beam loss measurement is located outside the beam line. Not all instrument types are installed at every cryomodule.

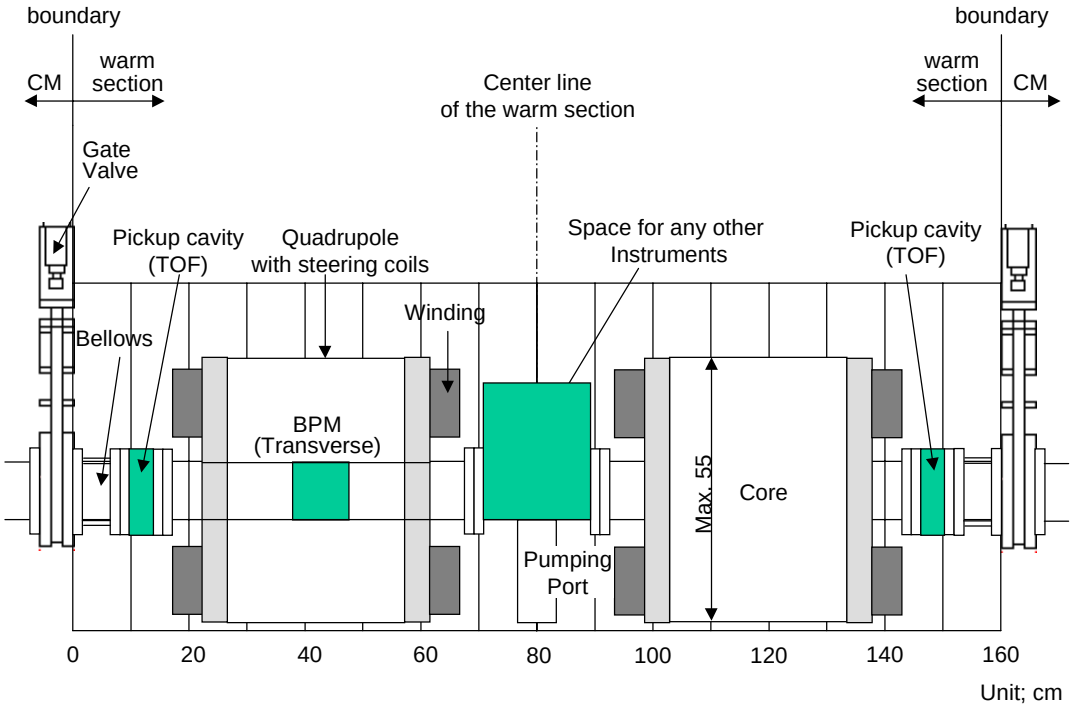

Fig. 8.1. Layout of the warm section between cryomodules.

9. CONVENTIONAL FACILITIES

9.1 INTRODUCTION

There are several scope changes to the conventional facilities which include: shortening of the linac tunnel and klystron building, new cryogenics building, new cavity processing and assembly area, changes in scope of the technical support building, reduction of installed electric power, and reduction of cooling capacity.

Figure 9.1 shows the site layout with the baseline warm linac, including linac tunnel, klystron building, ring and target buildings, central utility building, central lab-office building, and related facilities. Figure 9.2 shows the site layout as modified for the SC linac, including shorter linac tunnel and klystron building, new cryogenic building, and the new cavity processing and cryomodule assembly building.

Geometrical changes of the conventional facilities are shown in Table 9.1. The table shows changes in the linac tunnel, klystron building, and the klystron shop in the central lab office building, as well as the addition of a cryogenic building and SRF infrastructure building.

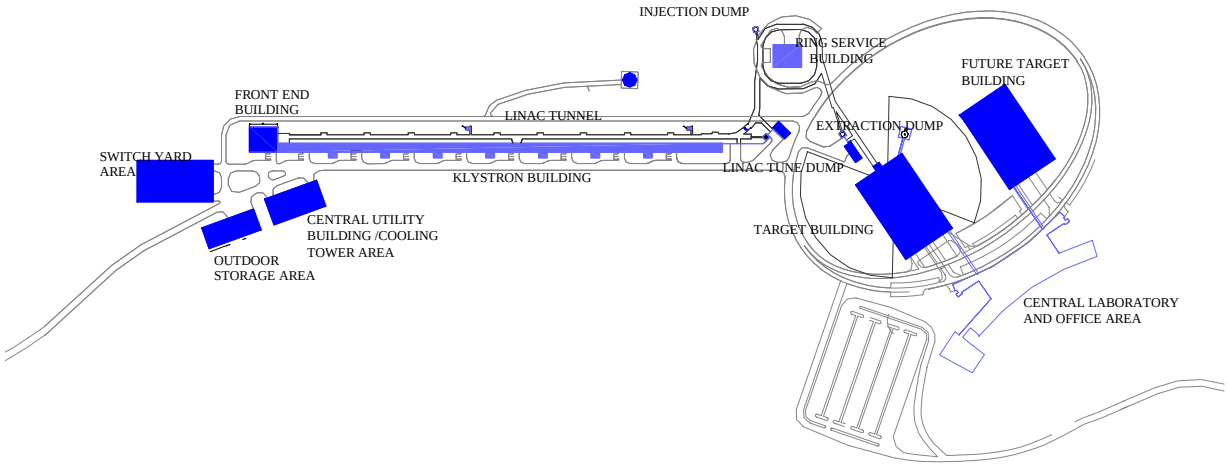

Figure 9.1 Site layout with the baseline warm linac.

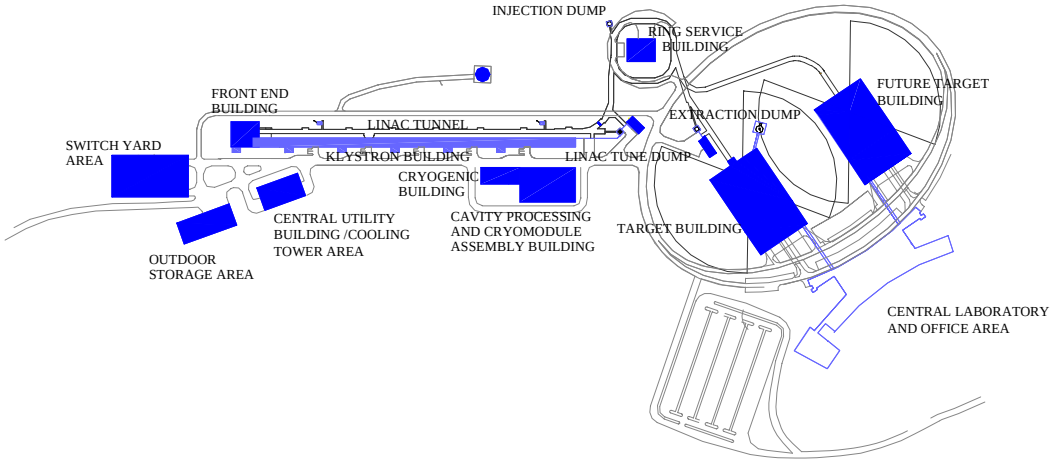

Figure 9.2 Site layout as modified for the SC linac.

Table 9.1 Conventional Facilities Comparison.

Facility	NC Linac	SC Linac	Δ (SC - NC)
Klystron Shop in the Central Lab Office Building (sq. ft.)	10,000	7,500	(2,500)
Cryogenic Building (sq. ft.)	0	6,000	6,000
SRf Infrastructure (sq. ft.)	0	25,000	25,000
Linac Tunnel (m)	464.8	327.9	(137)
Klystron Building (sq. ft.)	52.390	32.122	(20,268)

Technical changes to the conventional facilities are shown in Table 9.2. The impact on excavation, chilled water, tower water, peak and demand electrical power, and power for the cryogenics plant. The site-wide utility reduction of 6 MW and 13 MW, for chilled and tower water usage, respectively is shown

in the table. The reduction in linac electrical power demand is 13.1 MVA. It is interesting to note that the 200-MeV warm linac consumes more electrical power than 800 MeV of SC linac.

Table 9.2 Conventional Facilities Technical Data Comparison.

	NC Linac		SC Linac	
Linac Section Energy (MeV)	**2.5-194**	**194-1000**	**2.5-194**	**194-1000**
Excavation, cut and fill (cy)	97,144	275,056	97,144	193,914
Site-wide Chilled Water (MW)	5.5	15.5	5.5	9.5
Site-wide Tower Water (MW)	12.0	34.0	12.0	21.0
Peak Electrical Linac Power (MW)	23.1	92.1	23.1	29.0
Demand Electrical Linac Power (MVA)	4.1	16.5	4.1	3.4
Cryogenic Plant Power (MVA)	0.0	0.0	0.0	3.0

9.2 LINAC TUNNEL AND KLYSTRON GALLERY

The Linac tunnel and klystron building overall exterior dimensions are shortened in length by 137 meters (449.5 ft.), which was removed from the center portion of the tunnel. The baseline warm linac tunnel and klystron building are 464.8 meters (~1525 ft.) in length. The inside dimensions of the linac tunnel for the SC linac are 12 ft. wide by 10 ft high. The finish floor elevation of the linac tunnel remains at 1080.0 ft. above sea level and the finish grade of the earthen materials over the tunnel is 1108.5 feet. The klystron building internal working space dimensions are reduced from 30 ft. wide to 24 ft., but the building retains a 12-ft. ceiling height.

Table 9.3 shows the lengths of various sections of the linac and the net length reduction of 137m. This results in a construction cost reduction of $11.6M.

Table 9.3: Comparison of SC and NC Linac Length.

Cu Linac Length – Front End to 1001.5 MeV Point	456.74 m
Transition Energy – NC to SC	194.3 MeV
Cu Linac Length – Front End to 194.3 MeV Point	113.21 m
Cu Linac Length Replaced with SRF	343.54 m
SRF Linac Length 194.3 to 1001.5 MeV	206.60 m
Net Savings in Linac Tunnel and Klystron Building	136.94 m

9.3 CRYOGENIC BUILDING

The proposed cryogenic building is a standard high bay industrial building with the appropriate utility services to house the cryogenic refrigerators, compressors, and auxiliary equipment. The building measures approximately 60 ft. by 100 ft. and is located along the south side of the klystron building towards the higher energy end of the linac tunnel. A utility chase connects the cryogenic building to the linac enclosure. The cost of this building is $944k.

9.4 CAVITY PROCESSING AND CRYOMODULE ASSEMBLY BUILDING

Adjoining the cryogenic building is the cavity processing and cryomodule assembly building. This additional high bay standard industrial building measures approximately 125 ft. by 200 ft. and is utilized primarily for cavity surface preparation and assembly of linac cryomodules and related equipment. This building is located along the south side of the klystron building towards the high-energy end of the linac. The primary access road to this facility is along the south side of the building. The north side of the building has limited vehicular access due to the utility service runs to the klystron and linac buildings.

The Cavity Processing and Cryomodule Assembly Building is an above grade, steel frame, structure with an interior clear height of approximately 20 feet. All interior walls are reinforced concrete block with the exception of the plumbing walls between the restrooms. The concrete floor slab is constructed sufficiently flat to accommodate forklift traffic for moving equipment. It is planned to install a 5-ton overhead bridge crane in the building. Floor loading capacity is available to accommodate x-ray shielding for rf test areas as required.

The exterior skin of the building is constructed from insulated metal panels, masonry, pre-cast concrete, or other suitable material. The roof is standing-seam metal or composite built-up roofing over metal deck. The overall architectural style of the building is consistent with the chosen architecture for the entire SNS site.

Equipment access is provided by means of a minimum of two overhead truck doors. An access road and parking apron are provided to these locations sufficiently sized to allow for truck turnaround. Personnel access doors are provided as required by code.

The buildings are provided with air-conditioned air and ventilation, as well as the appropriate utilities such as electrical power and water, etc. to support the planned operations of the building.

The cavity processing and cryomodule assembly building is constructed at a cost of $157/sq. foot for a total cost of $3.9M. It provides approximately 25,000 sq. ft. of space.

9.5 CENTRAL LAB AND OFFICE (CLO) BUILDING

The klystron shop in the CLO is reduced from 10,000 sq. ft. to 7,500 sq. ft., because two of the four shielded klystron test stations are no longer required. The net saving is $400k.

9.6 CENTRAL UTILITIES BUILDING

The Central Utilities Building area of 15,000 square feet to support the baseline warm linac is reduced to 13,500 square feet. This reduction is the result of the chilled water load decreasing by 6 MW. The saving in building construction cost is $750k.

9.7 EXCAVATION

To construct the linac tunnel and the klystron gallery as proposed for the baseline warm linac from 194 to 1000 MeV, 275,000 cubic yards of earth must be cut and filled. The proposed SC case requires only a total of 194,000 cubic yards of cut and fill. This SC case provides a saving of $312k associated with the linac tunnel and klystron gallery excavation.

9.8 ELECTRICAL POWER SYSTEM

The total estimated power requirement for the SRF portion of the SNS linac is 3.4 MVA. The estimated power required for the corresponding portion of the normal conducting machine is 16.5 MVA. These power levels result in a 13.1 MVA reduction in power requirements for the SRF machine. Approximately 3.0 MVA are required to power the new cryogenic system plus cavity processing and cryomodule assembly area necessary for the SRF machine. A net power reduction of approximately 10.1 MVA is estimated for the SRF accelerator. Additionally, at least 1.5 MVA primary power reduction is anticipated from cooling water reductions. This power reduction results in considerable savings in both the SNS power plant cost and the required site distribution system. The existing power plant MVA rating can be reduced by 11.6 MVA. This reduction results in an estimated construction cost of approximately $1.5M. The installed cost for the site power distribution system is reduced due to shorter lengths, and lower voltage and power levels required to drive the rf system for the SRF machine. This reduction is estimated at $800k. It is estimated that savings of $2.3M for the Conventional Facilities Electrical Power System can be realized for the SRF machine as compared to the normal conduction machine.

9.9 CHILLED WATER AND TOWER WATER

The central chilled water load to support the SRF portion of the linac decreases by 6 MW from 15.5 MW to 9.5 MW due to the elimination of the structure cooling carts. The central tower water load has decreased by 13 MW from 46 MW to 33 MW due to reduction in structure cooling and klystron cooling loads. Cost of these systems includes chillers, chilled water piping system, cooling towers, tower water piping system and pumps. The saving from the chiller reduction is $839k and from the tower is $928k.

9.10 HEAT VENTILATION AND AIR CONDITIONING

Air-conditioning loads in both the linac and klystron buildings are decreased due to both reductions in the size of the facilities and the diminished heat gain from technical components. The decreased cooling load as a result of shortening the linac and klystron buildings by 137 meters and the narrowing of the klystron building by six feet amounts to approximately 53 tons (180 KW). The decrease in air-conditioning loads from technical components amounts to approximately 184 tons (650KW). The HVAC cost is included in the cost per square foot estimate for building construction, therefore there is no explicit change in the cost associated with linac length reduction.

9.11 NET COST DIFFERENCE

9.11.1 Construction cost savings

Table 9.4 is a summary of cost reductions and additions for conventional facilities associated with the SC linac. The net construction cost saving is $12.29M.

Table 9.4 Summary of cost reductions and additions for conventional facilities.

	Cost Saved ($M)	Cost Added ($M)
Linac Tunnel and Klystron Building	11.6	
Cryogenic Building		0.94
Cavity and Cryomodule Assembly Building		3.9
Central Lab Office	0.40	
Central Utility Building	0.75	
Excavation	0.31	
Electric Power System	2.30	
Chilled Water System	0.84	
Tower Water System	0.93	
Total	17.13	4.84
Net Savings (M$)	**12.29**	

9.11.2 Operating cost savings

The net savings in electric power is 11.6 MW as discussed in Section 9.8. Assuming 6000 hours of operation per year and $0.05 per kWh, the resulting saving is $3.5M per year. The assumed electric rate of $0.05 includes energy charge, demand charge, and amortization of the charge for Tennessee Valley Authority (TVA) equipment.

10. SUPERCONDUCTING RF PREPARATION FACILITIES (SRF INFRASTRUCTURE)

The construction plan is to procure niobium cavities from industrial vendors, who make cavities with niobium supplied by the SNS. Processing of cavities and the assembly and the testing of cryomodules are performed at the Oak Ridge site. The treatment of superconducting rf cavities requires the following infrastructure for cavity preparation and cryomodule assembly.

1. Eddy current surface inspection equipment for niobium sheets before shipping to vendors.
2. Cavity mechanical inspection system for welding and physical dimensions, when cavities are delivered by vendors.
3. Cavity frequency check and fine tuning system.
4. Buffered chemical polishing or electropolishing system to treat niobium surface.
5. High-pressure pure water rinsing system to clean the niobium surface.
6. Class 10, 100, and 1,000 clean rooms. Items 4 and 5 above are situated in the clean rooms.
7. Ultrahigh vacuum oven for cavity heat treatment at 800 to 1400°C.
8. Vertical cavity testing Dewars to test electromagnetic properties of cavity.
9. High and low rf power sources for cavity tests and high-power processing.
10. A cryoplant to support cavity testing activities.
11. Electron beam welding system in high vacuum for cavity repair if needed.

The infrastructure design is based on the assumption that all twenty nine (29) cryomodules are produced within the required schedule window of twenty one months. It also assumes that industry supplies roughly tuned cavities.

Figure 10.1 shows the TESLA Test Facility SRF infrastructure. In the figure, the clean rooms, chemistry area, and infrastructure are clearly visible. In addition to the aforementioned requirements, the TTF includes cavity testing, cavity assembly, and cryomodule assembly areas. This infrastructure is located in a building that measures 45 m $\times$ 100 m. SNS plans to build a similar size structure appropriate for construction of 29 SNS cryomodules.

The infrastructure must have cavity receiving, inspection and process capability. The receiving and inspection process includes dimensional inspection, weld inspection, frequency test, vacuum test, and rf bead pull. Surface processing capability includes ultrasonic rinse, bulk chemistry, internal low pressure rinse, high temperature bakeout, 800 ºC heat treatment, internal chemistry, heat treatment, tuning ($\pm$100 kHz), final chemistry, final high pressure rinse, and low temperature bakeout (150 ºC).

Single cavities are prepared for the vertical tests in class 10 and 100 cleanrooms, after surface treatment is complete. Open cavity operations are in class 10 cleanrooms and closed cavity operations are in class 100 cleanrooms. After completion of the vertical tests, the cavity is placed in a helium jacket in a class 10 clean room. Three or four of the cavities in the helium jacket make a cavity string, which is fixed in a space frame. Also installation of fine tuners on each cavity is performed.

The next assembly step is to make a cryomodule in class 100 cleanrooms. This procedure includes installation of the thermal shield, placement of the space frame in the cryostat, and installation of end caps and couplers.

The cost for the equipment in this facility is estimated to be 9M$.

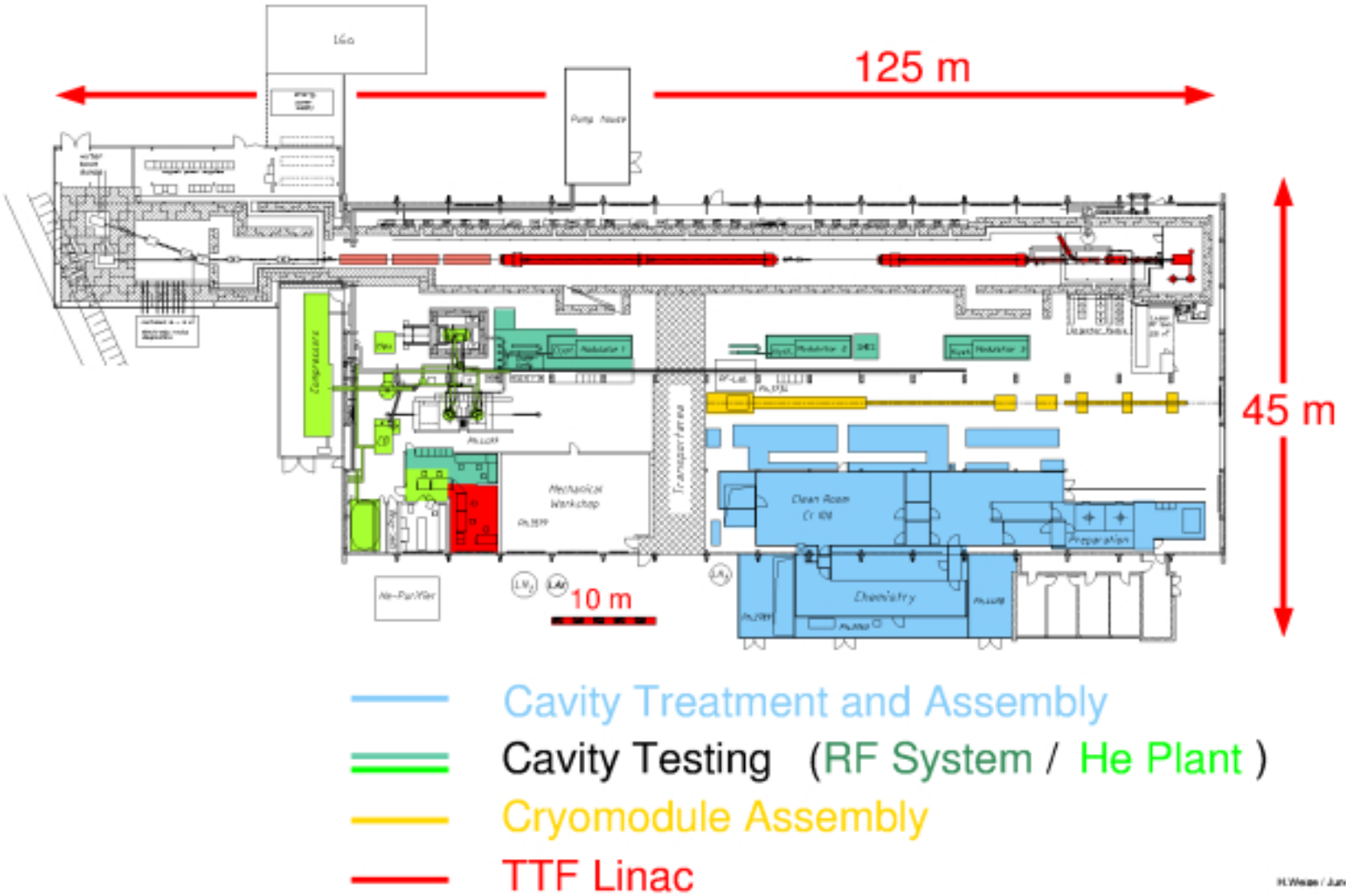

Fig. 10.1: The TTF superconducting rf infrastructure layout.

11. PROTOTYPING PLAN

The proposed superconducting linac sections between the energies of 194 MeV and 1000 MeV consist of two different types of cryomodules with two different cavity geometries, as described in Chapter 3. From 194 MeV to 331 MeV, three $\beta_g = 0.61$ cavities are assembled into each of nine cryomodules; above 331 MeV, 20 cryomodules with four $\beta_g = 0.76$ cavities each completes the superconducting linac sections.

From experience at other laboratories involved in superconducting accelerator technology, it is prudent to prototype these components prior to production of the whole system and to solve fabrication and performance issues at this stage. This chapter describes the plan for the prototyping effort. Due to the very tight schedule, it is restricted to:

I) Prototyping and testing of both types of cavities.
II) Prototyping and testing of the medium-β cryomodule.

The rationale for the decision to only prototype the medium-β module is as follows:

The medium-β cavities are more sensitive to the issues of mechanical stability, Lorentz force detuning, and microphonics. Prototyping efforts of the medium-beta cryomodule obviate the need for high-beta cryomodule prototyping. Q-value and accelerating gradient design values are comparable for both cavity types. However, the medium-β cryomodule requires fewer cavities and auxiliary components such as high power couplers, HOM couplers and tuners and fits better in a tight schedule. Assembly issues, QA and cleanliness issues can be addressed equally well for either cryomodule type.

Deliverables in this effort are:

- Four β = 0.61 niobium cavities, performance tested
- Two β = 0.76 niobium cavities, performance tested
- One copper cavity each of both types
- Six KEK-type high-power couplers, modified for 805 MHz
- One β = 0.61 cryomodule, tested (contains 3 β = 0.61 cavities & 3 couplers)
- One procurement package for the β = 0.61 cryomodule
- One procurement package for the β = 0.76 cryomodule

The cost and schedule summarized in Section 11.3 are based on the following assumptions:

- High-purity niobium can be obtained from LANL or elsewhere to allow a fast start of the cavity prototyping effort.
- The KEK high-power input coupler can be modified in a teaming effort with experts from KEK.
- The high-power rf system required for coupler and cryomodule testing is provided by SNS.
- Design, fabrication, and procurement of the deliverables are fast-tracked under a single management entity.

11.1 PROTOTYPING OF $\beta = 0.61$ AND $\beta = 0.76$ SIX-CELL CAVITIES

11.1.1 Fabrication and Testing

The cavities are fabricated from 3.5- to 4-mm-thick high-purity niobium with a residual resistivity ratio RRR $\geq$ 250. Cavity production is done in accordance with established manufacturing procedures: thorough material inspection for defects, deep drawing of half cells, machining for electron beam welding, cleaning, and electron beam welding. It is anticipated to use existing DOE, NSF, and other partner laboratory facilities (including CEA-Saclay, INFN-Milan, and TTF) and experience to accomplish these tasks.

The steps needed to arrive at the final product are listed below:

1. Manufacturing of deep-drawing dies for half-cells, made from Al 7075 in accordance with manufacturing drawings.
2. Deep drawing of copper prototype half-cells, both center and end cells.
3. Dimensional inspection of these half-cells.
4. Trimming of half-cells for electron beam welding.
5. Frequency measurements of half-cells and comparison to URMEL/MAFIA/ANSYS calculations.
6. Correction to trimming procedure or die geometry, if discrepancies are observed.
7. Fabrication of other cavity components such as beam pipes and coupler ports.
8. Electron beam welding of the 6-cell copper model.
9. Leak checking of models.
10. Modification of inelastic tuning equipment.
11. Frequency/field profile measurement and tuning of the copper model cavity/cavities.
12. QA of copper models and comparison of mechanical dimensions to design drawings.
13. Deep drawing of niobium half-cells and application of steps 3) to 12) to the niobium model.
14. Surface treatment (buffered chemical polishing and high pressure rinsing), assembly and cold testing of the prototype cavities.

As a minimum, the cryogenic tests should include the following measurements:

- Q_0 vs. T for 4.2K $\geq$ T $\geq$ 2.1 K (T - dependence of surface resistance)
- f vs. T for 4.2K $\geq$ T $\geq$ 2.1 K (pressure sensitivity of cavity)
- Q_0 vs. E_a at 2.1 K, all passband modes (info about possible quench)
- f vs. E_a at 2.1 K : (Lorentz force detuning)
- Test for Q - disease: hold cavity for 12 hrs @ 120 K, then retest

After initial tests, the cavities are heat-treated at T $\leq$ 800°C for 2–4 hrs in a titanium-lined furnace at a vacuum pressure P $\leq 2 \times 10^{-6}$ torr, followed by additional buffered chemical polishing and a retest.

Both tests establish whether an 800°C heat treatment improves cavity performance and is needed as a procedural step in cryomodule production. After the heat treatment step, the titanium He vessel is welded to the cavity. Because of a phase transition in the titanium at elevated temperatures around 800°C, the fabrication sequence has to be as indicated.

In addition, at room temperature the sensitivity of the cavity to external pressure (with respect to inelastic frequency changes) must be measured on at least one prototype cavity to determine the allowable He pressure during cooldown to avoid plastic deformation of the cavities.

11.2 PROTOTYPING OF THE β = 0.61 CRYOMODULE

11.2.1 Fabrication and Testing

As mentioned above, the fastest, most effective approach for prototyping this module is to use existing DOE, NSF, and other laboratory facilities and experience to accomplish these tasks, along with experienced industrial partners. There are several industrial firms supplying superconducting rf cavities to various laboratories throughout the world. The goal of this effort is to fabricate and fully rf test one major building block of the superconducting linac section of SNS. The following major components have to be fabricated for this prototype cryomodule:

11.2.1.1 Cavities

Three medium-β cavities are needed for installation in the prototype cryomodule; four β = 0.61 cavities are manufactured and tested during the cavity prototyping phase as outlined in Section 9.1. It is anticipated that three of these prototypes are used for the module.

11.2.1.2 Fundamental Power Couplers

The fundamental power coupler design is based on the KEKB input coupler, scaled to 805 MHz. There is already an agreement between the SNS and KEK management for close collaboration. Present scenarios foresee a close collaboration between SNS and KEK with its industrial partner in prototype development; manufacturing of five additional couplers, from which three will be chosen for the cryomodule, follows the prototyping stage. After the couplers are manufactured they must be rf tested and qualified for module assembly at an existing facility.

11.2.1.3 HOM Couplers

Damping requirements are determined from instability simulations and from knowledge of the cavity modes, shunt impedance, frequencies and manufacturing frequency spreads. The HOM coupler design is based on existing electron linac designs from DESY and CEA-Saclay. Prototyping and evaluation of the capabilities of the HOM coupler, including measurements on the prototype copper models, must be performed. Production of additional couplers for the module can be done in industry.

11.2.1.4 Tuner

The tuner design is based on existing designs, e.g., CEBAF, TTF, or APT tuner, adapted to the 805-MHz cavities. Prototypes can be manufactured locally or by qualified vendors; testing for functionality is done at existing facilities. Manufacturing of additional tuners for the module based on manufacturing drawings is done by industrial partners.

11.2.1.5 Rf Power Source for Cryomodule Testing

Power sources at 805 MHz exist at LANL. Prototypes of the 2.5-MW klystrons for the SNS baseline warm linac are currently undergoing vendor tests. One such system is needed at the facility where the module tests are carried out.

11.2.1.6 Cryomodule Hardware (End cans, vacuum vessel, thermal shield, magnetic shield)

Based on experience gained during the construction of CEBAF, these components can be fabricated by qualified industrial partners. Cryomodule hardware must be integrated with instrumentation for cryogenic testing, vacuum hardware, and rf testing equipment. The cavity string assembly requires an appropriate clean room facility. These tests have to include as a minimum:

- Cavity performance such as gradient and Q-value in an integrated system
- Lorentz force detuning and sensitivity to microphonics noise in a complex system
- Rf cross coupling between cavities
- Tuner functionality in a complex system
- Rf control system evaluation
- High power coupler capability
- Cryogenic performance of the cryomodule
- Functionality of instrumentation

11.3 COST AND SCHEDULE

Table 11.1 summarizes the estimated costs for cavity prototyping, fabrication, and testing of the medium-β cryomodule and the engineering costs for generating procurement packages for both module types. The estimates are based on actual costs for comparable components from different labs (e.g., KEK, TJNAF) or commercially available hardware.

The estimated direct costs for this total effort are $4.1M.

Table 11.1: Cost summary for prototyping effort

Item	Cost ($K)
Prototype cavities	
3 Niobium (2 + 2 -1)	255
2 copper	58
Tooling	45
Testing (2 tests per cavity)	98
Cryomodule	
Fabrication (including 3 additional cavities)	820
Tooling	80
Testing	100
Labor (not included above)	
Engineering module procurement packages	1,250
Prototyping, assembly ß = 0.61 module	1,254
11 man years @ $114K	
S & E	125
Total (direct costs)	**4,085**

A fast-track schedule that accomplishes the tasks described above by the fourth quarter of CY 2001 is shown in Fig. 11.1. The figure also shows that the procurement package for the construction is completed by July 1, 2001, and procurement contracts can be awarded by the end of the same CY.

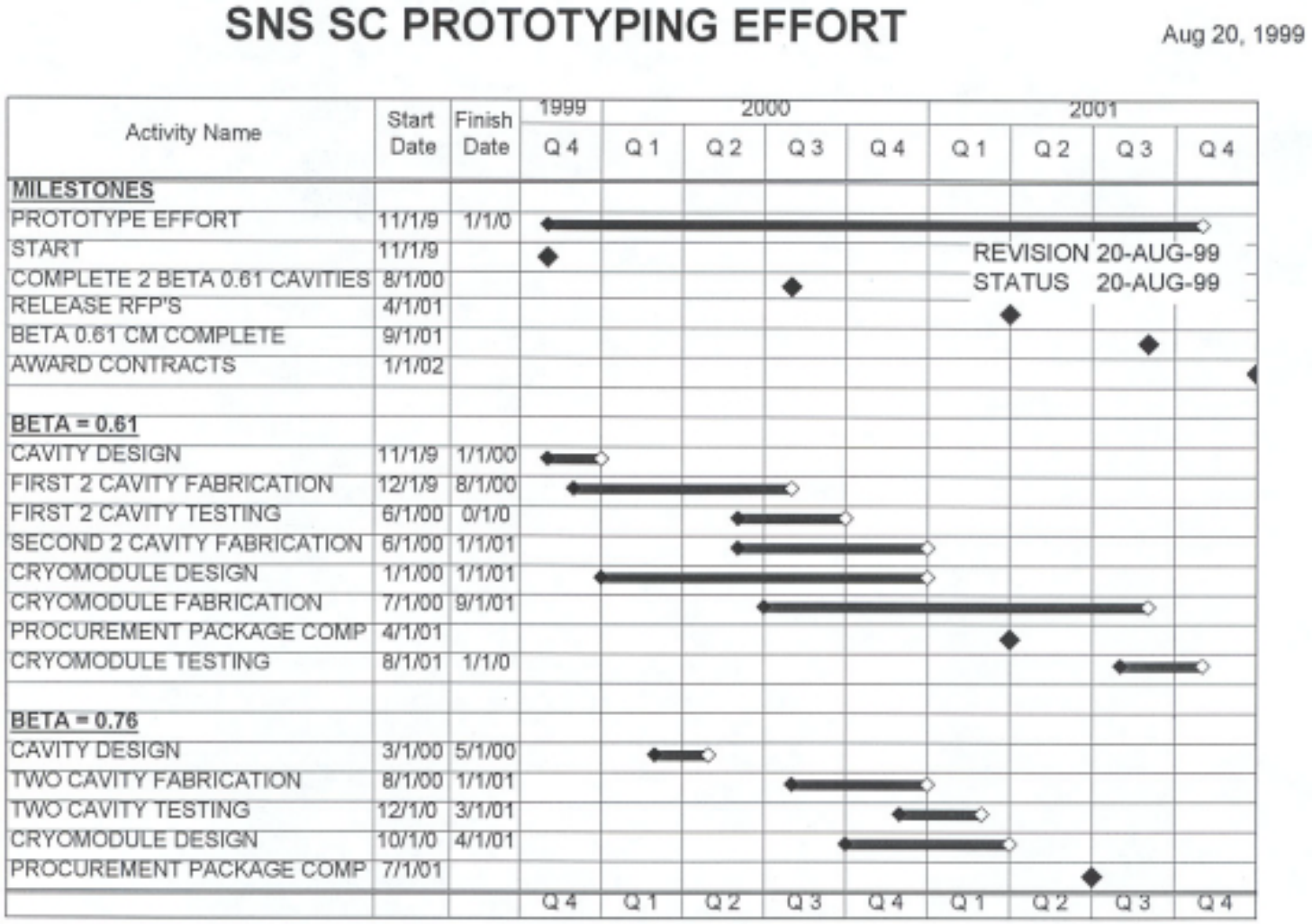

Fig. 11.1. SNS superconducting cryomodule prototyping schedule.

12. COST AND SCHEDULE

12.1 INTRODUCTION

In order to organize the cost and schedule of the SC linac, a separate work breakdown structure list (WBS) was created and is listed in Table 12.1. The baseline cost of $71.068M for the linac up to 194 MeV is retained. This SC cost estimate is separated into EDI, Procurements, and Installation, and rolled up to the third WBS level. It includes preconstruction R&D and cavity preparation and assembly area equipment, but does not include preoperational activities required for commissioning.

Table 12.1 WBS for the SC linac.

WBS NUMBER		WBS DESCRIPTION
1.11		***Superconducting Linac***
1.11.1		**Medium-Beta Cryomodule**
1.11.1.1		*Cold Mass*
1.11.1.1.1		Cavities
1.11.1.1.1.1		Cells
1.11.1.1.1.2		Bellows
1.11.1.1.1.3		Couplings
1.11.1.1.2		Auxiliary Cold Components
1.11.1.1.2.1		Ti Vessel
1.11.1.1.2.2		Space Frame Support
1.11.1.1.2.3		Tuner
1.11.1.1.2.4		HOM Loads
1.11.1.1.2.5		Directional Couplers
1.11.1.1.3		Cold Mass Component Assembly
1.11.1.2		*Cryostat*
1.11.1.2.1		Vacuum Vessel
1.11.1.2.2		End Caps
1.11.1.2.3		Thermal Shields
1.11.1.2.4		Cold Mass Support
1.11.1.2.5		Magnetic Shield
1.11.1.2.6		Instrumentation
1.11.1.2.7		Cold Waveguides
1.11.1.2.8		Tuner
1.11.1.2.9		Tuner Drive System
1.11.1.2.10		Cryostat Support
1.11.1.3		*Input Coupler*
1.11.1.4		*Cryomodule Assembly*
1.11.1.5		*Cryomodule Installation*
1.11.1.5.1		Installation Labor
1.11.1.5.2		Installation Equipment
1.11.1.5.2.1		Roughing Pump Cart
1.11.1.5.2.2		Other Equipment

1.11.2		**High-Beta Cryomodule**
1.11.2.1		*Cold Mass*
1.11.2.1.1		Cavities
1.11.2.1.1.1		Cells
1.11.2.1.1.2		Bellows
1.11.2.1.1.3		Couplings
1.11.2.1.2		Auxiliary Cold Components
1.11.2.1.2.1		Ti Vessel
1.11.2.1.2.2		Space Frame Support
1.11.2.1.2.3		Tuner
1.11.2.1.2.4		HOM Loads
1.11.2.1.2.5		Directional Couplers
1.11.2.1.3		Cold Mass Component Assembly
1.11.2.2		*Cryostat*
1.11.2.2.1		Vacuum Vessel
1.11.2.2.2		End Caps
1.11.2.2.3		Thermal Shields
1.11.2.2.4		Cold Mass Support
1.11.2.2.5		Magnetic Shield
1.11.2.2.6		Instrumentation
1.11.2.2.7		Cold Waveguides
1.11.2.2.8		Tuner
1.11.2.2.9		Tuner Drive System
1.11.2.2.10		Cryostat Support
1.11.2.3		*Input Coupler*
1.11.2.4		*Cryomodule Assembly*
1.11.2.5		*Cryomodule Installation*
1.11.2.5.1		Installation Labor
1.11.2.5.2		Installation Equipment
1.11.2.5.2.1		Roughing Pump Cart
1.11.2.5.2.2		Other Equipment
1.11.3		**Warm Beam Pipe Vacuum**
1.11.3.1		*Manifolds*
1.11.3.2		*Valves*
1.11.3.3		*Ion Pumps w/ Power Supply*
1.11.3.4		*Vacuum Fittings*
1.11.3.5		*Roughing Pump Cart*
1.11.3.6		*Vacuum System Installation*
1.11.4		**Magnet System**
1.11.4.1		*Quadrupoles*
1.11.4.2		*Corrector Magnets*
1.11.4.3		*Steering Magnets*
1.11.5		**Beam Diagnostics System**
1.11.6		**High Power RF System**
1.11.6.1		*IGBT Modulator*
1.11.6.2		*Klystrons*
1.11.6.3		*Amplifier*
1.11.6.4		*RF Transport*
1.11.6.4.1		Circulators
1.11.6.4.2		Windows

1.11.6.4.3		Waveguides
1.11.6.4.4		Ion Pumps w/ Power Supply
1.11.6.5		*RF System Installation*
1.11.7		**Low Level RF Systems**
1.11.7.1		*Low Level RF Control System*
1.11.7.2		*Cabling/Grounding*
1.11.7.3		*RF Reference & Distribution System*
1.11.7.4		*Low Level RF System Installation*
1.11.8		**Cryogenic System**
1.11.8.1		*Refigerator Systems*
1.11.8.1.1		Warm Compressors
1.11.8.1.2		Oil Coalescer
1.11.8.1.3		4.5 K Cold Box
1.11.8.1.4		2.1 K Cold Box
1.11.8.2		*Controls, Refrigerator/Cryomodule*
1.11.8.3		*Ancillary Equipment*
1.11.8.3.1		LHe DEWAR, 5,000 gal
1.11.8.3.2		LN2 DEWAR, 30,000 gal
1.11.8.3.3		External 80 K Purifiers
1.11.8.3.4		30,000 Gal He Storage Tanks
1.11.8.3.5		Instrument Air System
1.11.8.3.6		Contamination Equipment
1.11.8.3.7		External Piping
1.11.8.4		*Transfer Lines, Linac/Distribution*
1.11.8.4.1		Expansion/Anchor Boxes
1.11.8.4.2		Warm Gas Supply
1.11.8.4.3		Cooldown and Coupler Return
1.11.8.4.4		Guard Vacuum and Relief
1.11.9		**SC Assembly Facility**
1.11.9.1		*ORNL 1500W Refrigerator (Move)*
1.11.9.2		*Transfer Lines*
1.11.9.3		*Vertical Dewar*
1.11.9.3.1		Dewars, 2 R&D
1.11.9.3.2		Dewars, 3 Production
1.11.9.3.3		Vacuum Pumps, RGA, Auxiliary Equipment
1.11.9.3.4		Test Stands
1.11.9.4		*RF*
1.11.9.4.1		3-200W Cold Cavity, HOM Test
1.11.9.4.2		3-200kW Cold CM Test
1.11.9.5		*Chemistry*
1.11.9.5.1		Cabinets
1.11.9.5.2		HPR
1.11.9.5.3		Cavity Store
1.11.9.5.4		Clean, Handle, Ultrasonics
1.11.9.5.5		EBW
1.11.9.5.6		Inspection Equipment
1.11.9.6		*Hot Water Heater*
1.11.9.7		*800C Furnace*
1.11.11		**Project Services**
1.11.10.1		*Project Management*

1.11.10.2		*Project Controls/Business/Office Support*
1.11.10.3		*System Engineering*
1.11.10.4		*ES&H & QA/QC Support*
1.11.10.5		*Physics & Engineering Management*
1.12		**Conventional Facilities**
1.12.1		*Building*
1.12.2		*Clean Rooms*
1.12.2.1		R&D Clean Room
1.2.2.2		Production Clean Room
1.12.3		*Other Rooms*
1.12.3.1		Wet Chem Treatment
1.12.3.2		Ultra Pure Water
1.12.3.3		Chemical Area Store
1.12.3.4		QA/CMM Inspection
1.12.3.5		RF Test Warm
1.12.3.6		RF Test Cold
1.12.3.7		Furnace Area
1.12.3.8		Cold Material Test
1.12.3.9		Fabrication Area
1.12.3.10		Utility Area
1.12.3.11		CM Assembly Area
1.12.4		*EDI&A*
1.01.11		**Superconducting Linac R&D**
1.01.11.1		*Cavities*
1.01.11.2		*Cryomodule*
1.01.11.3		*Assembly/Testing*

12.2 COST ESTIMATE BASIS

Input data for the cost estimate comes from several sources, including vendor quotes, catalog prices, engineering judgment of experienced staff, and recent accelerator construction experience at other laboratories. Some of the cost data presented in this report are bottoms-up estimates and some are scaled from construction of existing facilities. The cost estimates presented here are in FY99 dollars.

The following lists specific cost estimate sources:

- The prototyping cost is estimated by TJNAF based on CEBAF experience.
- Cryomodule cost including cavities is based on bottoms-up and also rule-of-thumb estimates from industry experience. 250k$ per active meter includes helium jacket, couplers, and tuners, and HOM loads. The couplers, tuners, HOM loads account for 52k$ of the 250k$.
- Linac warm section costs are 75k$ per section, and include magnets, diagnostics, vacuum components.
- Refrigerator costs are estimated by TJNAF based on CEBAF experience.
- Cryogenic transport line are costed per unit length by TJNAF based on CEBAF experience.
- Rf system klystrons 22M$ are based on the first vendor quote received – waiting for additional vendor quotes.
- Power supply cost is based on a vendor quote.

- LLRF system and controls are based on TTF experience.
- The circulator cost of $7.15M is based on a vendor quote for 110 units.
- Rf transport costs are estimated per unit length for 13 m of length per klystron.
- Cryomodule processing facility equipment cost of $9M is estimated by TJNAF/SNS.
- Conventional construction cost adjustments are estimated using the same methods as for the baseline.

12.3 COST

12.3.1 Construction Cost

The cost in FY99 dollars of the SC linac from 194 MeV to 1000 MeV is estimated to be $118.6M, and its associated conventional facilities cost is $32.2M. These numbers should be compared to the baseline warm linac costs of $135.6M and $44.5M, respectively. Table 12.2 summarizes the cost of the SC linac from 194 MeV to 1000 MeV.

Table 12.2 Cost summary of the SC linac from 194 MeV to 1000 MeV.

	Cost	Subtotal
High beta linac section, HBLS		
Cost of HBLS completed cryomodules	$17,379K	
Additional cost for the first cryomodule (30% over average)	$261K	
HBLS test and installation cost	$3,107K	
Medium beta linac section, MBLS		
Cost of MBLS completed cryomodules	$5,996K	
Additional cost for the first cryomodule (30% over average)	$200K	
MBLS test and installation cost	$1,124K	
Assembly and processing		
Equipment in SCRF processing facility	$8,880K	
Total cost SC linac modules		**$36,947K**
Cryogenics		
Refrigerator procurement cost	$9,583K	
Inhouse design labor for cryosystem	$910K	
Cost of cryo distribution	$3,656K	
Cryo controls cost	$1,342K	
Ancillary equipment	$1,629K	
Cost of cryo power (included in conventional facilities)	$K	
Total cryo cost		**$17,121K**
RF power		
RF primary power cost (included in conventional facilities)	$K	
RF power supply cost	$15,682K	
Klystron total cost	$20,397K	
Circulator cost, one half of klystron cost	$10,198K	
RF control system cost	$9,651K	
RF transport cost	$2,782K	
Controls cost	$3,658K	
Grand total rf cost		**$62,368K**
Auxilliary linac components		
Cost of pumping, steering, focusing, and diagnostics	$2,175K	
Total SC linac cost for technical components		**$118,611K**
Conventional facilities		
Conventional facilities up to 194 MeV (unchanged)	$13,557K	
NC linac conventional facilities above 194 MeV		**$44,505K**
Conventional Facilities for SC linac		
Cryo building, (5000 sq. ft.)	$942K	
Cavity processing and cryomodule assembly building (25000 sq. ft.)	$3,935K	
Other linac facilities	$27,343K	
Total SC linac conventional facilities		**$32,220K**
Net change in conventional construction cost above 194 MeV		**-$12,285K**

Table 12.3 compares baseline linac costs and SC linac costs in FY99 dollars, showing the cost saving of 29.3M$.

Table 12.3 Cost comparison in FY99 dollars between NC and SC linacs for 194 MeV to 1000 MeV.

	NC		SC	Difference
Linac Segments (MeV)	2.5 – 194	194 – 1000	194 – 1000	
Technical Components (M$)	71.1	135.6	118.6	17.0
Conventional Facilities (M$)	13.6	44.5	32.2	12.3
Net Savings (M$)				**29.3**

12.3.2 Operating Cost

The net savings in electric power is 11.6 MW resulting in a reduction in operating costs for the SC linac option of $3.5M per 6000-hour operating year, compared to the cost of operating the warm baseline linac, as discussed in Section 9.11. This represents significant savings in the life-cycle operation cost of the facility.

12.4 SCHEDULE ESTIMATE BASIS

Input data for the schedule estimate comes from vendor discussions on delivery times and the CEBAF and TTF construction experience. As discussed in Chapter 11, a fast-track schedule that accomplishes the tasks described above by the end of 2001 is shown in Fig. 11.1. The figure also shows that the procurement package for the construction is completed by July 1, 2001, and procurement contracts can be awarded by December 20, 2001.

There are two potential critical path items in this schedule: one is cavity construction and cryomodule assembly and the other is klystron procurement.

The plan is that SNS provides certified niobium sheets to vendor or vendors to fabricate niobium cavities. Cavities are delivered to the SNS for processing. Two European vendors indicate that production of 20,000 cavities can be done over a 3-year period for the TESLA project. The SNS requirement of 107 cavities should be easily achievable within the scheduled 1.5 years. A niobium supplier reported that RRR300 niobium can be delivered to SNS for verification three months from receipt of order. This is a standard delivery time from several vendors.

The cavity preparation and cryomodule assembly building should be completed by the end of September 2001. The cavity first article arrives on site by April 1, 2002. The cavity preparation and assembly facility is designed to process 1.5 cavities per week, requiring about 74 weeks to process 110 cavities. The production rate of 1.5 cavities per week is slower than the actual production rate of four cavities or two-cavity pairs per week during CEBAF construction. The total number of cavities needed for the SNS SC linac is 107. Cryomodule assembly proceeds in parallel with cavity preparation, therefore the cryomodule assembly process completes shortly after the last cavity is processed. A medium-beta

cryomodule is assembled in two weeks for a total of 18 weeks. The high-beta cryomodules take 2.7 weeks each, thus the high-beta section is complete in about 54 weeks. The duration of cryomodule construction is 72 weeks.

When cryomodule assembly is completed, cryomodules are installed in the linac tunnel. In this way, cryomodule storage space is minimal, and as soon as installation of the last cryomodules is completed, installation of the linac completes.

The SNS SC linac requires 107 400-kW klystrons. A reliable, reputable vendor indicated that delivery of 107 klystrons within a two-year period is plausible. It is assumed in this schedule that the klystron development period is 17 months and the delivery period is 24 months, totaling 42 months.

12.5 SCHEDULE

The SC construction schedule is devised using the schedule estimate basis described in Section 12.4 and the warm linac baseline milestones noted below, while taking into account the prototyping schedule discussed in Chapter 11.

The baseline warm linac milestone is:

- October 1, 2001 central utilities available
- May 13, 2002 - Beneficial Occupancy Date (BOD) of the entire linac tunnel and klystron building
- April 1, 2004 - CCL installation completes
- July 5, 2004 - HEBT and Ring commissioning start – 1 GeV beam available

Pertinent prototype milestones impacting the construction schedule are:

- December 10, 1999 prototype niobium order
- February 1, 2000 prototype klystron and power supply order, 17 month duration
- February 1, 2000 prototype coupler order, 17 month duration
- October 2, 2000 prototype medium-beta cavity testing complete
- October 1, 2001 prototype medium-beta cryomodule complete

The following is a list of the production milestones:

- April 3, 2000 place order for long-lead refrigerator items
- July 17, 2000 production niobium order
- January 15, 2001 production die order
- April 2, 2001 production cavity rfp released
- August 1, 2001 place klystron and power supply order
- August 1, 2001 place coupler order
- September 17, 2001 BOD cryogenic building
- September 17, 2001 BOD SRF infrastructure building
- October 1, 2001 start installation refrigerator and SRF components
- December 17, 2001 Production cryomodule including cavities order
- March 1, 2002 first article cavity arrives.
- April 1, 2002 first cryomodule complete
- April 1, 2002 SRF infrastructure ready at SNS
- July 15, 2002 refrigerator component delivery complete
- January 2, 2003 refrigerator operational
- August 1, 2003 klystron, power supply, and coupler delivery complete
- September 1, 2003 last cryomodule construction complete
- October 1, 2003 cryomodule installation complete, begin commissioning
- January 2, 2004 begin cryomodule commissioning with beam.

- January 1, 2004 linac readiness review complete
- March 15, 2004 linac available for HEBT and Ring commissioning.

The schedule outlined above is four months shorter than the baseline schedule, thus it creates four months of schedule float. The summary schedule is shown in Figure 12.1.

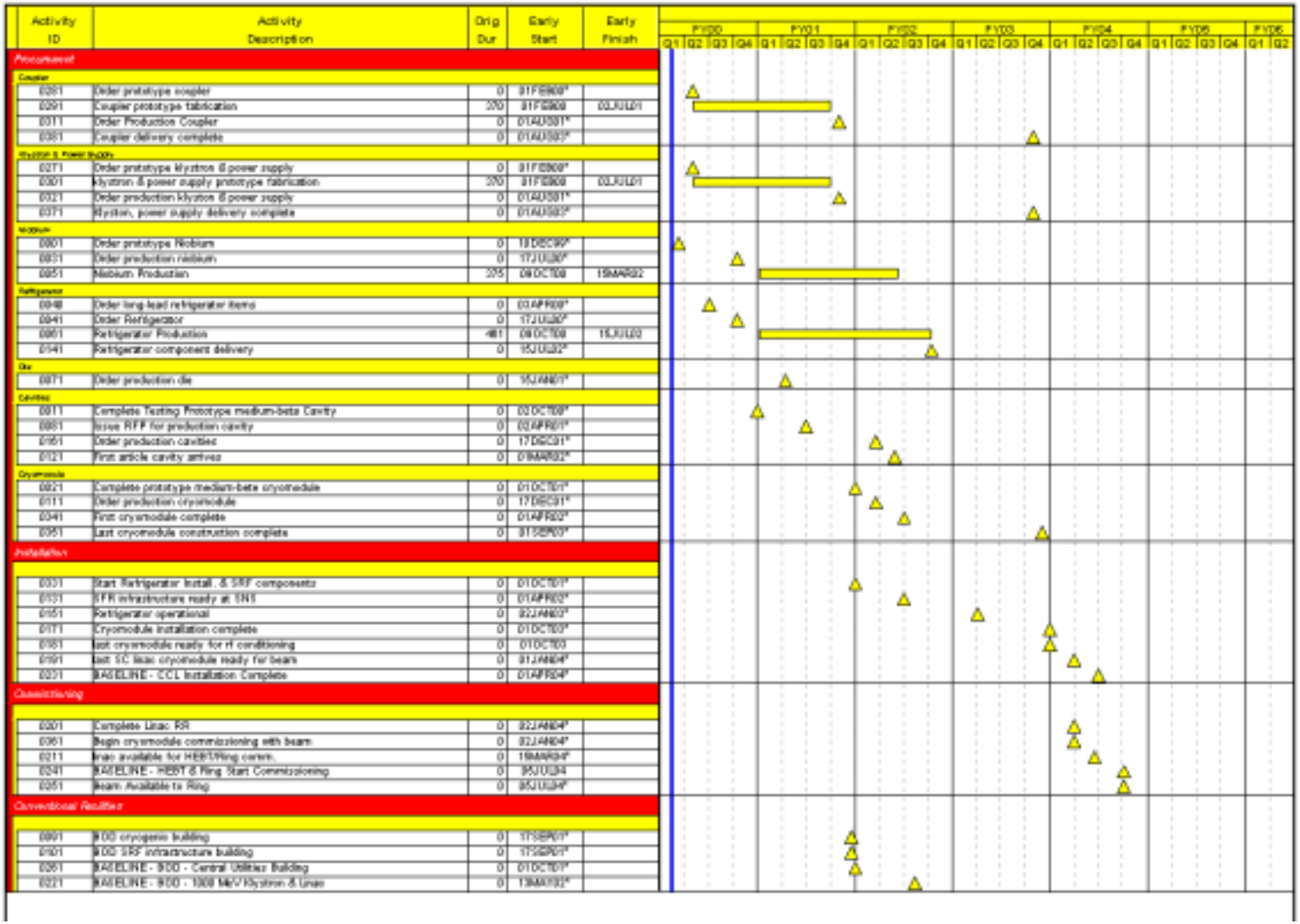

Figure 12.1 Summary Schedule for the SNS SC linac.

12.6 COST AND SCHEDULE SUMMARY

The total project cost of the SC linac option presented in this report is about $29.3M less than the warm baseline linac total project cost, including prototyping, technical equipment, and conventional facility scope reduction.

Due to the reduction of electric power and cooling required to operate the facility, the operating cost savings for the facility with SC linac are estimated to be at least $3.5M per year.

Due to the fact that less hardware is required, the construction duration is much shorter. Although actual construction of the SC linac starts later than the warm linac schedule, the SC linac is completed four months earlier. This four months can be used to obtain additional float for the Project.

13. REFERENCES

[1] M. Mizumoto, et al., “A High-Intensity Proton Linac Development the the JAERI Neutron Science Project,” Proceedings of the XIX International Linac Conference, LINAC98, Chicago, IL, (1999).

[2] C. Pagani, et al., “Status of the INFN High Current SC Proton Linac for Nuclear Waste Transmutation,” Proceedings of the XIX International Linac Conference, LINAC98, Chicago, IL, (1999).

[3] K. R. Crandall and D. P. Rusthoi, TRACE3D Documentation, Third Edition, LA-UR-90-4146, Los Alamos National Laboratory, (1990).

[4] B. Blind and R. Garnett, LINAC Code and a version of the PARMILA Code, private communication, 1999.

[5] J. Staples, private communication, 1999.

[6] S. Simrock, “Rf Control System for CEBAF,” Proceedings of the 1991 Particle Accelerator Conference, March 1991, San Francisco, CA, p.2515-2519 (1992).

APPENDIX A. Appendix A.

Table A.1 SNS SC Linac Parameter List.

Major Parameters	
Input H^- energy (MeV)	194.3
Output H^- energy (MeV)	1001.5
Output average beam power (MW)	2
Output average beam current	2
Macropulse repetition rate (Hz)	60
Macropulse beam period (ms)	0.974
Beam duty factor (%)	5.84
Chopper transmission	65
Chopper period (ns)	841
Peak macropulse current (mA)	56
Average macropulse current (mA)	36
Vacuum pressure (Torr)	$< 5 \times 10^{-8}$
Beam losses at 1 GeV (W/m)	<1

Length Allocations	
Cavity ends (cm)	22
Bellows (cm)	7
Cold to warm transitions (cm)	17.2
External valve and beam pipe (cm)	10
Relief valve and vacuum pumpout (cm)	5
Warm space between valves (cm)	160

Cell and Cavity Parameters	**Medium β**	**High β**
Geometrical beta	0.61	0.76
Cavity beta	0.64	0.79
Frequency (MHz)	805	805
Beta-lambda (m)	0.2272	0.283
Cell length (m)	0.1136	0.1415
Number of cells per cavity	6	6
Cavity active length (m)	0.6815	0.8491
Stiffening	yes	yes
R iris (cm)	5	5
Alpha (deg)	5	7
R dome (cm)	3.7	4.6
a/b	0.7	0.7
Coupling constant (%)	2	2
E_{max}/E_a interior cells	3	2.35
E_{max}/E_o interior cells	2.33	1.82
B_{max}/E_{max} (mT/MV/m)	1.99	2.12
B_{max}/E_a interior cells (mT/MV/m)	5.96	4.98
B_{max}/E_o interior cells (mT/MV/m)	4.64	3.86